INVESTIGATION OF THE PYROLYSIS OF LIGNIN BY USING COLLISION-INDUCED DISSOCIATION CHARGE-REMOTE FRAGMENTATION MASS SPECTROMETRY

by
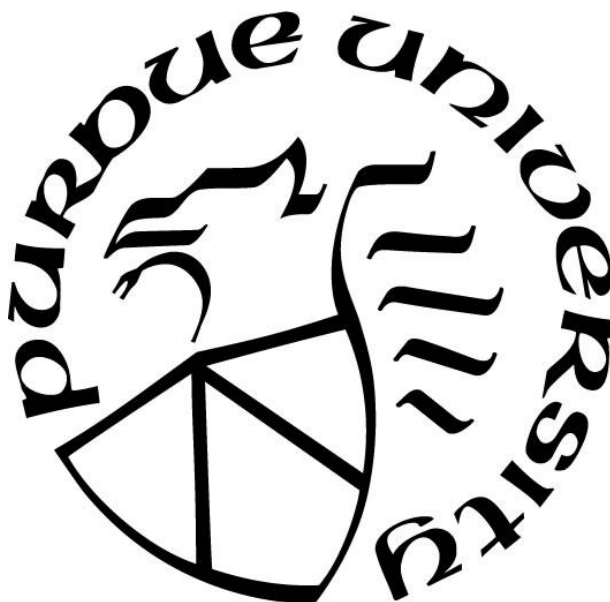
Cory Conder

A Dissertation

Submitted to the Faculty of Purdue University
In Partial Fulfillment of the Requirements for the degree of

Doctor of Philosophy

Department of Chemistry

West Lafayette, Indiana

May 2021

THE PURDUE UNIVERSITY GRADUATE SCHOOL
STATEMENT OF COMMITTEE APPROVAL

Dr. Paul Wenthold, Chair

Department of Chemistry

Dr. Hilkka Kenttämaa

Department of Chemistry

Dr. Herman Sintim

Department of Chemistry

Dr. Lyudmila Slipchenko

Department of Chemistry

Approved by:

Dr. Christine Hrycyna

To my wife, for her love and support

ACKNOWLEDGMENTS

I want to thank my wife Christina for standing by me through 5 years of graduate school. She truly knows the depth and breadth of the journey I took because she was my equal partner in every step, including weathering the storm of a pandemic (COVID-19) with two kids at home and a third on the way. I also want to thank my kids, Luke and Allison, for being the best kids in the world, and my parents for sending my mom to Indiana for a month to help my pregnant wife while I wrote my dissertation. I also am grateful to my research advisor, Paul, for letting me join his research group and for being my mentor. He really changed my life for the better, and I loved my time in his group.

Truly a lot of people have helped me succeed in graduate school, and without them I would not be where I am today. I want to thank Dr. Stephen Hoffman, Assistant Head of the Chemistry Department, Dr. Suzanne Bart, Associate Head, and Dr. Hilkka Kenttämaa for their words of encouragement at a critical time to keep me going towards my degree. I also want to thank Amber Jannasch and Bruce Cooper at the Bindley Bioscience Center who first got me interested in mass spectrometry and were happy to answer all my questions. I am also indebted to Konrad Kliewer (IT specialist), Marc Carlson (Electrical Engineer) and Erick Norwood (Instrument Technician) at the Amy Facility for doing a phenomenal job keeping our instruments running.

Other key people who helped me are Lynn Rider who assisted in formatting this dissertation, and Ned Gangwer, Building Deputy and Chemistry Maintenance Shop manager, who continues to keep the whole chemistry building running. I am also grateful for the life-long friendships I made with my labmates, Sabyasachy 'Babu' Mistry and Harshal Jawale. We enjoyed many long conversations together both inside and out of the lab, from research to religion as well as well as politics and soccer. I also want to thank my undergraduate research advisor, Dr. David Michaelis, for his continued support, as well as my high school physics and chemistry teacher, Linda Walter, for lighting the first spark and helping me recognize and develop my interest in science. She sacrificed a lot for her students so that we could enjoy a lifelong path of discovery and learning.

TABLE OF CONTENTS

LIST OF TABLES

LIST OF FIGURES

ABSTRACT

Mass spectrometry of negative ions is a convenient method for generating, isolating, and analyzing reactive intermediates that would otherwise be too short lived to detect. This ion approach is especially useful for studying the chemical properties of radicals. In this work, a negative charge-carrying group was attached to lignin model compounds and combined with collision-induced dissociation (CID) to generate and characterize radical species involved in the primary pyrolysis of lignin. The charge-tag served to increase the sensitivity of the model compounds using electrospray ionization mass spectrometry (ESI-MS) and promoted charge-remote fragmentations (CRF) upon being collisionally activated. The resulting product ions were comparable to the primary pyrolysis products of lignin; thus, CID-CRF proved to be an effective way of identifying the mechanisms by which lignin decomposes in the gas phase.

Additionally, this dissertation includes a review of nitrene anions. Nitrene anions are another class of reactive intermediates protected by an electron that provide a means for studying the corresponding neutral molecules via electron photodetachment spectroscopy and photoelectron spectroscopy. The added electron makes it possible for protected nitrene anions to be manipulated by external electric and magnetic fields of a mass spectrometer. Nitrene anions also display their own unique reactivities as reagents, which have been investigated using ion/molecule reactions. Mass spectrometry of negative ions has thereby provided information on the electronic states, reactivities, and thermochemical properties of nitrene intermediates.

CHAPTER 1. INTRODUCTION AND GUIDE TO DISSERTATION

1.1 Lignin

1.1.1 Origin and Applications

Lignin is a large molecule found in all terrestrial plants.[1] It is a carbon-dense material interwoven throughout plants to make them rigid and woody.[2] Thus, it derives its name from lignum, the Latin word for wood.[3] Together with cellulose and hemicellulose, lignin helps make up plant secondary cell walls (Figure 1.1). It has been described as the glue that holds plants together.[2, 4] As such, it has been investigated as an industrial adhesive.[5, 6] Its hydrophobicity helps to form channels in plants for transporting water.[4] It also makes the plant secondary cell wall less permeable to pathogen invasion.[7]
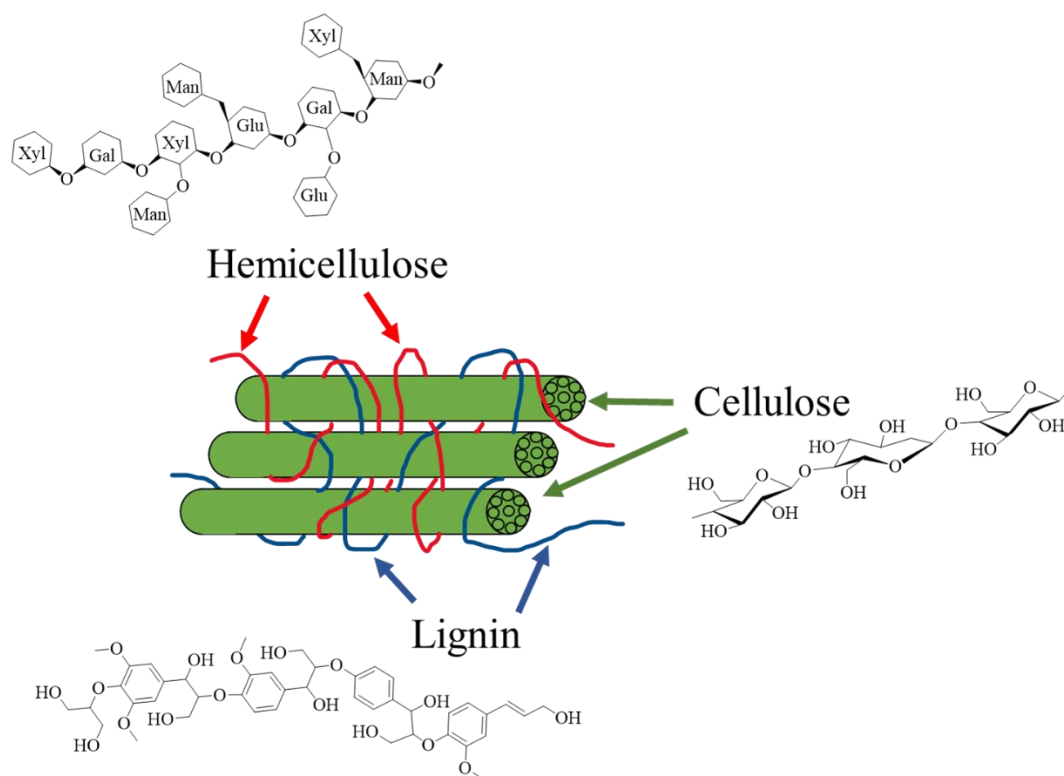
Figure 1.1 A representation of lignin, cellulose, and hemicellulose in plants

Because of its abundance, lignin has been investigated as a renewable energy source. Lignin is estimated to contain 30 percent of all non-fossil organic carbon, second only to cellulose.[2]

Not only is lignin easily available in plants, but it is also available as a byproduct of the pulping process.[8] Because plants make lignin by removing CO_2 from the atmosphere, burning lignin-based fuels is a sustainable CO_2 neutral process.[9] Lignin growth is even a carbon sink when it is transferred to soil through roots or by mixing biochar with soil.[10]

Lignin has also been explored as a feedstock for many valuable chemicals such as ethyl benzene (for organic synthesis), guaiacol (for medicinal purposes), and vanillin (for flavoring).[11] It can be upgraded into liquid transportation fuels.[12] It has even been utilized for its detergent-like properties. After sulfite pulping, the resulting lignosulfonates contain many strong polar and non-polar groups which have been used to lubricate deep oil well drills.[13] Other applications for lignin include stabilizing agent for ceramics,[14] concrete additive,[15] and sequestering metal ions in the environment.[16]

Although a highly useful material, lignin is also extremely recalcitrant, which hinders the valorization of biomass such as the production of ethanol and paper from plants.[17, 18] Some studies have found a negative correlation between lignin and plant growth.[19] Thus, transgenic species are often sought that contain a lower lignin content and increased biomass volume.[20] Multiple methods have been used for separating lignin from the rest of the fibrous material in plants including physical, chemical and biological treatments.[21-28] After treatment, the resulting heterogenous mixtures may be more compatible with liquid fuels, but substantial purification costs are often required for upgrading the mixtures into value-added chemicals.[21] Thus, the search continues to improve the process for separating lignin from plants to make biomass a viable chemical and energy source.[29, 30]

1.1.2 Molecular Structure

Unlike cellulose, which is a linear chain of repeating glucose subunits, lignin is composed of a diverse set monomers and linkages that branch out into a large molecule of kilodalton scale.[30-33] While no two lignin molecules are the same, common characteristics are shared between all kinds of lignin.[31] Examples of common chemical linkages found throughout lignin are shown in Figure 1.2. These include condensed (C-C) bonds and etheric (C-O-C) bonds. The strength of these bonds helps to protect plants from being digested by microbes and enzymes;[22, 34] however, the

difficulty of breaking these bonds is also what hinders the conversion of biomass into value-added chemicals.[35]
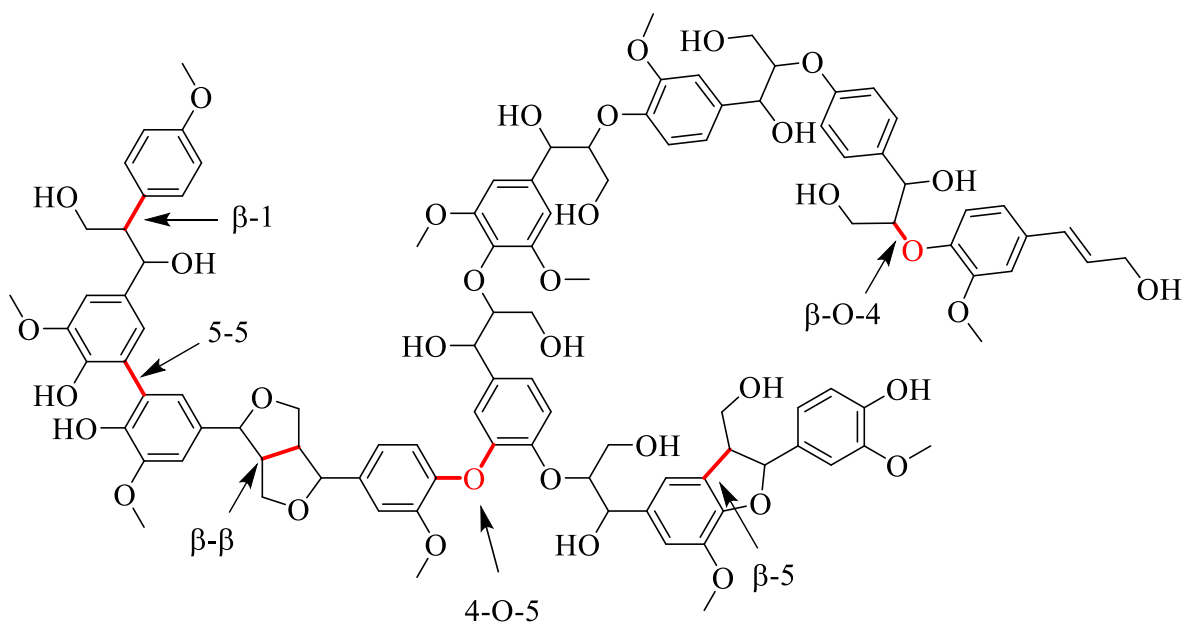
Figure 1.2 Common chemical linkages in lignin

Lignin is composed of three monolignols (H, G, and S subunits), which vary in amounts among different kinds of wood (Figure 1.3).[33] The majority of hardwood has been found to be composed of G and S subunits whereas softwood contains mostly G and a smaller amount of H.[33, 36] The ratio of H, G, and S subunits has been found to have an impact on the recalcitrance of lignin.[30] For example, transgenic switchgrass with a reduced S/G ratio had reduced recalcitrance compared to a wild type.[37] Additionally, biomass with a greater ratio of H-type lignin to G- and S-type was shown to decompose faster under certain conditions.[38] In another study, by varying the ratio of H, G, and S subunits, either through the careful selection of plant species or by genetic engineering, the phenol and ketone content in the resulting bio-oil was significantly impacted.[39]

H subunit   G subunit   S subunit

p-coumaryl alcohol   coniferyl alcohol   sinapyl alcohol
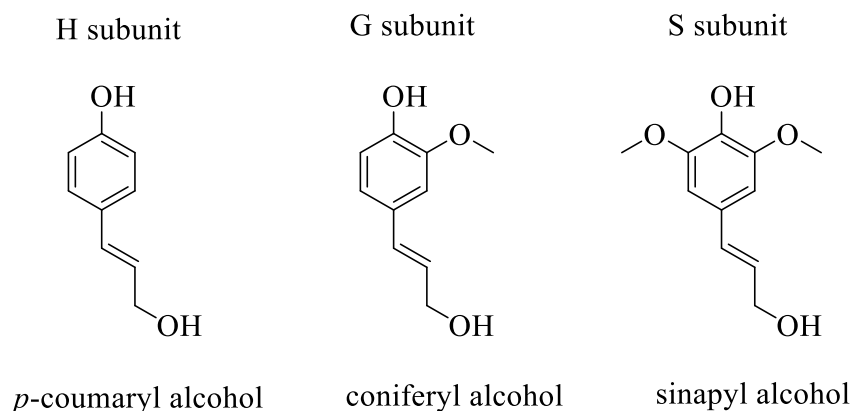
Figure 1.3 The three major monomers of lignin

Other common characteristics of lignin include certain functional groups such as hydroxy (OH), methoxy (OCH$_3$), carbonyl (CO), and carboxyl groups (COOH).[40] To study the influence of these groups on the recalcitrance of lignin, smaller model compounds are often used and subjected to the same treatment processes as native lignin.[41] The impact of these structural motifs is reflected in the rate at which the model compounds degrade and in the resulting products that form. Many studies focus on the monolignols; however, hundreds of model compounds containing the same moieties and linkages as lignin have been used to study the factors controlling how lignin breaks down under certain conditions.[30-33, 42] A few examples are shown in Figure 1.4.

phenol   guaiacol   syringol   methyl coumarate

anisole   dimethoxybenzene   catechol   vanillin   4-hydroxybenzoic acid
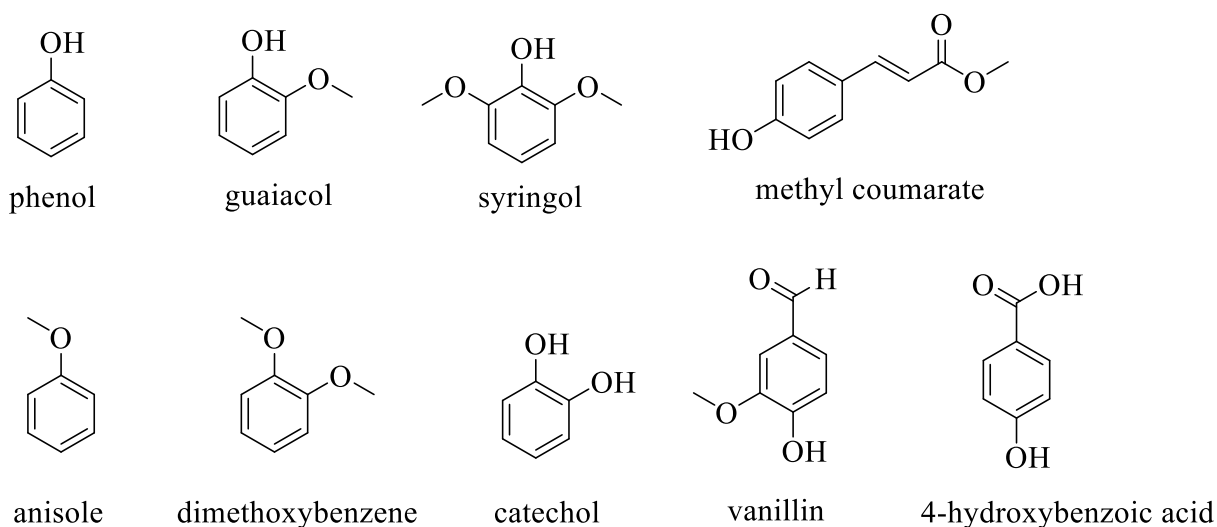
Figure 1.4 Examples of lignin model compounds

17

1.1.3 Thermal Treatments

Lignin has a higher energy content than cellulose and is similar to the energy density of coal,[19] and this energy can be released by adding heat. Additionally, the resulting smoke condensate from burning lignin can be collected, which contains many useful aromatic compounds. Thus, thermal treatments are a common approach for utilizing lignin and for investigating the effects of structural motifs on the conversion of lignin (or lignin model compounds) into valuable chemicals.[43] Three main thermal treatments of lignin exist which are pyrolysis, gasification, and combustion (Figure 1.5). Gasification uses steam and high temperatures to produce carbon monoxide, hydrogen, and carbon dioxide, also known as syngas, along with slag and ash.[44] In contrast, pyrolysis is done under high temperatures in the absence of oxygen and results in a liquid product. This liquid mixture is known as pyrolysis oil, biocrude or bio-oil.[45]
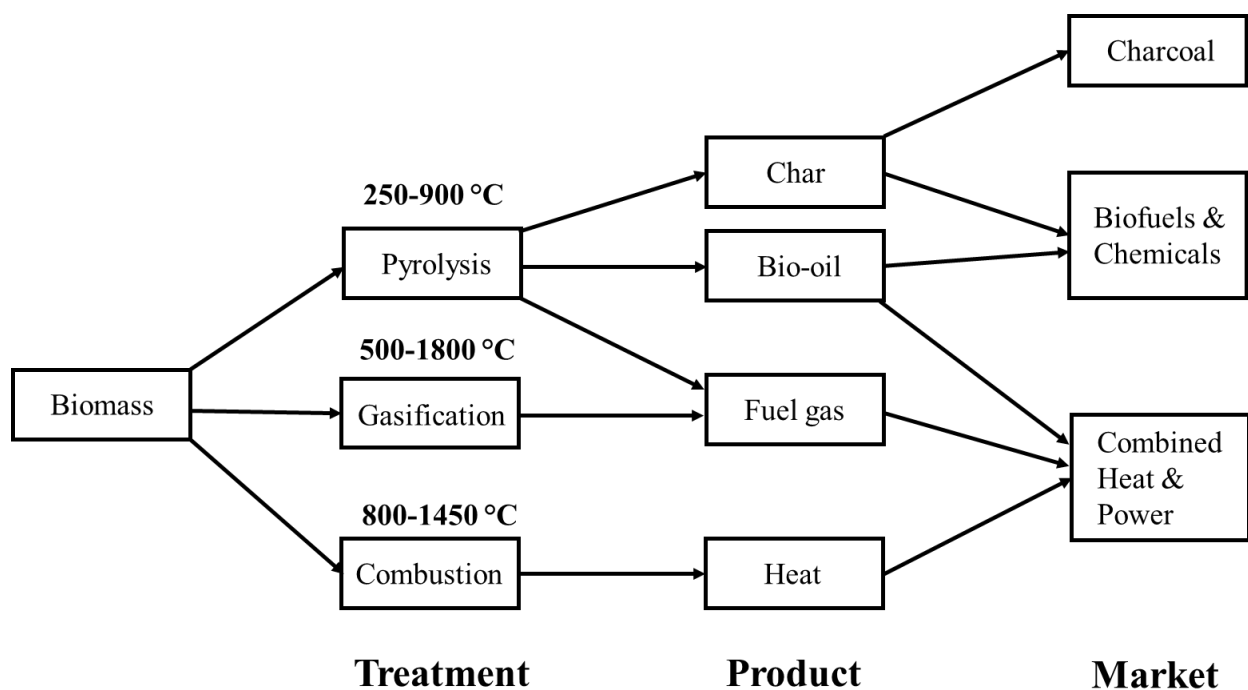
Figure 1.5 Thermal treatments of biomass[43]

In addition to the valuable chemicals produced from heating lignin, thermal treatments have another major advantage over other treatment options because the exuded gases can be used as fuel to run the overall process, which removes the need for an external energy source. However, the biggest obstacle facing the production of biofuels and chemicals from lignin is the high

downstream costs required to purify and upgrade the products. Producing a cleaner, initial bio-oil mixture would reduce the associated purification costs, which can be done by identifying the factors that control product selectivity during thermal treatments.

This work is focused on understanding the fundamental chemical reactions that occur during pyrolysis that contribute to the formation of desired products while eliminating unwanted byproducts. Two of the most important factors controlling product selectivity in pyrolysis is temperature and residence time, which affects the ratio of bio-oil to char formation.[29, 46] However, maximizing liquid yield is only the first step in obtaining a cleaner bio-oil mixture.[36, 47] A better understanding of the fundamental chemical reactions that occur during the conversion of lignin into bio-oil could is the necessary next step to obtaining a cleaner product.

A common byproduct during pyrolysis is polycyclic aromatic hydrocarbons or PAHs, which are toxic to the environment and poison catalysts used for upgrading bio-oil.[47-49] PAH growth is thought to occur via secondary reactions of radical intermediates that form during pyrolysis (Scheme 1.1). However, little is known about the mechanism of their formation because of the difficulty associated with isolating reactive intermediates. Predictions of the radical intermediates leading to PAH formation rely heavily on theoretical computations rather than experimental evidence, although advancements have been made in isolating and detecting highly transient species. A few examples of analytical techniques used for deducing the chemical reactions involved during pyrolysis will be discussed in the next section.

Scheme 1.1

Lignin   PAH

19
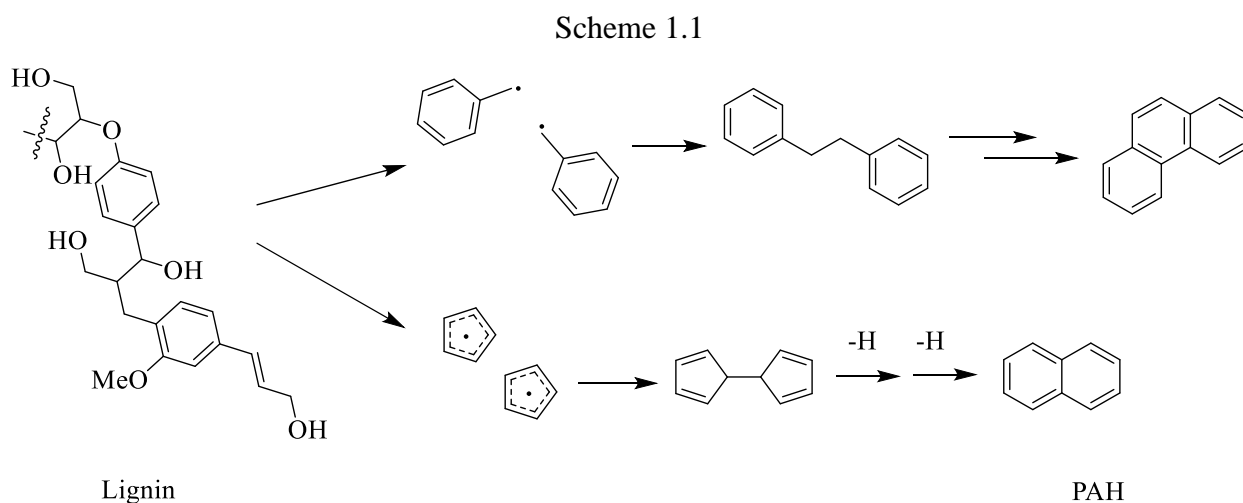
1.2 Analytical Techniques for Studying Lignin Pyrolysis

Analytical chemistry simply stated is the science of characterizing and quantifying matter. It can be used to rate the efficacy of different pyrolysis methods for converting biomass into valuable chemicals, i.e., it can tell you what raw material you started with and what molecules you ended with and thereby reveal whether a desired chemical transformation was successful. Some of the more common analytical techniques for characterizing the starting structure of lignin along with its decomposition products are nuclear magnetic resonance (NMR),[12, 33] thermogravimetry-Fourier transform infrared spectroscopy (TF-FTIR),[50, 51] and pyrolysis-gas chromatography mass spectrometry (Py-GC/MS).[45, 52] These analytical tools have helped identify several factors that can lead to a cleaner bio-oil upon pyrolysis of lignin.

1.2.1 Thermogravimetric Analysis

Thermogravimetric analysis (TGA) is a useful method that helps to identify the temperature at which certain structural features in lignin begin to decompose.[53] It does this by measuring the mass change of a sample over time as it is heated. TGA is commonly coupled with another analysis method such as Fourier-transform infrared spectroscopy (FTIR) or gas-chromatography-mass spectrometry (GC-MS) or to identify the volatile components that are lost upon heating. An example is shown in Figure 1.6. The first thermal feature shows primary pyrolysis reactions occurring around 350 °C whereas the peaks at 450 °C and 600 °C are due to secondary pyrolysis reactions.
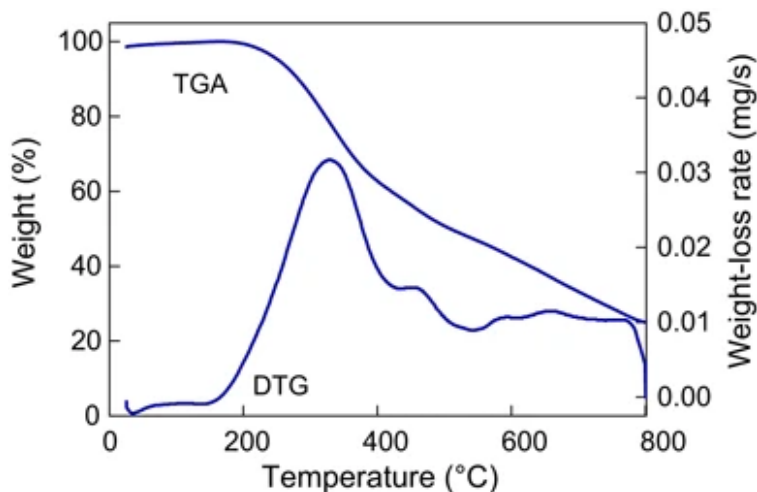
Figure 1.6 "Thermogravimetric analysis of milled wood lignin isolated from Japanese cedar (*Cryptmeria japonica*)" by Kawamoto[36, 54]/licensed under CC BY 4.0

TGA is also a convenient method for screening catalysts that can increase the bio-oil yield and product selectivity of lignin pyrolysis. When mixed with lignin, zeolites can promote deoxygenation reactions which reduces the amount of phenols in the resulting bio-oil and increases the amount of hydrocarbons that are typically found in gasoline, including benzene, toluene, and xylene.[55] In contrast, metal oxides and hydroxide catalysts can be used to increase phenol content in the resulting bio-oil.[56] In addition to screening catalysts, TGA has been used to evaluate the effects of various atmospheres on the pyrolysis of lignin.[57]

1.2.2   Gas Chromatography-Mass Spectrometry

Another analytical technique for studying the pyrolysis of lignin is gas chromatography mass spectrometry (GC-MS). Because many primary pyrolysis reactions occur in the gas phase, GC-MS is well suited for characterizing pyrolysis products. It can be coupled to a pyrolysis chamber to identify the temperature at which lignin molecules decompose like TGA-MS. The temperature at which specific volatile fragments from lignin can be detected via pyrolysis-GC-MS has been described by Kawamoto.[36] During the primary pyrolysis stage (<400 °C), compounds containing methoxy groups are abundant in the gas phase including substituted guaiacols, syringols, and side chains containing unsaturated alkyl groups (Figure 1.7). As the temperature is increased (>400 °C), methoxy groups and side chains begin to fragment resulting in a greater abundance of hydroxy-containing molecules such as phenols, cresols, and catechols.

21
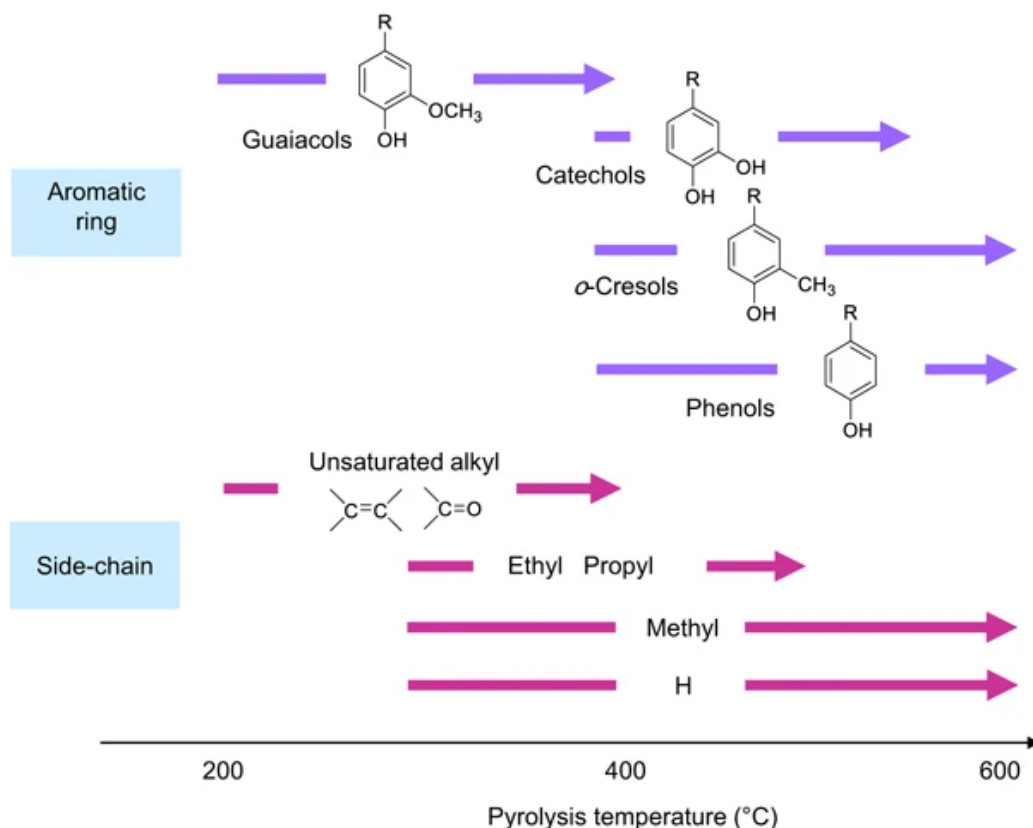
Figure 1.7 "Effect of pyrolysis temperature on aromatic substitution pattern and side-chain structure of the products from G-type lignin" by Kawamoto[36]/licensed under CC BY 4.0

While pyrolysis-GC-MS has been useful for identifying and quantifying many pyrolysis products involved in the thermal degradation of lignin, it is unable to detect primary pyrolysis intermediates that undergo secondary reactions too quickly. Rather than trap the reactive intermediates, strategies are often employed to ensure that only minimal amounts of secondary reactions occur in order to simplify studies of lignin degradation. This can be done by reducing the sample to extremely dilute concentrations so that bimolecular reactions are rare.

1.2.3 Supersonic Expansion

Although bimolecular reactions can convolute studies of lignin degradation, they also play an important role in the formation of pyrolysis products. Lignin is known to decompose quickly via both radical and concerted mechanisms involving many intermediate steps.[58-60] Thus, it is important to devise methods that can isolate reactive intermediates, including radicals, that form during cleavage of various lignin linkages and cracking of alkyl chains.[61] The intermediates

involved are often too short-lived to detect because they quickly undergo bimolecular reactions, and the steps in the thermochemical decomposition of lignin must be inferred from the end products.[62] While dilution can help prevent bimolecular reactions, it also decreases the sensitivity of primary pyrolysis products by lowering their concentrations below the lower limits of detection.

Several methods have been investigated for isolating radical intermediates. Mukarakate et al.[48] found that laser ablation with short pulses of lignin compounds led to shorter heating times and fewer secondary reactions than in a traditional thermal chamber, and the primary products could then be isolated and ionized using supersonic expansion and resonance-enhanced multiphoton ionization (REMPI). The ions were then detected using reflectron time-of-flight mass spectrometry (TOFMS). Similarly, using a flash reactor and supersonic expansion, Kidwell et al.[63] found that they could detect radical intermediates using Fourier microwave spectroscopy. While both methods were successful at isolating radical intermediates, neither could eliminate bimolecular reactions completely.

1.3   Charge-Remote Fragmentation Mass Spectrometry

To study the decomposition of lignin in the gas phase, including isolating reactive intermediates, we proposed using electrospray ionization (ESI) coupled with collision-induced dissociation mass spectrometry (CID-MS). CID-MS is a powerful technique for characterizing the structure of organic molecules and has often been applied to lignin pyrolysis products.[32, 42, 64] In addition to providing structural information on a target molecule, CID-MS can also reveal the mechanistic steps by which a molecule breaks after undergoing a collision. It was Adams and Gross[65] who first proposed that collision-induced fragmentations at a location remote from the charge site can be analogous to thermolytic cleavage of a neutral molecule. Thus, by attaching a charge-carrying group to lignin and subjecting it to CID-CRF, reactive intermediates in the thermal degradation of lignin can be isolated and analyzed. The advantage of CRF is that it reveals the fragmentation of native lignin, as opposed to the deprotonated molecule. A more detailed explanation of the steps involved in CID-CRF including the ionization process will be discussed below.

1.3.1 Electrospray Ionization

ESI is a soft ionization technique used to volatilize molecules with little to no fragmentation and is capable of getting very large molecules, including lignin, into the gas phase (Figure 1.8). It works by dissolving a sample in a volatile solvent, which is then sprayed out of a needle with a high applied voltage. The liquid, now highly charged, cannot contain such high charges and is broken up into many tiny aerosol droplets. The droplets are composed of solvent molecules as well as the dissolved sample. As the droplets travel into the orifice of the mass spectrometer, the solvent molecules are evaporated in a heated capillary, which leaves the sample molecules desolvated in the gas phase and ready for analysis (Figure 1.9).[66]
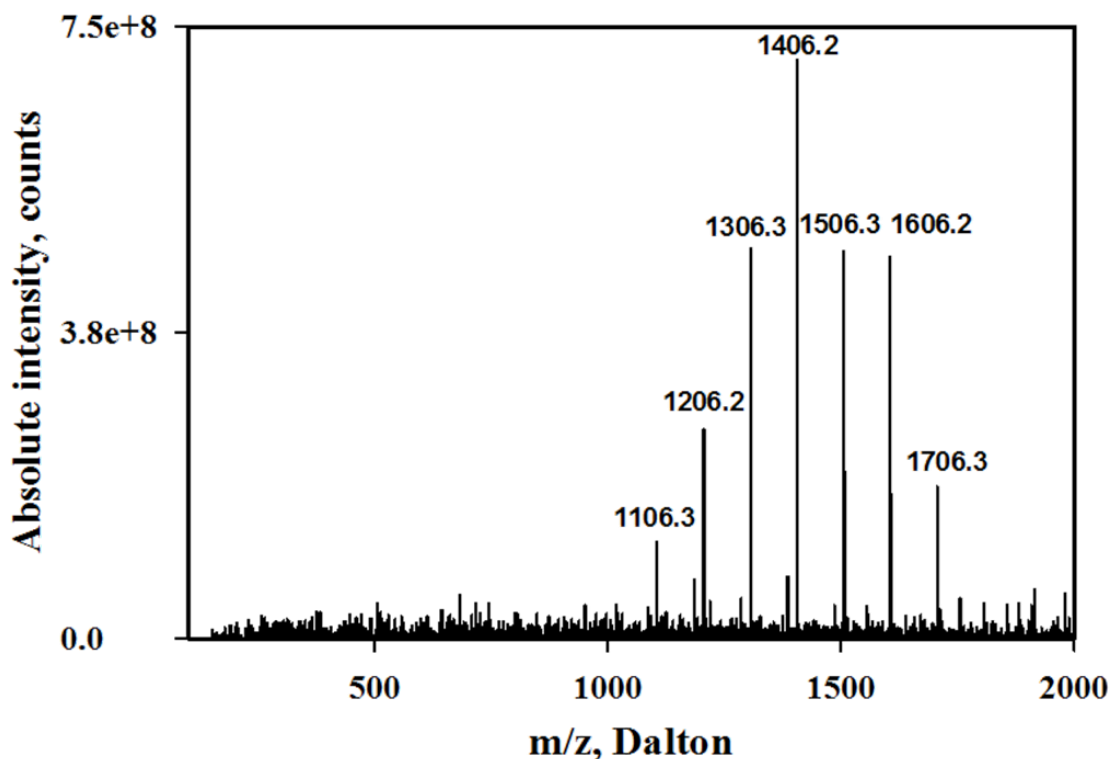
Figure 1.8 A full mass spectrum of sulfonated lignin
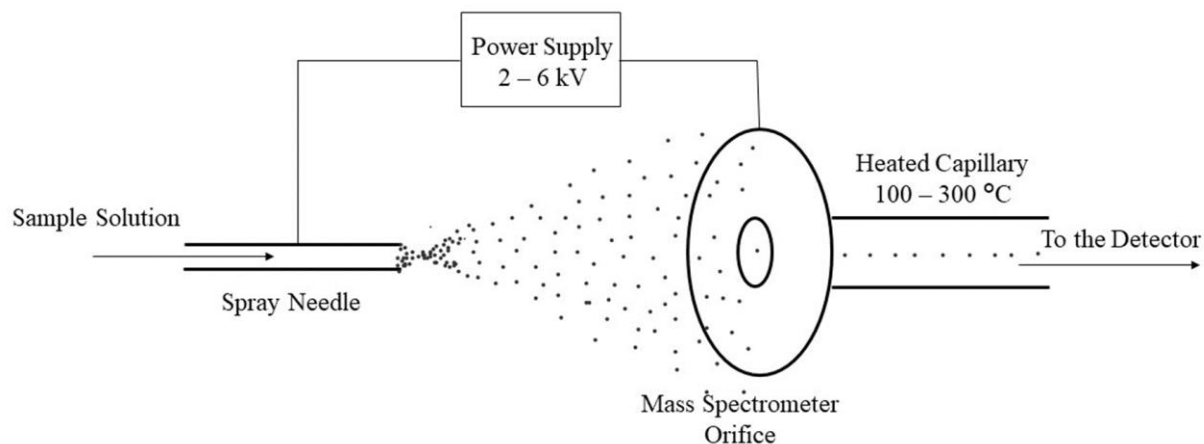
Figure 1.9 Diagram of electrospray ionization source

An advantage of ESI is that secondary reactions between molecular ions is not possible because their charges repel each other. This aids in the isolation and detection of reactive intermediates that otherwise would undergo further reactions and be too short lived to detect. As a result, the true primary pyrolysis products or unimolecular decomposition products of lignin can be isolated and characterized that have not undergone secondary reactions. Eliminating secondary reactions also simplifies the resulting spectra, which makes structural assignments easier to make. Furthermore, ESI does not require the high temperatures that are required by pyrolysis, so the fragmentations steps can more easily be controlled.

1.3.2   Collision-Induced Dissociation

After lignin has been ionized via ESI, the next step is to induce dissociation to observe how it fragments, which can be done using tandem mass spectrometry (MS/MS). One common way of carrying out MS/MS is with a triple quadrupole where mass filters and collision chambers selectively fragment ions of a specific mass-to-charge ratio (m/z) and send their product ions to a detector that counts their relative abundance (Figure 1.10).[67] Thus, in addition to the molecular weight of the starting ion, MS/MS can help yield structural information based on the product ions that form. The selection-fragmentation-detection sequence can also be repeated on the product ions to gain further information.
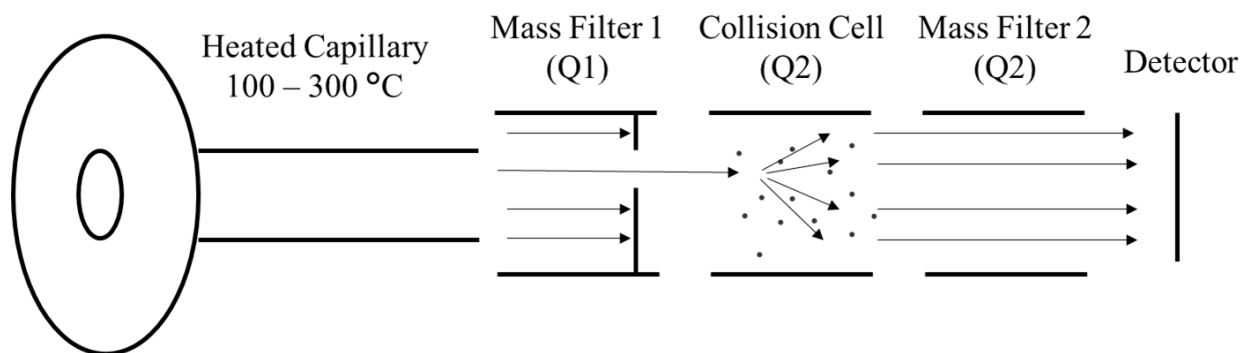
Figure 1.10 A diagram of a triple quadrupole mass filter

Similarly, MS/MS for carrying out CID can be performed using an ion trap. Ion traps differ from triple quadrupoles because the collision cell and the mass filters are combined into one, such as in a Paul trap or a Penning trap. A Paul trap uses static and oscillating electric fields to capture and hold ions whereas a Penning trap uses an electric field to confine ions axially and a magnetic field to confine particles axially. The ions are then collided with an inert gas to induce fragmentation, and the product ions are detected.

A simplified example of CID is shown in Scheme 1.2. When the target ion, M^-, is subjected to CID, it undergoes cleavage of the A-B bond. The resulting product ion, $[M - A]^-$, now has a smaller mass by an amount equal to the mass of A. Thus, it can be deduced that M^- contained a terminal A group. The process can be repeated on the product ion, $[M - A]^-$, which undergoes cleavage of the B-C bond resulting in $[M - A - B]^-$ revealing that the original ion M^- also contained a B group. Finally, repeating the process once more results in cleavage of the C-D bond forming a product with a mass equal to $[M - A - B - C]^-$, which is just the fragment D^-.

Scheme 1.2

$$A\text{-}B\text{-}C\text{-}D^- \longrightarrow A + B\text{-}C\text{-}D^- \longrightarrow B + C\text{-}D^- \longrightarrow C + D^-$$

$$M^- \qquad\qquad [M - A]^- \qquad\qquad [M - A - B]^- \qquad\qquad [M - A - B - C]^-$$
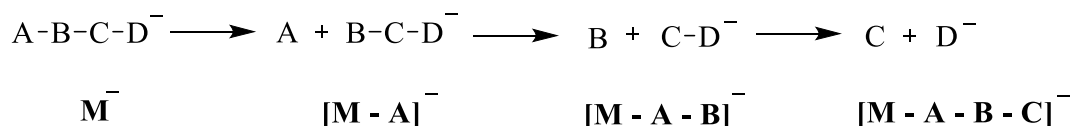
In contrast to pyrolysis, fragmentations in CID are easier to control because they are caused by collisions with an inert gas rather than by high temperatures. The kinetic energy of the collisions can be controlled by applying an electrical potential to the target ions. Low-energy CID is typically carried out with ion energies less than 1 kiloelectron volt (keV) whereas high-energy CID is in the

range of 1 keV to 20 keV. When the molecular ion collides with an inert gas, such as helium, nitrogen, or argon, fragmentation is induced. Low-energy CID results in more rearrangement reactions and charge-driven loss. As the molecular ion kinetic energy increases, the odds of direct bond cleavage and charge-remote fragmentation increases.[68]

1.3.3   Charge-Remote Fragmentation

Charge-remote fragmentation is well-known to occur during the analysis of many naturally occurring biological molecules such as lipids, steroids, and peptides. Bile salts were some of the first molecules studied using CRF. Bile salts are synthesized in the liver from cholesterol and undergo enzymatic modifications which make them acidic. Using fast atom bombardment combined with tandem mass spectrometry, Tomer and coworkers[69] observed that bile salts underwent markedly different fragmentation patterns compared to radical cations of bile salts generated by electron ionization (EI). Rather than initiating fragmentation at the carboxylate charge site as was the case with EI, CRF resulted in bonds fragmenting in the cholesterol rings far enough away from the charge site that it could be concluded that the charge site was not involved in the fragmentation (Figure 1.11).
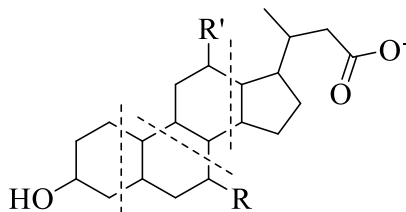
Figure 1.11 An example of a bile salt which may undergo CRF

Another example of CRF occurring is in the mass spectrometric analysis of fatty acids, which have been shown to undergo parallel losses of C_nH_{2n+2} starting from the alkyl terminus and fragmenting anywhere between C5 and C16 (Figure 1.12).[70] The distance between these carbons and the negatively-charged carboxylate group ensures that the fragmentation is not initiated by the charge site.
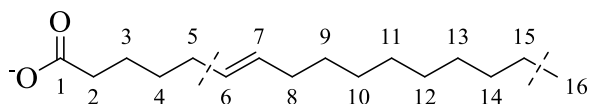
Figure 1.12 An example of a fatty acid which may undergo CRF

Peptides may also undergo CRF. In our previous work, we have shown that a sulfonate charge tag can be used to track the fragmentation of a canonical (non-zwitterionic) amino acid, **PheSO₃⁻**, and a peptide, **GlyPheSO₃⁻** in the gas phase (Figure 1.13).[71, 72] The carbon-sulfur bond is convenient for CID-CRF because it does not cleave under high energy, so the SO_3^- generally remains attached to the product ion. Thus, it should be possible to use sulfonated lignin model compounds to gain insights into the gas-phase degradation of neutral lignin. In addition to functioning as a charge tag for lignin, lignosulfonates themselves represent a valuable raw material worthy of study because they are a byproduct of the pulping process.[73]
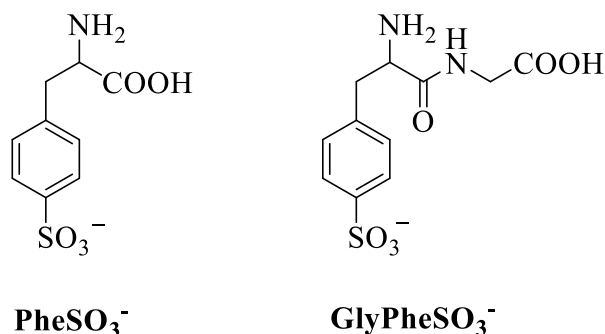
Figure 1.13 Examples of an amino acid and a peptide with a sulfonate charge tag.

1.4   Guide to Dissertation

In summary, lignin is a valuable biopolymer with wide ranging applications from renewable energy to chemical production to concrete. However, it is also extremely recalcitrant so that extraction of lignin from plants is a slow process requiring high costs. Thermal treatments are commonly employed to valorize lignin because of its high energy density. Nevertheless, the fundamental chemical reactions involved in the pyrolysis of lignin are still poorly understood. A better understanding of the reactive intermediates that form during lignin pyrolysis can shed light on the factors that control product selectivity. Several existing analytical methods such as TGA,

pyrolysis-GC-MS, and pyrolysis coupled to supersonic expansion and mass spectrometry have been utilized to characterize primary pyrolysis products.

In this work, we applied CID-CRF to study the degradation products of lignin, which can improve the sensitivity of reactive intermediates and does not require high temperatures. The only requirement is that a suitable charge tag can be found that does not interfere with the neutral fragmentation processes of lignin. Additionally, high-energy CID must be used in order induce CRF, which is then comparable to how lignin would fragment under pyrolysis conditions. The results of CID-CRF applied to various lignin model compounds will be presented herein.

Chapter 2 is a review of nitrene anions. While not directly related to lignin, Chapter 2 takes an in-depth look at how anions can be used to investigate the properties of reactive intermediates, including radical, diradical, and triradical species. Many of the primary pyrolysis products of lignin are radical intermediates, which can be generated in abundant populations as distonic radical ions via ESI/MS/MS. Similarly, nitrene anions are protected nitrene intermediates which can be used to gain information on the chemical properties of the neutral molecule, including electronic states and thermochemical data, via spectroscopy and mass spectrometry. Furthermore, the reactivities of nitrene anions are reviewed as well.

Chapter 3 contains the results of CID-CRF applied to several methoxy-substituted lignin model compounds: namely, anisole, guaiacol, *ortho*-dimethoxybenzene, and *meta*-dimethoxybenzene. The results are compared to pyrolysis studies. Additionally, evidence was found for the formation of radical intermediates that had not been reported previously. Supporting calculations were carried out to determine the energy effects of the charge tag on the ground states and transition states of intermediates involved in the decomposition of the model compounds.

Chapter 4 contains the results of CID-CRF applied to phenethyl phenyl ethers (PPE). PPE is a model compound of the β-O-4 linkage, which is the most abundant linkage in lignin. Analysis of the product ions was used to elucidate whether initial fragmentation proceeded via homolytic cleavage or a concerted elimination reaction. Calculations were carried out to gain insights into the transition state complex leading to the observed products. The unimolecular decomposition products of 1-methoxy-PPE and 1,2-dimethoxy-PPE are also reported.

Chapter 5 presents computational data on the effects of varying charge and location of the charge site on the potential energy surfaces of the model compounds. Based on the results,

suggestions are made for improving the charge tag. In addition, future directions for the project are discussed including identifying the thermolysis of other organic small molecules.

1.5   References

1. Lu, F.; Ralph, J., Chapter 6 - Lignin. In *Cereal Straw as a Resource for Sustainable Biomaterials and Biofuels*, Sun, R.-C., Ed. Elsevier: Amsterdam, 2010; pp 169-207.

2. Boerjan, W.; Ralph, J.; Baucher, M., Lignin Biosynthesis. *Annual Review of Plant Biology* **2003,** *54* (1), 519-546.

3. SjÖStrÖM, E., Chapter 4 - LIGNIN. In *Wood Chemistry (Second Edition)*, SjÖStrÖM, E., Ed. Academic Press: San Diego, 1993; pp 71-89.

4. Shrotri, A.; Kobayashi, H.; Fukuoka, A., Chapter Two - Catalytic Conversion of Structural Carbohydrates and Lignin to Chemicals. In *Advances in Catalysis*, Song, C., Ed. Academic Press: 2017; Vol. 60, pp 59-123.

5. Mankar, S.; Chaudhari, A.; Soni, I., Lignin in phenol-formaldehyde adhesives. *International Journal of Knowledge Engineering* **2012,** *3*, 116-118.

6. Kalami, S.; Arefmanesh, M.; Master, E.; Nejad, M., Replacing 100% of phenol in phenolic adhesive formulations with lignin. *Journal of Applied Polymer Science* **2017,** *134* (30), 45124.

7. Nair, A.; Ithnin, N. B.; Sim, H. L.; Appleton, D. R., Energy Crops. In *Encyclopedia of Applied Plant Sciences (Second Edition)*, Thomas, B.; Murray, B. G.; Murphy, D. J., Eds. Academic Press: Oxford, 2017; pp 164-176.

8. Refaat, A. A., 5.13 - Biofuels from Waste Materials. In *Comprehensive Renewable Energy*, Sayigh, A., Ed. Elsevier: Oxford, 2012; pp 217-261.

9. Bergs, M.; Völkering, G.; Kraska, T.; Pude, R.; Tung, X. D.; Kusch, P.; Monakhova, Y.; Konow, C.; Schulze, M., Miscanthus x giganteus Stem Versus Leaf-Derived Lignins Differing in Monolignol Ratio and Linkage. *International Journal of Molecular Sciences* **2019,** *20* (5).

10. Jansson, C.; Wullschleger, S. D.; Kalluri, U. C.; Tuskan, G. A., Phytosequestration: Carbon Biosequestration by Plants and the Prospects of Genetic Engineering. *BioScience* **2010,** *60* (9), 685-696.

11. Cao, L.; Yu, I. K. M.; Liu, Y.; Ruan, X.; Tsang, D. C. W.; Hunt, A. J.; Ok, Y. S.; Song, H.; Zhang, S., Lignin valorization for the production of renewable chemicals: State-of-the-art review and future prospects. *Bioresource Technology* **2018,** *269*, 465-475.

12. Chu, S.; Subrahmanyam, A. V.; Huber, G. W., The pyrolysis chemistry of a β-O-4 type oligomeric lignin model compound. *Green Chemistry* **2013,** *15* (1), 125-136.

13. Browning, W. C., Lignosulfonate Stabilized Emulsions in Oil Well Drilling Fluids. *Journal of Petroleum Technology* **1955,** *7* (06), 9-15.

14. Cerrutti, B. M.; de Souza, C. S.; Castellan, A.; Ruggiero, R.; Frollini, E., Carboxymethyl lignin as stabilizing agent in aqueous ceramic suspensions. *Industrial Crops and Products* **2012,** *36* (1), 108-115.

15. Jankowska, D.; Heck, T.; Schubert, M.; Yerlikaya, A.; Weymuth, C.; Rentsch, D.; Schober, I.; Richter, M., Enzymatic Synthesis of Lignin-Based Concrete Dispersing Agents. *ChemBioChem* **2018,** *19* (13), 1365-1369.

16. Guo, X.; Zhang, S.; Shan, X.-q., Adsorption of metal ions on lignin. *Journal of Hazardous Materials* **2008,** *151* (1), 134-142.

17. Fernández-Rodríguez, J.; Erdocia, X.; Hernández-Ramos, F.; Alriols, M. G.; Labidi, J., Chapter 7 - Lignin Separation and Fractionation by Ultrafiltration. In *Separation of Functional Molecules in Food by Membrane Technology*, Galanakis, C. M., Ed. Academic Press: 2019; pp 229-265.

18. Doherty, W. O. S.; Mousavioun, P.; Fellows, C. M., Value-adding to cellulosic ethanol: Lignin polymers. *Industrial Crops and Products* **2011,** *33* (2), 259-276.

19. Novaes, E.; Kirst, M.; Chiang, V.; Winter-Sederoff, H.; Sederoff, R., Lignin and Biomass: A Negative Correlation for Wood Formation and Lignin Content in Trees. *Plant Physiology* **2010,** *154* (2), 555.

20. Bonawitz, N. D.; Kim, J. I.; Tobimatsu, Y.; Ciesielski, P. N.; Anderson, N. A.; Ximenes, E.; Maeda, J.; Ralph, J.; Donohoe, B. S.; Ladisch, M.; Chapple, C., Disruption of Mediator rescues the stunted growth of a lignin-deficient Arabidopsis mutant. *Nature* **2014,** *509* (7500), 376-380.

21. Beckham, G. T.; Johnson, C. W.; Karp, E. M.; Salvachúa, D.; Vardon, D. R., Opportunities and challenges in biological lignin valorization. *Current Opinion in Biotechnology* **2016,** *42*, 40-53.

22. Shin, S. K.; Ko, Y. J.; Hyeon, J. E.; Han, S. O., Studies of advanced lignin valorization based on various types of lignolytic enzymes and microbes. *Bioresource Technology* **2019,** *289*, 121728.

23. Dai, J.; Patti, A. F.; Saito, K., Recent developments in chemical degradation of lignin: catalytic oxidation and ionic liquids. *Tetrahedron Letters* **2016,** *57* (45), 4945-4951.

24. Costa, S.; Rugiero, I.; Larenas Uria, C.; Pedrini, P.; Tamburini, E., Lignin Degradation Efficiency of Chemical Pre-Treatments on Banana Rachis Destined to Bioethanol Production. *Biomolecules* **2018,** *8* (4), 141.

25. Merklein, K.; Fong, S. S.; Deng, Y., Chapter 11 - Biomass Utilization. In *Biotechnology for Biofuel Production and Optimization*, Eckert, C. A.; Trinh, C. T., Eds. Elsevier: Amsterdam, 2016; pp 291-324.

26. Sagues, W. J.; Bao, H.; Nemenyi, J. L.; Tong, Z., Lignin-First Approach to Biorefining: Utilizing Fenton's Reagent and Supercritical Ethanol for the Production of Phenolics and Sugars. *ACS Sustainable Chemistry & Engineering* **2018,** *6* (4), 4958-4965.

27. Rinaldi, R.; Jastrzebski, R.; Clough, M. T.; Ralph, J.; Kennema, M.; Bruijnincx, P. C. A.; Weckhuysen, B. M., Paving the Way for Lignin Valorisation: Recent Advances in Bioengineering, Biorefining and Catalysis. *Angewandte Chemie International Edition* **2016,** *55* (29), 8164-8215.

28. Zakzeski, J.; Bruijnincx, P. C. A.; Jongerius, A. L.; Weckhuysen, B. M., The Catalytic Valorization of Lignin for the Production of Renewable Chemicals. *Chemical Reviews* **2010,** *110* (6), 3552-3599.

29. Britt, P. F.; Buchanan, A. C., III; Martineau, D. R., Flash Vacuum Pyrolysis of Lignin Model Compounds: Reaction Pathways of Aromatic Methoxy Groups. Oak Ridge National Lab., TN (US): United States, 1999.

30. Parthasarathi, R.; Romero, R. A.; Redondo, A.; Gnanakaran, S., Theoretical Study of the Remarkably Diverse Linkages in Lignin. *The Journal of Physical Chemistry Letters* **2011,** *2* (20), 2660-2666.

31. Tolbert, A.; Akinosho, H.; Khunsupat, R.; Naskar, A. K.; Ragauskas, A. J., Characterization and analysis of the molecular weight of lignin for biorefining studies. *Biofuels, Bioproducts and Biorefining* **2014,** *8* (6), 836-856.

32. Huaming Sheng, W. T., Jinshan Gao, James S. Riedeman, Guannan Li,; Tiffany M. Jarrell, M. R. H., Linan Yang, Priya Murria, Xin Ma,; John J. Nash, a. H. I. K., (−)ESI/CAD MSn Procedure for Sequencing Lignin Oligomers Based on a Study of Synthetic Model Compounds with β-O-4 and 5-5 Linkages. *Analytical Chemistry 89* (24), 13089–13096.

33. Vanholme, R., Demedts, B., Morreel, K., Ralph, J., & Boerjan, W., Lignin biosynthesis and Structure. *Plant Physiology* **2010,** *155* (3), 895-905.

34. Horwath, W., Chapter 12 - Carbon Cycling: The Dynamics and Formation of Organic Matter. In *Soil Microbiology, Ecology and Biochemistry (Fourth Edition)*, Paul, E. A., Ed. Academic Press: Boston, 2015; pp 339-382.

35. Scott, J. L.; Buchard, A., 17 - Polymers from plants: Biomass fixed carbon dioxide as a resource. In *Managing Global Warming*, Letcher, T. M., Ed. Academic Press: 2019; pp 503-525.

36. Kawamoto, H., Lignin pyrolysis reactions. *Journal of Wood Science* **2017,** *63* (2), 117-132.

37. Fu, C.; Mielenz, J. R.; Xiao, X.; Ge, Y.; Hamilton, C. Y.; Rodriguez, M.; Chen, F.; Foston, M.; Ragauskas, A.; Bouton, J.; Dixon, R. A.; Wang, Z.-Y., Genetic manipulation of lignin reduces recalcitrance and improves ethanol production from switchgrass. *Proceedings of the National Academy of Sciences* **2011,** *108* (9), 3803.

38. Li, M.; Pu, Y.; Ragauskas, A. J., Current Understanding of the Correlation of Lignin Structure with Biomass Recalcitrance. *Frontiers in chemistry* **2016,** *4*, 45-45.

39. Torri, I. D. V.; Paasikallio, V.; Faccini, C. S.; Huff, R.; Caramão, E. B.; Sacon, V.; Oasmaa, A.; Zini, C. A., Bio-oil production of softwood and hardwood forest industry residues through fast and intermediate pyrolysis and its chromatographic characterization. *Bioresource Technology* **2016,** *200*, 680-690.

40. El Mansouri, N.-E.; Salvadó, J., Analytical methods for determining functional groups in various technical lignins. *Industrial Crops and Products* **2007,** *26* (2), 116-124.

41. Patil, N. D.; Tanguy, N. R.; Yan, N., 3 - Lignin Interunit Linkages and Model Compounds. In *Lignin in Polymer Composites*, Faruk, O.; Sain, M., Eds. William Andrew Publishing: 2016; pp 27-47.

42. Marcum, C. L.; Jarrell, T. M.; Zhu, H.; Owen, B. C.; Haupert, L. J.; Easton, M.; Hosseinaei, O.; Bozell, J.; Nash, J. J.; Kenttämaa, H. I., A Fundamental Tandem Mass Spectrometry Study of the Collision-Activated Dissociation of Small Deprotonated Molecules Related to Lignin. *ChemSusChem* **2016,** *9* (24), 3513-3526.

43. Bridgwater, A. V., Review of fast pyrolysis of biomass and product upgrading. *Biomass and Bioenergy* **2012,** *38*, 68-94.

44. Helsen, L.; Bosmans, A., Waste-to-Energy through thermochemical processes: matching waste with process. *Invited Presentation* **2010**, 133-180.

45. Bahng, M.-K.; Mukarakate, C.; Robichaud, D. J.; Nimlos, M. R., Current technologies for analysis of biomass thermochemical processing: A review. *Analytica Chimica Acta* **2009,** *651* (2), 117-138.

46. Britt, P. F.; Buchanan, A. C.; Cooney, M. J.; Martineau, D. R., Flash Vacuum Pyrolysis of Methoxy-Substituted Lignin Model Compounds. *The Journal of Organic Chemistry* **2000,** *65* (5), 1376-1389.

47. Xu, L.; Zhang, Y.; Fu, Y., Advances in Upgrading Lignin Pyrolysis Vapors by Ex Situ Catalytic Fast Pyrolysis. *Energy Technology* **2017,** *5* (1), 30-51.

48. Mukarakate, C.; Scheer, A. M.; Robichaud, D. J.; Jarvis, M. W.; David, D. E.; Ellison, G. B.; Nimlos, M. R.; Davis, M. F., Laser ablation with resonance-enhanced multiphoton ionization time-of-flight mass spectrometry for determining aromatic lignin volatilization products from biomass. *Review of Scientific Instruments* **2011,** *82* (3), 033104.

49. Cheng, H.; Wu, S.; Huang, J.; Zhang, X., Direct evidence from in situ FTIR spectroscopy that o-quinonemethide is a key intermediate during the pyrolysis of guaiacol. *Analytical and Bioanalytical Chemistry* **2017,** *409* (10), 2531-2537.

50. Yang, H.; Yan, R.; Chin, T.; Liang, D. T.; Chen, H.; Zheng, C., Thermogravimetric Analysis−Fourier Transform Infrared Analysis of Palm Oil Waste Pyrolysis. *Energy & Fuels* **2004,** *18* (6), 1814-1821.

51. Li, B.; Lv, W.; Zhang, Q.; Wang, T.; Ma, L., Pyrolysis and catalytic pyrolysis of industrial lignins by TG-FTIR: Kinetics and products. *Journal of Analytical and Applied Pyrolysis* **2014,** *108*, 295-300.

52. Chang, G.; Huang, Y.; Xie, J.; Yang, H.; Liu, H.; Yin, X.; Wu, C., The lignin pyrolysis composition and pyrolysis products of palm kernel shell, wheat straw, and pine sawdust. *Energy Conversion and Management* **2016,** *124*, 587-597.

53. Sebio-Puñal, T.; Naya, S.; López-Beceiro, J.; Tarrío-Saavedra, J.; Artiaga, R., Thermogravimetric analysis of wood, holocellulose, and lignin from five wood species. *Journal of Thermal Analysis and Calorimetry* **2012,** *109* (3), 1163-1167.

54. Asmadi, M.; Kawamoto, H.; Saka, S., Gas- and solid/liquid-phase reactions during pyrolysis of softwood and hardwood lignins. *Journal of Analytical and Applied Pyrolysis* **2011,** *92* (2), 417-425.

55. Liao, W.; Wang, X.; Li, L.; Fan, D.; Wang, Z.; Chen, Y.; Li, Y.; Xie, X. a., Catalytic Alcoholysis of Lignin with HY and ZSM-5 Zeolite Catalysts. *Energy & Fuels* **2020,** *34* (1), 599-606.

56. Naron, D. R.; Collard, F. X.; Tyhoda, L.; Görgens, J. F., Production of phenols from pyrolysis of sugarcane bagasse lignin: Catalyst screening using thermogravimetric analysis – Thermal desorption – Gas chromatography – Mass spectroscopy. *Journal of Analytical and Applied Pyrolysis* **2019,** *138*, 120-131.

57. Shen, D.; Hu, J.; Xiao, R.; Zhang, H.; Li, S.; Gu, S., Online evolved gas analysis by Thermogravimetric-Mass Spectroscopy for thermal decomposition of biomass and its components under different atmospheres: Part I. Lignin. *Bioresource Technology* **2013,** *130*, 449-456.

58. Klein, M. T.; Virk, P. S., Model pathways in lignin thermolysis. 1. Phenethyl phenyl ether. *Industrial & Engineering Chemistry Fundamentals* **1983,** *22* (1), 35-45.

59. Beste, A.; Buchanan, A. C., Kinetic simulation of the thermal degradation of phenethyl phenyl ether, a model compound for the β-O-4 linkage in lignin. *Chemical Physics Letters* **2012,** *550*, 19-24.

60. Elder, T.; Beste, A., Density Functional Theory Study of the Concerted Pyrolysis Mechanism for Lignin Models. *Energy & Fuels* **2014,** *28* (8), 5229-5235.

61. Mante, O. D.; Rodriguez, J. A.; Babu, S. P., Selective defunctionalization by TiO2 of monomeric phenolics from lignin pyrolysis into simple phenols. *Bioresource Technology* **2013,** *148*, 508-516.

62. Nguyen, T. T. P.; Mai, T. V. T.; Huynh, L. K., Detailed kinetic modeling of thermal decomposition of guaiacol – A model compound for biomass lignin. *Biomass and Bioenergy* **2018,** *112*, 45-60.

63. Kidwell, N. M.; Vaquero-Vara, V.; Ormond, T. K.; Buckingham, G. T.; Zhang, D.; Mehta-Hurt, D. N.; McCaslin, L.; Nimlos, M. R.; Daily, J. W.; Dian, B. C.; Stanton, J. F.; Ellison, G. B.; Zwier, a. T. S., Chirped-Pulse Fourier Transform Microwave Spectroscopy Coupled with a Flash Pyrolysis Microreactor: Structural Determination of the Reactive Intermediate Cyclopentadienone. *The Journal of Physical Chemistry Letters* **2014,** *5* (13), 2201-2207.

64. Jarrell, T. M.; Marcum, C. L.; Sheng, H.; Owen, B. C.; O'Lenick, C. J.; Maraun, H.; Bozell, J. J.; Kenttämaa, H. I., Characterization of organosolv switchgrass lignin by using high performance liquid chromatography/high resolution tandem mass spectrometry using hydroxide-doped negative-ion mode electrospray ionization. *Green Chemistry* **2014,** *16* (5), 2713-2727.

65. Adams, J.; Gross, M. L., Charge-remote fragmentations of closed-shell ions. A thermolytic analogy. *Journal of the American Chemical Society* **1989,** *111* (2), 435-440.

66. Banerjee, S.; Mazumdar, S., Electrospray Ionization Mass Spectrometry: A Technique to Access the Information beyond the Molecular Weight of the Analyte. *International Journal of Analytical Chemistry* **2012,** *2012*, 282574.

67. Grebe, S. K.; Singh, R. J., LC-MS/MS in the Clinical Laboratory - Where to From Here? *The Clinical biochemist. Reviews* **2011,** *32* (1), 5-31.

68. Yan, Y.; Ubukata, M.; Cody, R. B.; Holy, T. E.; Gross, M. L., High-Energy Collision-Induced Dissociation by MALDI TOF/TOF Causes Charge-Remote Fragmentation of Steroid Sulfates. *Journal of The American Society for Mass Spectrometry* **2014,** *25* (8), 1404-1411.

69. Tomer, K. B.; Jensen, N. J.; Gross, M. L.; Whitney, J., Fast atom bombardment combined with tandem mass spectrometry for determination of bile salts and their conjugates. *Biomedical & Environmental Mass Spectrometry* **1986,** *13* (6), 265-272.

70. Jensen, N. J.; Tomer, K. B.; Gross, M. L., Gas-phase ion decomposition occurring remote to a charge site. *Journal of the American Chemical Society* **1985,** *107* (7), 1863-1868.

71. Koirala, D.; Kodithuwakkuge, S. R.; Wenthold, P. G., Mass spectrometric study of the decomposition pathways of canonical amino acids and α-lactones in the gas phase. *Journal of Physical Organic Chemistry* **2015,** *28* (10), 635-644.

72. Koirala, D.; Mistry, S.; Wenthold, P. G., Participation of C-H Protons in the Dissociation of a Proton Deficient Dipeptide. *Journal of The American Society for Mass Spectrometry* **2017,** *28* (7), 1313-1323.

73. Brudin, S.; Schoenmakers, P., Analytical methodology for sulfonated lignins. *Journal of Separation Science* **2010,** *33* (3), 439-452.

CHAPTER 2.   MASS SPECTROMETRY STUDIES OF NITRENE ANIONS

A version of this chapter is pending publication with Mass Spectrometry Reviews by Wiley. Harshal Jawale and Paul Wenthold are contributing authors.

2.1   Introduction

2.1.1   Nitrenes

Nitrenes are a fascinating class of reactive intermediates that contain a neutral hypovalent nitrogen atom (R-N) and are isoelectronic with carbenes. Because of their unique chemical reactivity, nitrenes have been utilized in applications such as organic synthesis,[1-3] photoaffinity labeling,[4, 5] and cross-linking experiments.[6] They have also been observed in the interstellar medium.[7] Nitrenes are commonly formed by thermolysis or photolysis of azides which undergo expulsion of N_2, analogous to how carbenes are formed from diazo compounds. Despite their similarities, nitrenes and carbenes have very different reactivity. For example, carbenes easily react with C-H bonds to form adducts[8-11] whereas nitrenes tend to undergo intramolecular rearrangements to form polymeric tar.[12, 13]

In the early 1980s, spectroscopic work resulted in conflicting information about the chemical properties and spin states of nitrenes due to the extreme difficulty of isolating them as intermediates. Photolysis of nitrene precursors generates nitrenes in an excited state,[14] and the excess energy causes nitrenes to quickly isomerize into multiple intermediates that all absorb in a similar range. For example, the photolysis of phenylazide (PhN$_3$) produces phenylnitrene (PhN), ketenimine, and cyanocyclopentadienyl radical that all absorb between 300 and 400 nm, which complicated the isolation and characterization of PhN.[13, 15-18] Similarly, it was assumed that alkylnitrenes could not be detected because of a barrierless 1,2-shift of hydrogen or alkyl groups.[19]

With improvements in trapping experiments and other methods such as flash photolysis, spectroscopic assignments of many nitrenes have now been well established. Many observations of nitrenes or their primary photolysis products have been made in low-temperature matrices.[20-24] These experiments were often carried out using nanosecond laser flash photolysis or nanosecond time-resolved infrared.[14, 25] However, the lifetime of some reactive intermediates such as ^{1}PhN is

about 1 ns in organic solvents at room temperature.[14] Other singlet nitrenes, such as *o*-biphenylnitrene (*o*-BpN) and 1-napthylnitrene (1-NpN) have even shorter lifetimes (16 and 12 ps, respectively);[26, 27] thus, ultra-fast absorption spectroscopy is often required for their detection.

2.1.2 Nitrene anions

An alternate approach to isolating reactive intermediates is to introduce a negative charge and manipulate the resulting anions using mass spectrometry. Anions have the advantage of being easier to generate and detect in the gas phase than their neutral counterparts. They are also less prone to undergo rearrangement reactions and fragmentations, so an added electron can thereby function as a protecting group.[28-30] This negative ion approach can be used to produce high yields of biradical negative ions, or distonic radical anions, regioselectively.[31] These protected intermediates can then be used in mass spectrometric studies to investigate free-radical chemistry, the acid-base properties of radicals, and in electron photodetachment spectroscopy (EPD) and negative ion photoelectron spectroscopy (PES) to probe the singlet-triplet energy gaps of the corresponding neutral biradicals and to measure their electron affinities.[32, 33]

Pioneering work in this area by Squires, Wenthold, and coworkers produced a series of radical anions, diradical anions, and even triradical anions such as benzynes, *m*-xylylene, trimethlyenemethane (TMM), and tetramethyleneethane (TME) in a flowing afterglow.[31, 32, 34, 35] Mass spectrometry of negative anions has also been used to study a number of other transient species such as cubyl radical, phenyl radical, and vinyl radical.[36-39] Nitrenes are likewise diradical intermediates with short lifetimes due in part to having an empty p orbital on the nitrogen that enables intramolecular rearrangements (Figure 2.1). In contrast, nitrene anions have an extra valence electron leaving no vacant orbitals, which effectively slows down rearrangement reactions and increases their lifetimes.[40] Nitrene anions are thus more stable than neutral nitrenes and can be used to determine a wide range of thermochemical data.[30, 41]
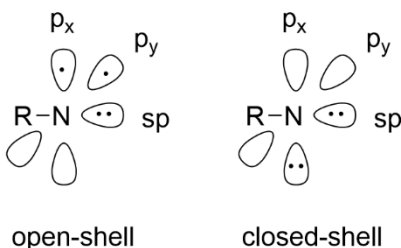
Figure 2.1 Two possible ways that the non-bonding electrons in nitrenes can be distributed. One is an open-shell structure, and the other is a closed-shell structure.

In addition to providing valuable insights into the nature of neutral nitrenes, nitrene anions have their own unique properties as reactants, which can also be investigated using mass spectrometry. Anionic substituents have been shown to be capable of tuning the reactivity of nitrenes, and their products have been explored using ion/molecule reactions.[40, 42-49] In this work, we review advancements in the field of nitrene anion chemistry, from their formal synthesis and reactivity to their characterization via spectroscopy and mass spectrometry, and characterization of the thermochemical properties of nitrenes.

2.2   Electronic Structure of Nitrenes

Because any work on nitrene anions is intrinsically linked to nitrenes, it is useful to begin with a discussion on the underlying electronic structure of nitrenes. In any case, the electronic configuration of nitrenes and nitrene anions are closely related because they differ by only one electron. Nitrenes are nominally sp hybridized with a bonding sp orbital, a non-bonding sp orbital, and two (non-hybridized) p orbitals. A lone pair of electrons fills the non-bonding sp orbital, and two more electrons are distributed between the p_x and p_y orbitals. Most nitrenes have a triplet ground state with singlet excited states that can have electronic configurations p_x^2, p_y^2, or p_xp_y. The lowest-energy excited state for nitrenes is usually an open-shell singlet, in contrast to what occurs in isoelectronic carbenes, where the lowest-energy excited state generally a closed-shell singlet.[13, 50] This can be explained by looking at the molecular orbital diagrams for carbenes and nitrenes. Because carbenes are sp^2 hybridized, the closed-shell singlet is made by pairing two non-bonding electrons in a lower-energy non-bonding sp^2 orbital whereas electron repulsion in nitrenes raises the energy of the closed-shell state relative to the open-shell state (Figure 2.2).

39
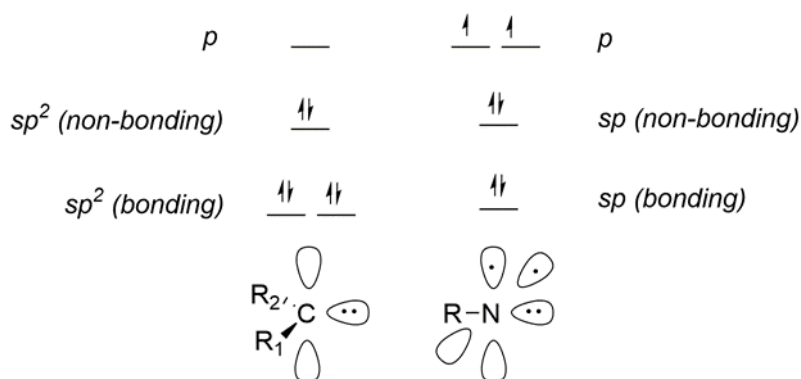
Figure 2.2 Molecular orbital diagrams for carbenes (left) and nitrenes (right)

The difference in the electronic structure of carbenes and nitrenes leads to a large difference in reactivity. Because of excess thermal energy that is retained upon formation, both carbenes and nitrenes are initially formed in an excited state. However, carbenes can quickly undergo intersystem crossing (ISC) from the closed-shell singlet to the ground state triplet, which can then undergo bimolecular chemistry.[13, 50, 51] This is because the change in angular momentum from flipping the spin of an electron is accommodated by a change in orbitals ($\sigma \rightarrow \sigma\pi$) to allow for efficient spin-orbit coupling (SOC). In contrast, ISC for nitrenes is much slower because momentum is not as easily conserved going from an open-shell singlet to a triplet state without a change in orbitals ($\sigma\pi \rightarrow \sigma\pi$), resulting in slow SOC.[52, 53] As a result, nitrenes are stuck in the open-shell singlet excited state, which undergoes intramolecular rearrangements faster than ISC. An example of this is seen in the photolysis of PhN_3 where the primary photolysis product ^1PhN isomerizes and multiple intermediates form (Figure 2.3). In addition to isomerizing, ^1PhN can also abstract a proton to form nitrenium ion.[14, 54]
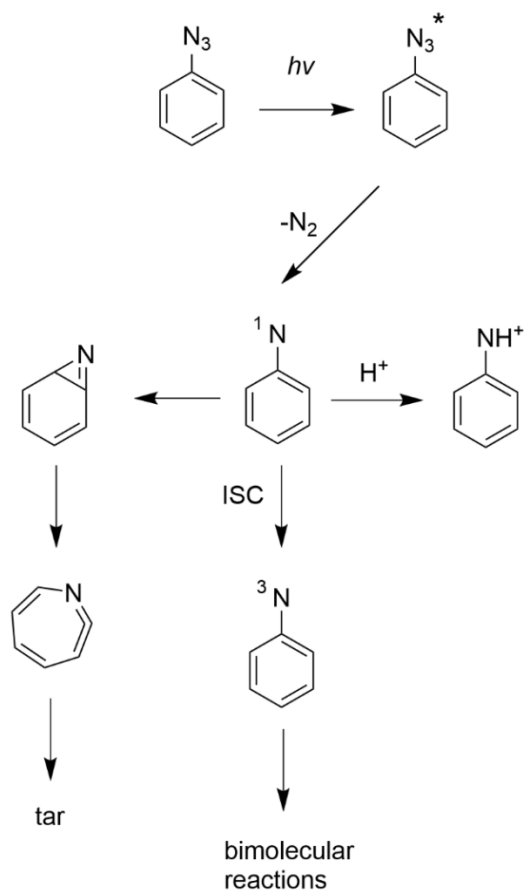
Figure 2.3 Key intermediates in the photolysis of phenylazide[14]

The singlet-triplet splitting is important in controlling the reactivity of nitrenes. A large singlet-triplet splitting leads to more intramolecular rearrangements. A smaller gap leads to faster relaxation into the triplet ground state and the possibility of bimolecular reactions. Substituents can be added to stabilize the open-shell singlet to prolong its lifetime,[51] to stabilize the closed-shell singlet, which undergoes ISC to the triplet ground state faster. The ground-state triplet is less likely to undergo rearrangement reactions because electrons of the same spin cannot be paired. Much theoretical and experimental work on nitrenes has been centered around tuning the singlet-triplet gap,[15, 51, 55, 56] and nitrene anions have played a significant role in accomplishing this.

2.3   Classes of Nitrene Anions

2.3.1   Introduction

Nitrene anions play many roles in addition to functioning as protected nitrene intermediates. They participate in a wide range of chemical reactions depending on their class or how they are synthesized. There are formally two approaches that could be used to introduce a negative charge into a nitrene. The first would involve the addition an electron to a nitrene, creating a radical anion. Alternatively, anionic nitrenes from neutral nitrenes can be created by removing a cation, such as a proton. Because neutral nitrenes are unstable and therefore not viable as ion precursors, these approaches are not used to synthesize the ions, but the ions that would be formed have distinguishing characteristics that provide a basis for organization and discussion.

A general description of the different classes of nitrene anions is provided in the sections below. Details of the characterization and reactivity of the ions will be given in later sections.

2.3.2   Nitrene Radical Anions

Nitrene radical anions formally correspond to ions formed by an addition of an electron to an even-electron nitrene. Practically, they can be formed by using electron ionization (EI) of an appropriate precursor, such as an azide. Adding an electron to an azide results in dissociative attachment with loss of N_2, leaving behind a nitrene radical anion, as seen in the formation of phenylnitrene radical anion (PhN$^-$) from PhN$_3$ (Equation 2.1).[40]

$$PhN_3 \xrightarrow{\;e^-\;} PhN^- + N_2$$

(2.1)
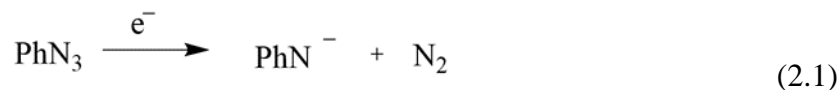
Nitrene radical anions still have an sp hybridized nitrogen, so they have a lone pair of electrons in a non-bonding sp orbital and three more valence electrons distributed between two non-bonding σ and π orbitals. This reduces the number of electronic states from 4, as in the nitrene, to 2. For example, PhN$^-$ has two possible electronic states; namely, the $\pi^2\sigma$ ground state and a $\sigma\pi^2$ excited state (Figure 2.4). Although calculations predict the $\pi^2\sigma$ state to be favored for PhN$^-$,[53, 57] it does not have to be so for all nitrene anions.
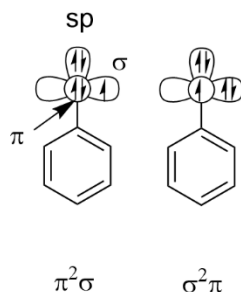
Figure 2.4 The two possible electronic configurations of phenylnitrene radical anion

As mentioned earlier, nitrene radical anions contain an extra valence electron which prevents intramolecular rearrangement reactions from occurring as quickly as they do for neutral nitrenes. This aids in their most significant role as protected nitrene intermediates in photodetachment and photoelectron spectroscopy studies for probing the spectroscopic properties of nitrenes. Their reactivity has also been examined.

2.3.3   Deprotonated Nitrenes

Deprotonation of nitrenes can occur if the nitrene has an acidic hydrogen. Depending on the location of the acidic hydrogen, nitrene anions formed by removing a proton can have the charge centered on the nitrogen or on a separate atom. In theory, a molecule with a proton bound to the nitrogen, such as imidogen (NH), can be deprotonated to give an even-electron anion with a formal charge of -1, as shown in Equation 2.2. However, this can only be done in theory as deprotonation of NH leads to a radical anion that is unbound with respect to electron detachment.[58]

$$HN \xrightarrow{\text{-H}^+} N^-$$

(2.2)

In practice, the charge must be at a separate site from the nitrogen center such that the nitrogen atom retains its formal charge of 0. These types of ions can be formed by deprotonation of a molecule containing an azide group. Similar to electron attachment, deprotonation provides the necessary energy for spontaneous loss of N_2 to form the resulting nitrene anion, as in Equation 2.3.

43

(2.3)
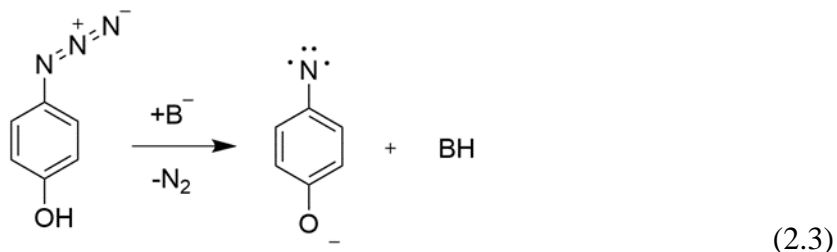
The resulting anion is not necessarily a pure nitrene and may have a mix of nitrene and imide character. For example, the *ortho-* and *para*-quinonimide anions have contributing nitrene and quinonimide resonance structures (Figure 2.5). In contrast, the *meta* isomer is purely a nitrene with no imide character.
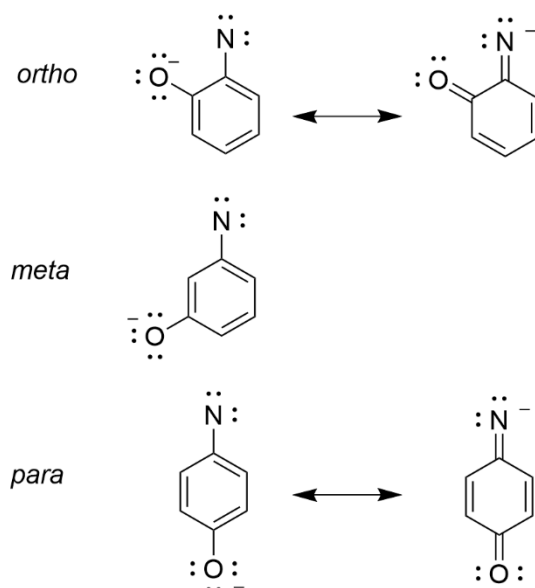
Figure 2.5 Resonance structures of nitrenephenoxide anions show that deprotonated nitrenes may have both nitrene and quinonimide characteristics

Deprotonated nitrenes are still nominally nitrenes, or at least have nitrene character in that they have resonance contributions from structures with 6 electrons on nitrogen. Therefore, they will have the same electronic states as nitrenes, including σ^2, π^2 and $\sigma\pi$ singlets and a $\sigma\pi$ triplet. However, the energy ordering of the states is not necessarily the same, especially in terms of the energies of the closed-shell states, even to the extent of having a singlet ground state.[56]

2.3.4 Imide Anions

Deprotonation of a nitrene on the carbon connected to the nitrogen nominally would result in the formation of an imide anion, $R_2C=N^-$, and not a nitrene. However, nitrene character can be introduced into the ion by the addition of electron withdrawing groups. For example, Rau and Wenthold[42] have shown that benzaldimide (deprotonated benzaldimine), formed by reaction of trimethylsilybenzaldimine with fluoride, Equation 2.4, has an open-shell $\sigma\pi$ electronic structure if there is a sufficiently electron-withdrawing group on the aromatic ring. However, most imide anions have negligible nitrene character.

$$(2.4)$$
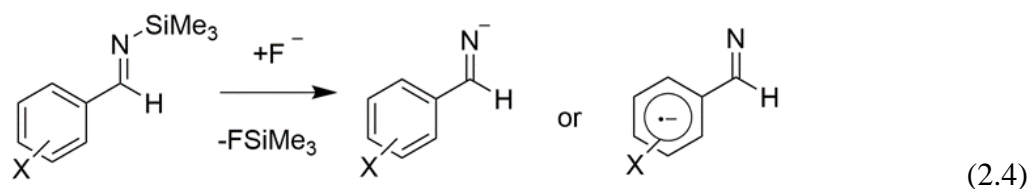
2.4 Spectroscopy of Nitrene Anions – Characterization of the Electronic States of Nitrenes and Nitrene Anions

2.4.1 Introduction

An important application of nitrene anions is as a means for investigating the properties of nitrenes in the gas phase. Free of solvent effects that potentially stabilize electronic states, experiments with gaseous ions can simplify the characterization of nitrenes. This section discusses the advancements in the direct spectroscopic observation of nitrene anions. Some examples include imidogen (HN^-),[59-65] methylnitrene (CH_3N^-),[19] phenylnitrene (PhN^-),[53, 66-69] and substituted phenylnitrene anions.[53]

2.4.2 NH⁻

The simplest nitrene anion is NH^-. The first experimental study of NH^- was carried out by Celotta, Bennett, and Hall.[70] Using a 488-nm Ar^+ laser beam with a crossed-beam apparatus, they carried out negative-ion photoelectron spectroscopy (NIPES) of NH_2^- anion, formed by glow-discharge ionization of NH_3. A small amount of NH^- was also formed, which allowed them to measure the corresponding electron affinity of NH (EA = 0.38 ± 0.03 eV). Engelking and

Lineberger[60] increased the amount of NH^- by using HN_3 for the source gas in place of NH_3 and increased the NIPES signal with a more powerful laser. Although the resolution was poor in resolution, the measured spectrum had two peaks in the photoelectron spectrum, corresponding to transitions from the $X^2\Pi$ state of NH^- to the $X^3\Sigma^-$ and $a^1\Delta$ states of NH, with an energy splitting of 1.579 ± 0.017 eV, in close agreement with theory as well as the results of photolysis experiments with neutral NH_3.[63, 71] They also revised the electron affinity of NH (EA = 0.381 ± 0.014 eV).

In the mid-1980s, Neumark et al.[62] reported the infrared spectrum of NH^- by carrying out autodetachment spectroscopy using a coaxial laser-ion beam spectrometer and monitoring the neutrals and ejected electrons. As in the previous work, the NH^- was a produced by ionization of HN_3 in a hot-discharge source. The autodetachment resonances showed transitions in the R branch from NH^- (v=0) to NH^- (v=1) with a resolution better than 20 MHz. Transitions were also observed in the Q branch with a smaller resolution to calculate equilibrium vibrational constants, which allowed them to measure an electron affinity of 0.370 ± 0.004 eV. Later, using autodetachment spectroscopy of NH^- and detecting the kinematic velocity of the neutral molecule, Al-Za'al, Miller, and Farley[64] were able to increase the resolution of the rotation-vibration spectrum and reported an electron affinity with a precision a thousand times higher than previous work (EA(NH) = 0.374362(5) eV).

2.4.3 CH_3N^-

Little is known about the electronic states of alkylnitrenes. The simplest alkylnitrene, methylnitrene, is an intermediate in many combustion processes[72] and is thought to have a triplet ground state (X^3A_2) C_{3v} symmetry and a singlet first excited state ($\tilde{a}^1E$).[19] However, singlet CH_3N is unstable and quickly undergoes a hydrogen atom shift to become methyleneimine, CH_2NH (Equation 2.5).

$$\begin{array}{cc} H{-}\overset{H}{\underset{H}{C}}{-}N{:} \longrightarrow & \overset{H}{\underset{H}{C}}{=}\overset{H}{N}{\cdot\cdot} \end{array} \tag{2.5}$$
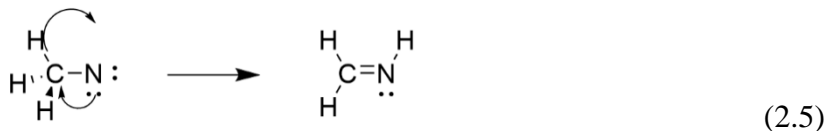
Formation of the imine was first proposed in the early 1930s during pyrolysis studies[73] of methylazide (CH_3N_3) and later confirmed by photoionization spectroscopy.[74] Nevertheless,

methylnitrene remained elusive despite many early attempts to isolate it. An accurate measurement of the electron affinity for CH_3N was not reported until decades later when Travers et al.[19] reported negative ion photoelectron spectroscopy of CH_3N^-, formed by ionization of methylazide in a discharge source. The electron affinity of CH_3N was found to be 0.022 ± 0.009 eV, with a singlet-triplet splitting of 1.352 ± 0.0011 eV.

2.4.4 PhN$^-$

PhN is perhaps the most famous nitrene, and PhN$^-$ has been investigated in many spectroscopy studies. This radical anion was first investigated in the early 1980s.[40, 47] In the study of two primary reaction channels between aryl azides and nitrenes, they proposed that the reduction product PhN$^-$ would avoid the competing rearrangement products of PhN. They were able to synthesize PhN$^-$ via dissociative electron attachment with PhN_3 in a flowing afterglow apparatus. Shortly thereafter, Drzaic and Brauman[67, 68] recognized PhN$^-$ as an approach for obtaining spectroscopic information on PhN. They reported the first direct measurement of the electron affinity of 33.7 ± 0.3 kcal/mol (1.46 ± 0.02 eV) obtained by using energy-resolved photodetachment (PD) spectroscopy in an ion cyclotron resonance spectrometer. They also were able to estimate a singlet-triplet splitting of 4.3 kcal/mol for PhN based on the increased PD yield at the corresponding energy in the spectrum.

In 1992, Travers et al.[66] reported the 488 nm photoelectron spectrum of PhN$^-$, prepared from PhN_3 using a hot cathode ion source. The spectrum contained intense bands corresponding to the formation of the ground-state triplet (EA(PhN) = 1.45 ± 0.2 eV) and peaks attributed to the excited singlet state. Because the ions were rotationally and vibrationally hot, the initial peaks for the singlet band were assigned as hot bands. This assignment was confirmed by remeasuring the spectrum by taking the 351 nm photoelectron spectrum with thermal ions formed in a flowing afterglow ion source. Although the 351 nm spectrum is not shown, they explain that it confirms that the initial bands of the singlet state in the 488 nm spectrum are hot bands (see reference 5 in Travers et al.[66]) and that the singlet origin indicates a singlet-triplet splitting of approximately 18 kcal/mol.

Shortly thereafter, McDonald and Davidson[69] reported another value for the electron affinity of PhN$^-$ by using PD spectroscopy in a flowing afterglow. Based on the onset of the

photodetachment signal, they determined the electron affinity of PhN to be 1.429 ± 0.011 eV, in reasonable agreement with the previously reported values. On the basis of observed transitions in the PD curve, they assigned a singlet-triplet splitting of 18.33 kcal/mol for PhN, in excellent agreement with the value obtained by using NIPES. Curiously, they observed lower energy transitions for the singlet, which were assigned to hot bands, as had been the case for the NIPES study,[66] despite the fact that the ions formed in the flowing afterglow source should be vibrationally cooler than those in the glow-discharge.

As part of a NIPES study of chlorinated aromatic nitrenes (vide infra), Wijeratne et al.[53] measured the 355 nm photoelectron spectrum of PhN$^-$ for comparison with the previous work of Ellison and co-workers.[66] Surprisingly, they found that the weak features previously described as hot bands for the singlet band were still present in the spectrum, despite using a pulsed expansion source to cool the ions. Moreover, the intense bands that had been attributed to the origin of the singlet excited state were not apparent in the 355 nm spectrum. In a reanalysis of the unpublished spectrum cited by Travers et al.,[66] it was discovered that the intense singlet-state feature was likely due to phenoxide impurity, whereas the weaker features assigned to hot bands corresponded to the standard progression of the singlet band. The reanalysis of the spectrum resulting in a revised value of the singlet triplet splitting, with $\Delta E_{ST} = 14.8 \pm 0.5$ kcal/mol, in good agreement with modern theoretical predictions.[75] Interestingly, the first singlet transition observed in the PD spectrum reported by McDonald and Davidson,[69] originally assigned as a hot band, is also found at an energy of 14.8 kcal/mol, suggesting that it is likely the origin for the onset of singlet formation.

2.4.5   ClPhN$^-$

Wijeratne et al.[53] have carried out a photoelectron spectroscopy study of chloro-substituted phenylnitrene anions to examine the effect of chlorination on the electronic structure. The ions used in the study were formed from the corresponding chlorinated phenyl azides using a pulsed-expansion ionization source.[76-78]

The 355 nm photoelectron spectra obtained are shown in Figure 2.6. The lower-energy features were assigned to the triplet states, and the higher-energy features were assigned to the singlets. The origins of the triplet states are assigned as "A" and vibrational peaks are labeled "B-D". Likewise, the origins of the singlet states are labeled "a" and vibrational peaks "b-c". The

spectra made it possible to measure the electron affinities for ortho-, meta-, and para-substituted (chlorophenyl)nitrene as 1.79 ± 0.05, 1.82 ± 0.05, and 1.72 ± 0.05 eV, respectively.
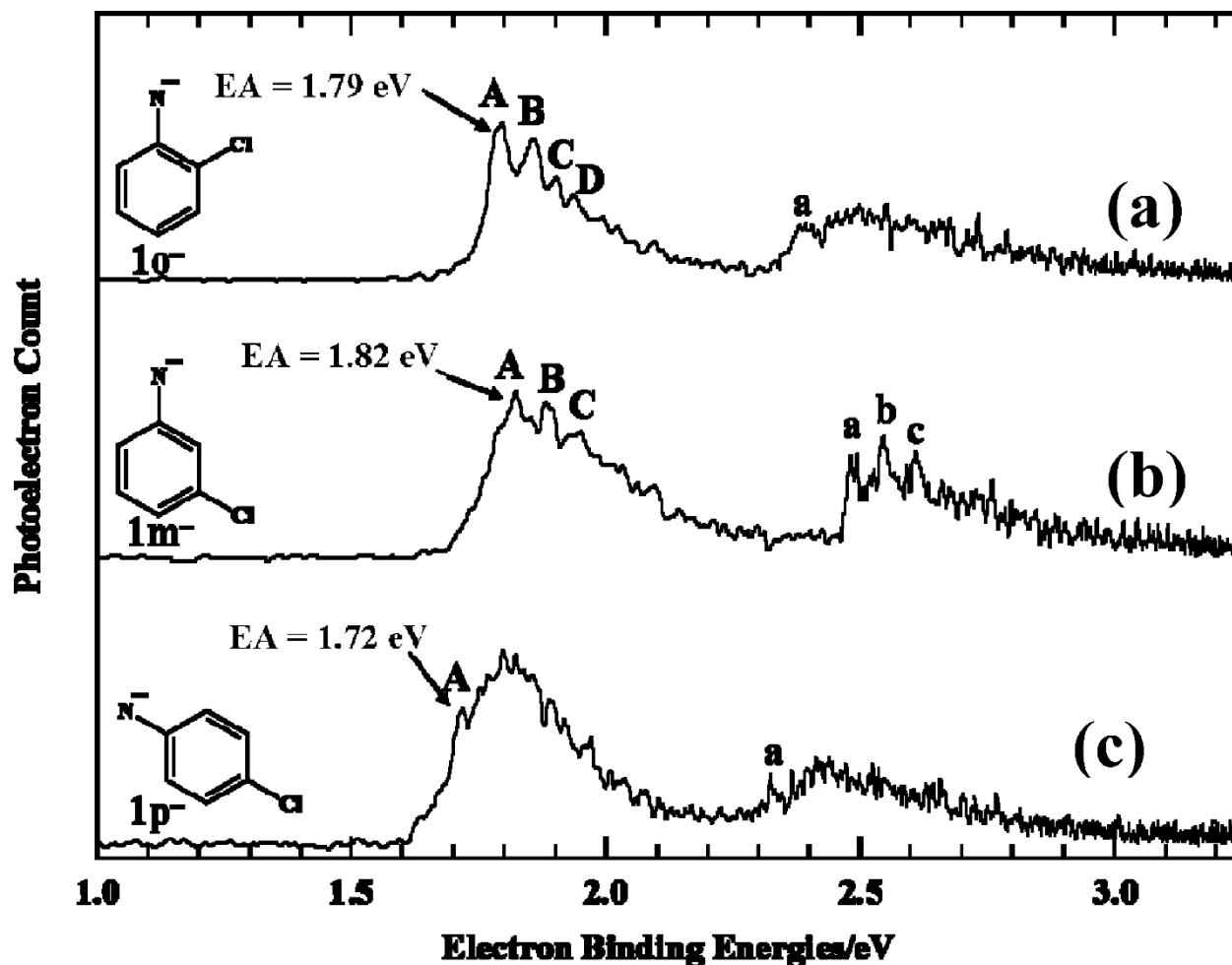
Figure 2.6 Photoelectron spectra of the (a) ortho-, (b) meta-, and (c) para-isomers of (chlorophenyl)nitrene anions at 355 nm. The region from 2.2 to 2.8 eV was scaled up by 2.5 to observe the origin of the singlet state more clearly. The origins of the triplet states are assigned as "A" and the other vibrational peaks are labeled as B−D. The origins of the singlet states are assigned as "a" for each isomer, and vibrational peaks are labeled b−c. Reprinted with permission from *J. Phys. Chem. A* 2009, 113, 34, 9467-9473.[53] Copyright 2009 American Chemical Society.

From the photoelectron spectra, it could be determined that the chlorine did not affect the order of the electronic states of the aromatic nitrene, with the open-shell singlet state still the lowest energy singlet state. However, subtle differences were observed in the shapes of the spectral features for the singlet states for the ortho- and para-singlet states, which were interpreted as

indicating that the chlorine substituent has a detectable effect on the energies and structures of the open-shell singlet states. The effect was attributed to one-electron resonance delocalization involving the chlorine atom (Scheme 2.1), which allows for favorable delocalization of the π electron that reduces the electron-pair repulsion between the unpaired electrons.[79] The result is a lowering of the singlet state energy (by about 1 kcal/mol) and a shortening of the C–N bond in the ortho- and para-isomers compared to that in the meta-isomer, where no resonance stabilization occurs.

Scheme 2.1
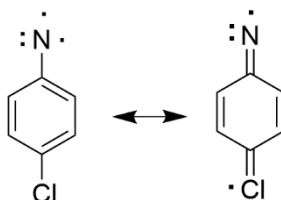
2.4.6 Quionimides

The PES of quinonimides has been carried out by Hossain et al.[80] Benzoquinones play an important role as electron acceptors in various biological processes[81, 82] as well as in chemical applications.[83, 84] The ortho and para isomers have Kekulé valence structures and low-energy closed-shell singlet electronic states, whereas the meta isomer has a non-Kekulé structure with an open-shell triplet ground state. Incorporating substituents into the aromatic ring lead to variations of lower-energy, stable Kekulé structures with closed-shell elecronic states, or to higher-energy, non-Kekulé structures with high-spin electron coupling.

o-Bzq   m-Bzq   p-Bzq
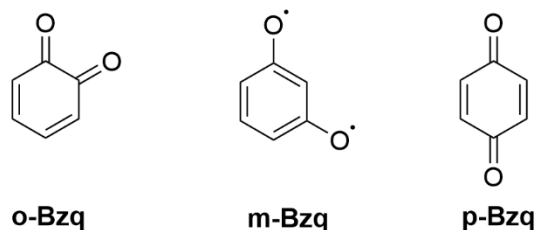
As will be discussed in the next section, the reactivity of ortho-, meta-, and para-quinoidal imides[56] shows that the electronic structure of the para isomer actually exhibits characteristics

consistent with a thermally accessible triplet state. Accordingly, Hossain et al.[80] used negative ion photoelectron spectroscopy (NIPES) to study the electronic properties of the quinonimides and also determine spectroscopic properties of the corresponding quinoniminyl radicals. The NIPES experiments were carried out using a time-of-flight (TOF) photoelectron spectrometer with an ESI source. ESI of o-, m- and p-azidophenoxide ions occurs by dissociation (M - H - N2) to create benzoquinone product anions, **o-BzqN⁻**, **m-BzqN⁻**, and **p-BzqN⁻**.

o-BzqN⁻   m-BzqN⁻   p-BzqN⁻

The photoelectron spectra gave electron affinities of 1.715 and 1.67 ± 0.01 eV for **o-BzqN⁻** and **p-BzqN⁻**, respectively. By modeling of the Frank-Condon profiles for the photoelectron bands, it was concluded that the para isomer, **p-BzqN⁻** is a ground state singlet whereas the ortho isomer is a triplet ground state nitrene. The meta isomer was found to rearrange to **p-BzqN⁻** and other unidentified isomers, and consequently could not be characterized.

2.5   Reactivity

2.5.1   Introduction

Mass spectrometry has been used in investigating the reactivity of nitrene anions in ion-molecule reactions. Nitrene anions can act as both Lewis bases and as radical intermediates. Radical chemistry stems from the configuration of valence electrons in the open-shell structure whereas two-electron chemistry can occur in either the closed-shell or open-shell structures. Because of their electron deficiency, nitrene anions are electrophilic as well. As will be discussed below, PhN⁻ sets the basis for much of what is known about the reactivity of nitrene anions. However, as the field of nitrene anions has been increasing, a number of other rich examples have surfaced as well. This section highlights the unique reactivity that has been found for nitrene anions.

2.5.2 PhN⁻

The reactivity of PhN⁻ has been thoroughly investigated. A summary of the reactivity of PhN⁻ is shown in Figure 2.7. PhN⁻ can be generated by dissociative electron attachment of PhN_3. Because PhN⁻ has an odd number of electrons, it is a ground-state doublet and does not have the multiplicity problem of other nitrenes (triplet vs singlet).[40] Thus, it can easily participate in reactions with other molecules.
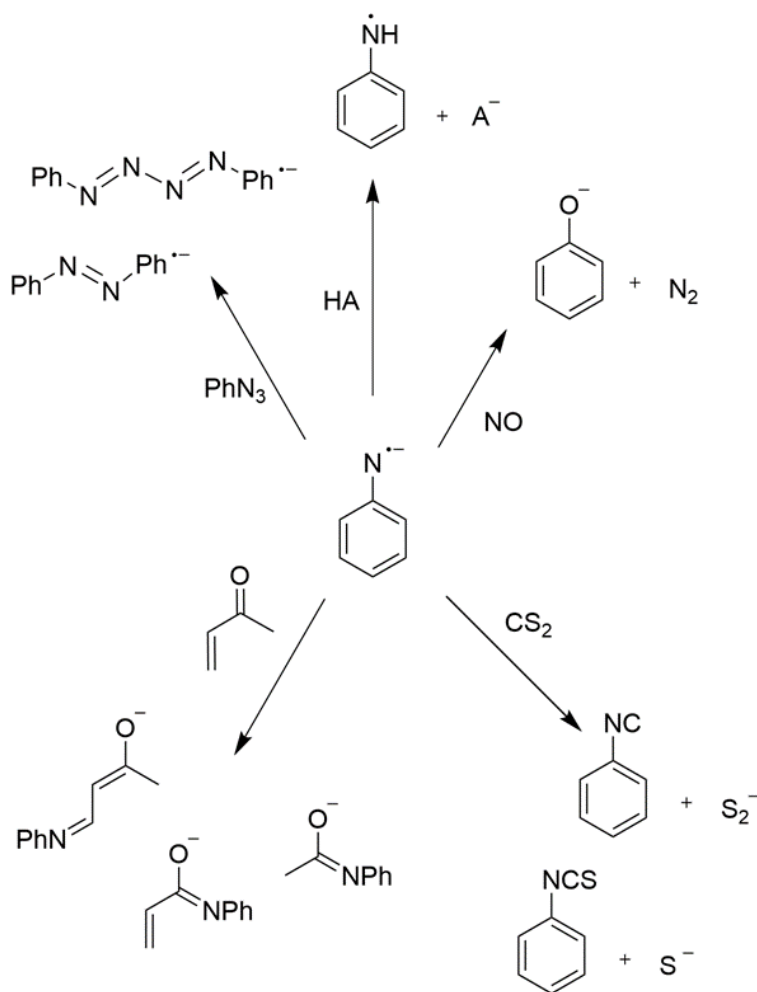
Figure 2.7 Reactions with PhN⁻

One of the first reactivity studies on PhN⁻ was carried out by McDonald and Chowdhury.[40] They observed that PhN⁻ can react with PhN_3 by addition to Nα to produce azobenzene radical

anion and nitrogen (Equation 2.6) and to NY˙ to produce 1,4-diphenyltetrazadiene radical anion (Equation 2.7).

$$PhN^{\bullet-} + PhN_3 \longrightarrow Ph\text{-}N\text{=}N\text{-}Ph^{\bullet-} + N_2$$

(2.6)

$$PhN^{\bullet-} + PhN_3 \longrightarrow Ph\text{-}N\text{=}N\text{-}N\text{=}N\text{-}Ph^{\bullet-}$$

(2.7)
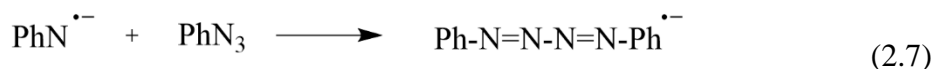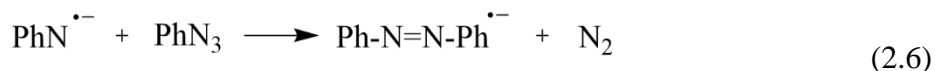
McDonald, Chowdhury, and Setser[47] also determined the proton affinity of PhN⁻ in a flowing afterglow using a series of proton donors with known acidity. For strong acids, PhNH was the major product. For weak acids that could not protonate PhN⁻, bimolecular reactions were observed instead. PhN⁻ was found to form clusters with alcohols through a sequence of reactions. PhN⁻ also reacted with CH_3CN to form $C_8H_8N_2^-$ as the major product. On the basis of whether the proton transfer was observed, the proton affinity of the anion was deduced to be 372 ± 2 kcal/mol, which leads to $\Delta H_f(PhN^-) = 60 \pm 2$ kcal/mol.[47, 85]

PhN⁻ also undergoes addition to certain α,β-unsaturated compounds. Gas-phase studies of 1,2- vs. 1,4 additions of nucleophiles to α,β-unsaturated compounds is difficult because both reactions lead to products with the same m/z values. Additionally, solution-phase studies indicate that 1,2 additions are easily reversible, so the results from gas-phase studies yield little information on the difference in reactivities of the two sites. However, hypovalent radical anions can be used to solve the reactivity of α,β-unsaturated compounds.[43]

Hypovalent species such as R_2C^-, RN⁻, O⁻, and S⁻ can add to α,β-unsaturated compounds irreversibly because they contain both an unpaired electron and a lone pair.[44, 49] After the lone pair adds to the carbon, the radical can initiate irreversible β fragmentation, as shown in Scheme 2.2. The resulting product ions have different m/z values; thus, the preference for 1,2 vs. 1,4 additions can be identified. Whereas as R_2C^-, and O⁻ have large H atom (HA) and H+ (PA) affinities giving them short lifetimes, RN⁻ has smaller calculated HA and PA values making it a better nucleophile for gas-phase reactions.[49]

Scheme 2.2
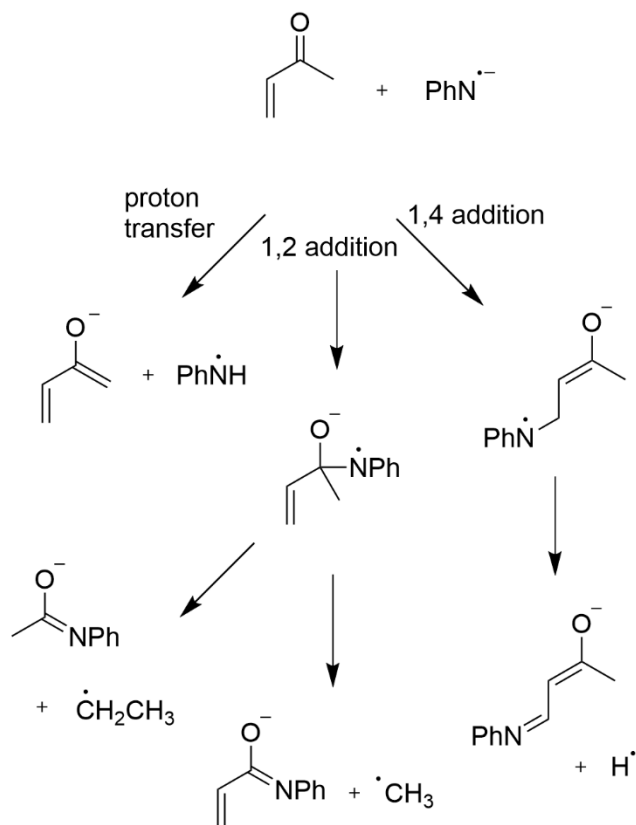
As seen with additions to α,β-unsaturated compounds, PhN⁻ also adds to carbonyls. Most gas-phase nucleophiles add to carbonyls reversibly making information about the reactivity of carbonyl sites difficult to uncover. Nevertheless, addition of PhN⁻ followed by irreversible β fragmentation can yield valuable information on the reactivity of carbonyl sites, as shown in Scheme 2.3.

Scheme 2.3
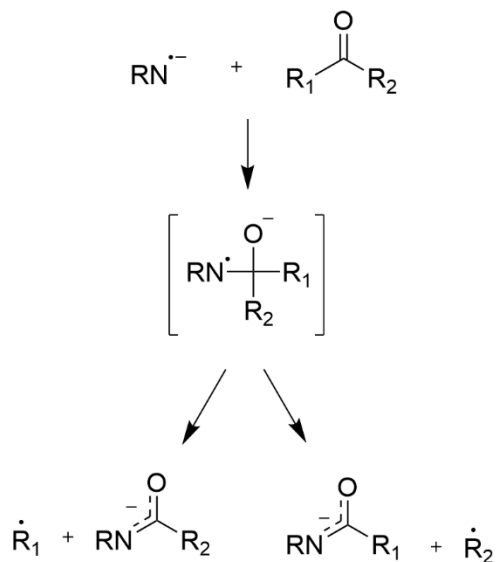
Nitric oxide (NO) is a reagent that reacts specifically with open-shell anions in the gas phase.[86] Ion/molecule reactions involving NO can thus aid in investigating electronic structure. Wijeratne and Wenthold[93] observed that PhN$^-$ reacted with NO via nitrogen-oxygen exchange to form phenoxide, as shown in Equation 2.8.

$$(2.8)$$
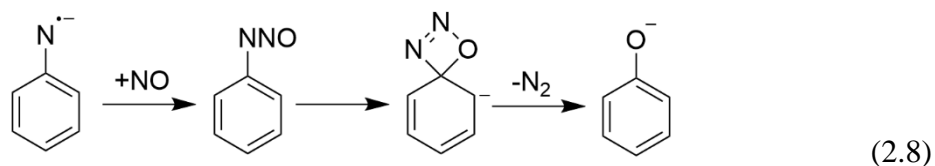
They also observed that PhN$^-$ reacted with carbon disulfide (CS_2) by C^+ or CS^+ abstraction forming S^- and S_2^- (Equation 2.9).
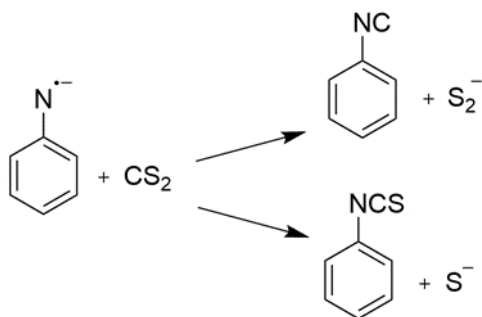
(9)

2.5.3 Pyridinyl-*n*-oxide Nitrenes

Radical stabilizing groups[87] are one route to altering the electronic structure of nitrene intermediates. Although the effect of these groups is predicted to be small, usually reducing the singlet-triplet splitting by less than 2 kcal/mol, some larger effects do occur.[88] Furthermore, other radical stabilizing groups are predicted to have an unusually small singlet-triplet splitting, as seen with 2-furanylnitrene.[89] To determine the effects of a radical stabilizing group on PhN⁻, Koirala, Poole, and Wenthold[57] investigated the reactivity of 3- and 4-pyridinylnitrene-n-oxide radical anions, **3PNO⁻** and **4PNO⁻**, respectively, formed by ionization of the corresponding azides in a flowing afterglow ion source.
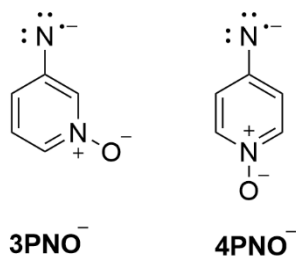
The pyridinium is an electron acceptor, but the oxide is a π donor. While the n-oxide does not participate in resonance at the 3-position, two types of stabilization are available at the 4-position (Figure 2.8).

56
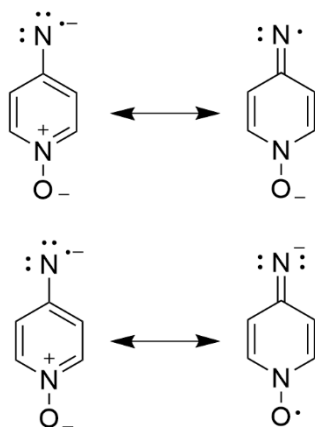
Figure 2.8 Resonance structures of **4PNO⁻**

The radical anions were generated using EI of azide precursors, then cooled to ambient temperature (298 K) by helium buffer gas downstream in a flow tube where they underwent ion/molecule reactions. Although the n-oxide was not predicted to alter the ground state of **4PNO⁻**, differences in reactivity between **3PNO⁻** and **4PNO⁻** were observed. One significant difference is that the reaction of **4PNO⁻** with NO leads to more adduct ion whereas the reaction with **3PNO⁻** only leads to trace amounts. Both are observed to undergo N-O exchange.

Upon reaction with CS_2, **3PNO⁻** and **4PNO⁻** again displayed different reactivity. Nucleophilic attack of the oxygen in the anion at the carbon in CS_2 was only observed for **4PNO⁻**. This led to sulfur-oxygen transfer and to formation of CS_2O^- (Equation 2.10), which was not observed for **3PNO⁻** indicating that the *n*-oxide moiety does not interact with the substituent in the *meta* position.

(2.10)
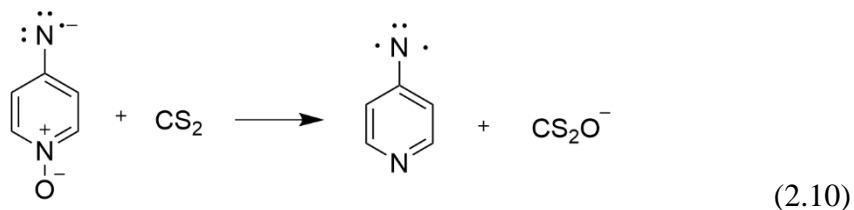
This work confirmed that sufficiently strong π-donors oxygen-atom transfer, which is consistent with condensed-phase studies[90] but had not previously been observed for aromatic n-oxides.

57

2.5.4 Quinonimides

Rau, Welles, and Wenthold[56] showed that anionic-π donors can lead to a closed-shell singlet ground state. They investigated reactions of anion-substituted (CH_2^-, O^-) aromatic nitrenes with O_2, NO, and CS_2. The ions were synthesized by reaction of precursor azide molecules *m*- and *p*-azidotoluene and *p*-azidophenol with hydroxide and fluoride ions, respectively, in a flow tube, resulting in closed-shell nitrene anions, as shown in Equations 2.11, 2.12, and 2.13.

$$(2.11)$$

$$(2.12)$$

$$(2.13)$$
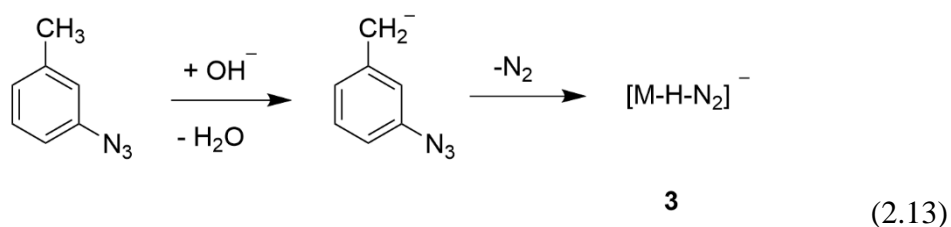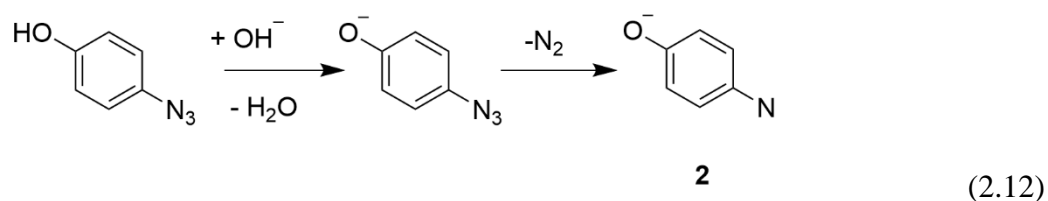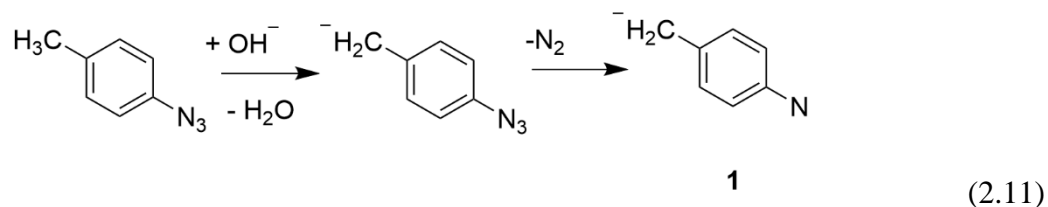
Differences were observed in the products of the deprotonated nitrene anions **1-3** when they react with NO. The compounds with CH_2^- (**1** and **3**) only undergo adduct formation with NO, whereas ion **2**, with the O^-, results in nitrogen-oxygen exchange in addition to adduct formation (Equation 2.14).

$$[\mathbf{2} + NO]^{-}$$

$$+ \ N_2$$

(2.14)
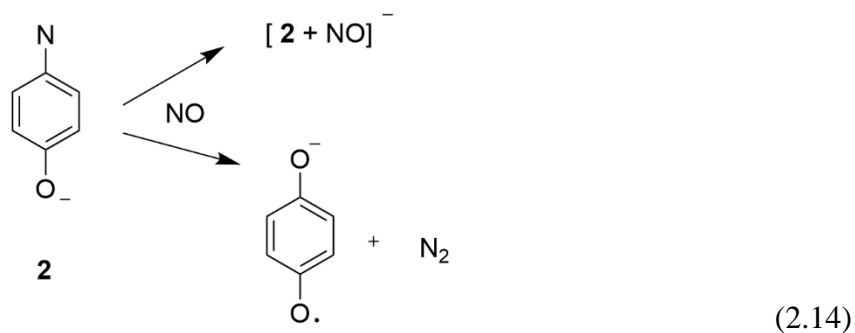
Both *para* isomers (**1** and **2**) undergo sulfur-nitrogen exchange with CS_2 to form NCS^-; however, **3** once again only undergoes adduct formation. The differences in the observed reactivity of the deprotonated nitrene anions with NO and CS_2 provide insight into the ion electronic structures. Because NO is known to undergo reactions with open-shell anions,[31, 91, 92] it was expected that **1** undergoes only adduct formation because it is a closed-shell anion. In contrast, **2** formed a 60/40 mixture of adduct and semiquinone anion (Equation 2.14), which implies it has an accessible open-shell structure. In addition, reaction of **2** with molecular oxygen results solely in nitrogen-oxygen exchange, which is indicative of a low-energy, accessible triplet state.

Calculations carried out on the singlet-triplet energy gaps of other nitrene derivatives led to the prediction that functional groups that could fine tune the electronic structure of nitrenes. Figure 2.9 is the result of those calculations showing a range of electron donating groups that create a spectrum of molecules with a mix of quinone and nitrene resonance contributions. The stronger the electron donor, the greater the quinone contribution and which increases the likeliness of the molecule undergoing bimolecular reactions.
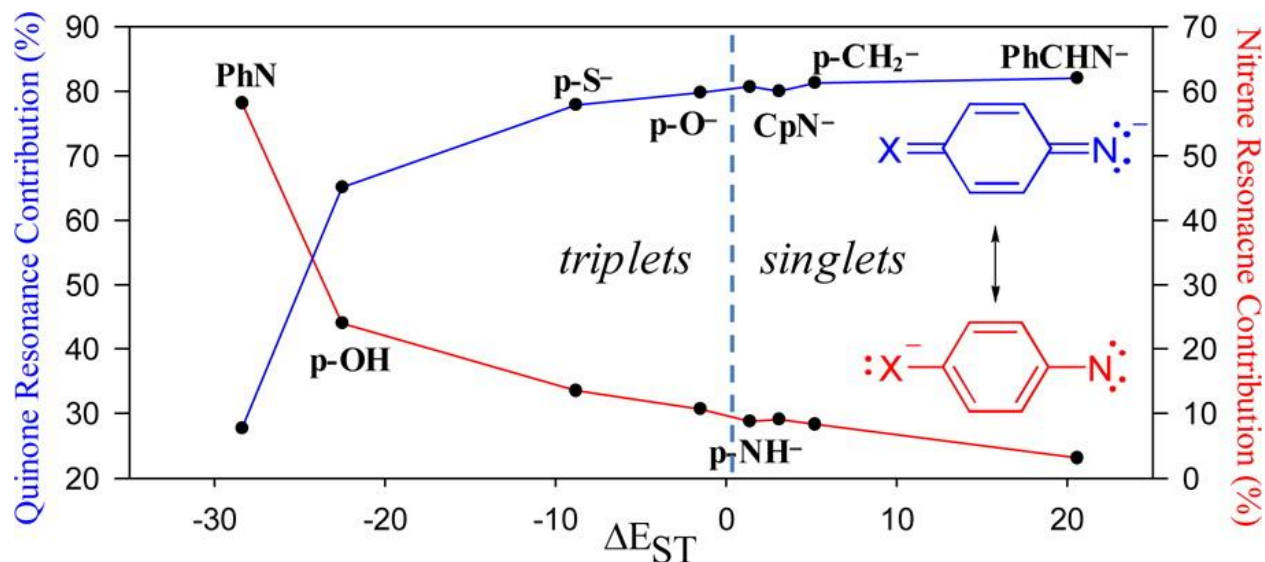
Figure 2.9 Calculated anionic substituent effects on the singlet-triplet splitting of phenylnitrene. Reprinted with permission from *J. Am. Chem. Soc.* 2013, 135, 2, 683–690.[56] Copyright 2013 American Chemical Society.

2.5.5 Benzoylnitrenes

Wijeratne and Wenthold[45, 93, 94] have extensively studied the reactivity and thermochemistry of benzoylnitrene radical anions, which were generated by 70 eV electron ionization of benzoylazide and analyzed with a triple quadrupole mass spectrometer. Acylnitrenes have been confirmed to be ground state singlets[95, 96] because they are stabilized by the carboxylate through resonance.[97, 98] Similarly, benzoylnitrene radical anion is also stabilized via resonance, as shown in Equation 2.15.

(2.15)
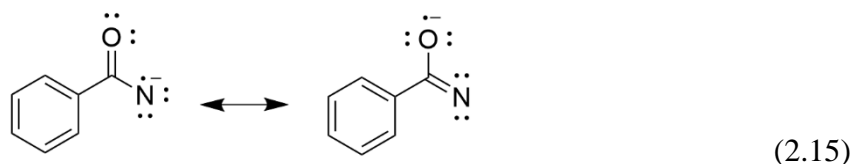
As with aromatic nitrene anions, benzoylnitrene anions react with NO by nitrogen-oxygen exchange forming benzoate anion as the major product (Equation 2.16). The reaction is again proposed to involve an initial radical coupling of the benzoyl nitrene anion and the nitric oxide forming a benzoylnitrosate anion, followed by the formation of a 4-membered transition state that gives the benzoate after elimination of a nitrogen molecule.

(2.16)
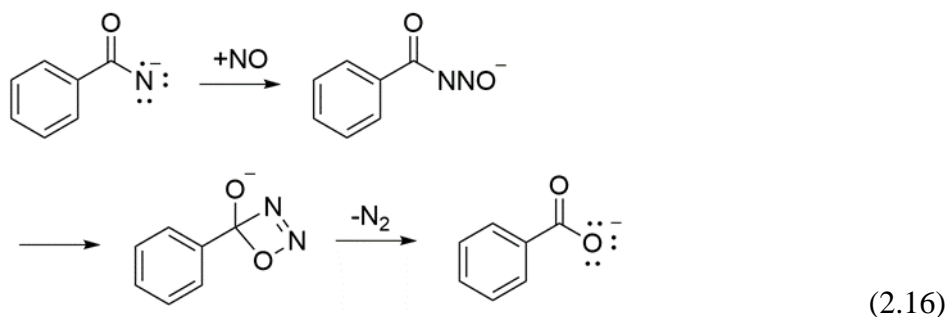
The reaction also produces a small amount of benzonitrile, which is produced by oxygen anion transfer (Equation 2.17).

(2.17)
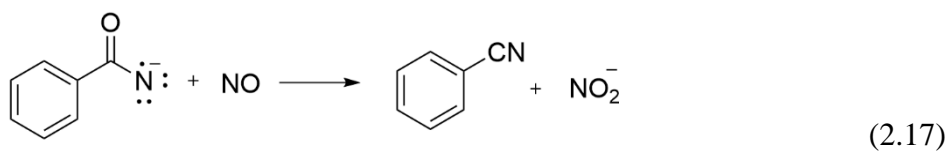
The reaction with nitrogen dioxide also undergoes a nitrogen-oxygen exchange leading to formation of benzoate anion and N_2O. This reaction is presumed to follow a similar mechanism as the reaction with NO, with initial formation of phenylnitroso anion followed by a rearrangement. This reaction produced additional products, as shown in Scheme 2.4, but to a much smaller extent.

Scheme 2.4
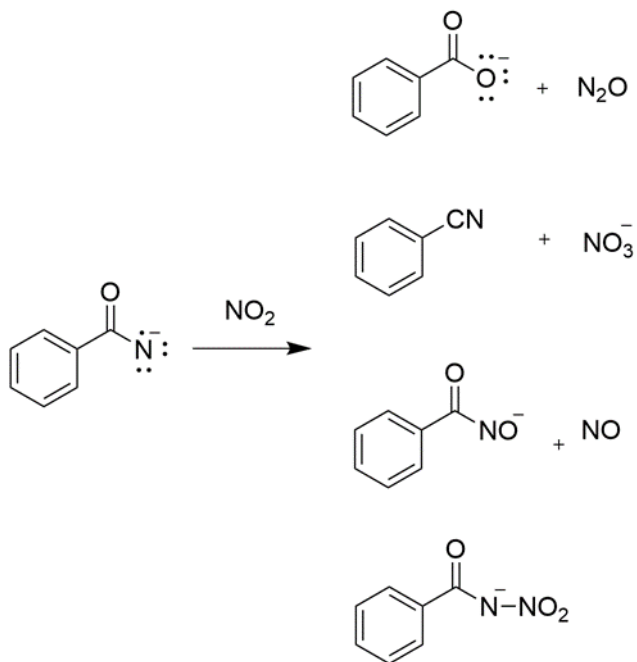
The reaction of benzoyl nitrene anion with the Lewis acid CS_2 yields benzonitrile as the main product along with CS_2O^- (Equation 2.18). Oxygen anion transfer is also observed in the reaction with SO_2, where the major products are benzonitrile and SO_3^- (Equation 2.19). This reaction is accompanied by the formation of SO, indicating oxygen abstraction by the benzoylnitrene anion. Reaction of benzoyl nitrene anion with other Lewis acids such as CO_2 and N_2O does not occur.[93]

(2.18)

(2.19)
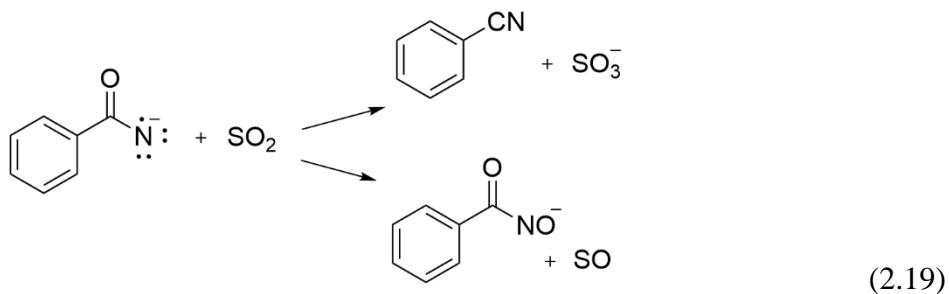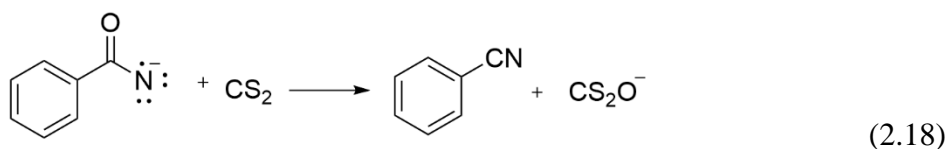
Atomic oxygen ion, O^-, is well-known to undergo reactions by H_2^+ transfer.[99] Consequently, O^- has been used extensively for the synthesis of radical anions of reactive molecules, including carbenes and diradicals. A similar type of H_2^+ transfer was also observed in the reactions of benzoylnitrene anions with select reagents with high acidities. The reagents vary from various substituted phenols to other substrates such as acetic acid and 1,1,1,3,3,3-hexafluoro-2-propanol, as shown in Equations 2.19 and 2.20.[45]

(2.19)

(2.20)
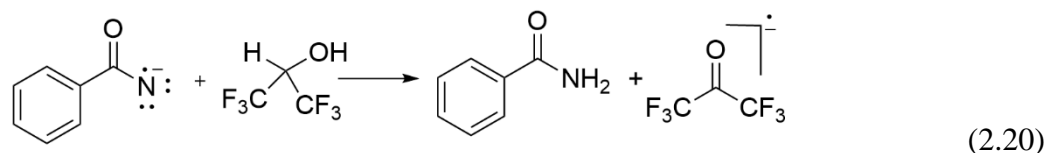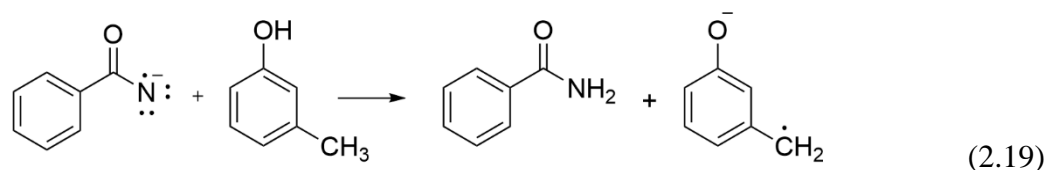
2.5.6   Benzaldimides

In the same way that strong π donors can increase the quinone character of nitrenes, electron withdrawing groups can increase the nitrene character of imides. An example is para-substituted quinonimide anion, as shown in Equation 2.22.

(2.22)
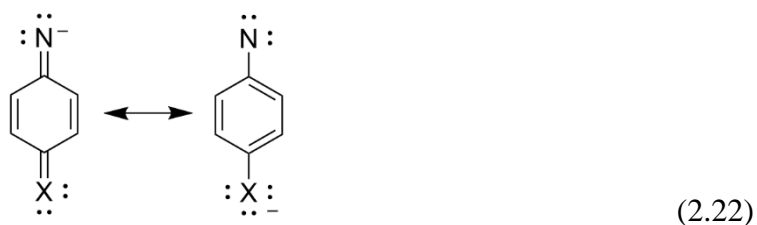
While imide anions are formally the conjugate bases of imines, they can be synthesized by reactions of n-trimethylsilylimines with fluroride ion (Equation 2.23).

$$(2.23)$$
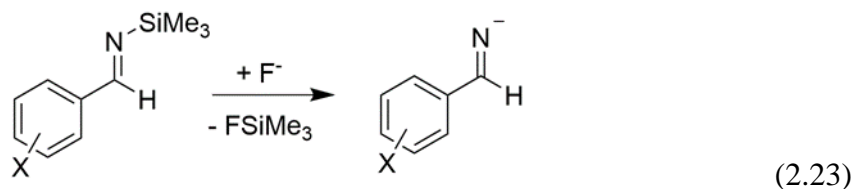
The nitrene character of these molecules can be confirmed through ion/molecule reactions with NO and CS_2 which have distinct reactivities towards open-shell and the closed-shell nitrenes.[56] Using these reagents, Rau and Wenthold[42] examined the reactivities of substituted benzaldimide anions (Equation 2.24).

$$X = H, p\text{-}CH_3, p\text{-}CN, m\text{-}NO_2, p\text{-}NO_2$$

$$(2.24)$$
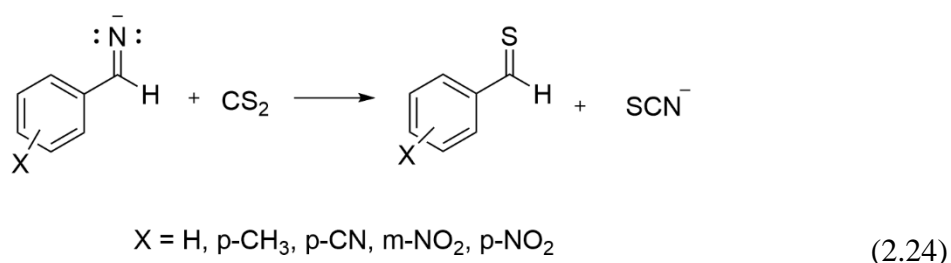
In their studies, various substituted benzaldimides reacted with CS_2 by nitrogen-sulfur exchange, thus confirming the presence of a nitrogen-based anion. The mechanism of the NCS-formation is predicted to involve direct addition of CS_2 forming a thiocaboxylate which forms a 4-membered transition state followed by the substitution (Scheme 2.5).

Scheme 2.5
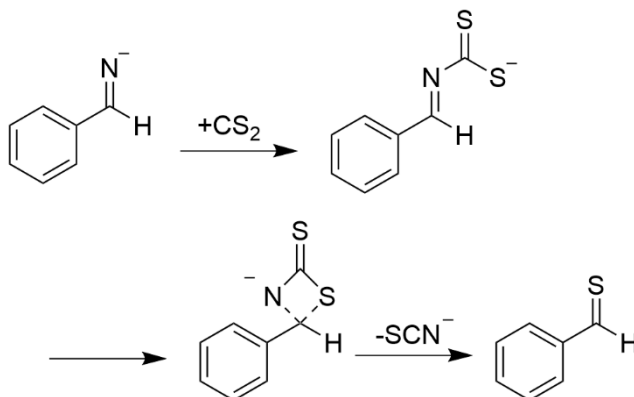
The ions also reacted with CS_2 by hydride transfer forming HCS_2^- and the corresponding benzonitriles (Equation 2.25). This was unique because other imide anions such as benzophenone do not react with CS2 via hydride transfer.[56]

$$X = H, p\text{-}CH_3, p\text{-}CN, m\text{-}NO_2, p\text{-}NO_2 \tag{2.25}$$
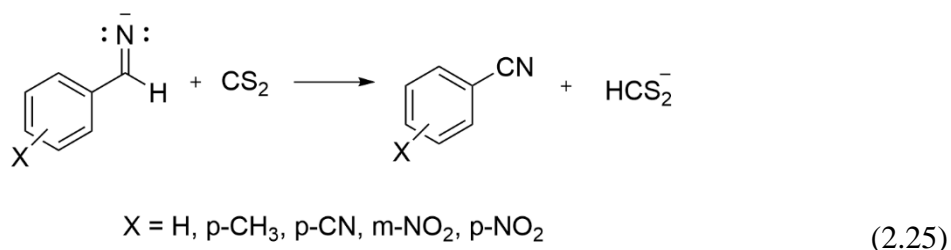
In reactions with NO, most imide anions form adducts indicating the presence of a closed-shell anion. In contrast, *p*-nitrobenzaldimide was found to react with NO via N-O exchange forming benzaldehyde radical anion (Equation 2.26). The formation of the NO adduct as well as the N-O exchange product is indicative of that *p*-nitrobenzaldimide has an accessible open-shell (presumably) triplet electronic state.

$$\tag{2.26}$$
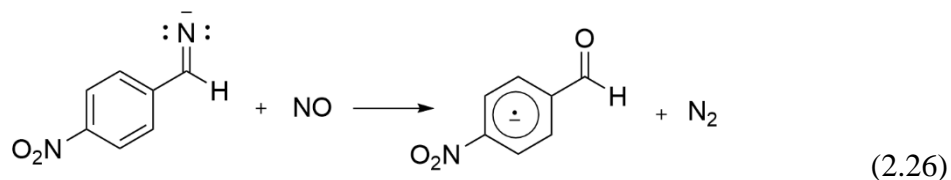
2.6   Thermochemistry

The focus of many of the studies included in this review has been on the determination of the thermochemical properties of nitrene anions and the corresponding nitrenes. Thermochemical properties, such as enthalpies of formation, gas-phase acidities, and electron affinities, aid in understanding the reactivity of nitrenes and nitrene anions, and many of the traditional mass spec approaches have been used in this regard.[100]

As discussed in the spectroscopy section, nitrene electron affinities can be measured from a photodetachment or photoelectron spectrum. From features in the photodetachment and photoelectron spectra, it can be possible to determine the energy difference between the triplet and singlet states of the nitrene, ΔE_{ST}. Anion proton affinities (or, conversely, the gas-phase acidity of

the conjugate acid, $\Delta G_{acid}(RNH)$) have been measured by using proton-affinity bracketing, wherein the proton affinity is deduced from the occurrence or non-occurrence of proton transfer in the reaction of proton donors with known gas-phase acidities. With reliable estimates of ΔS_{acid} values the free energy values can be converted to $\Delta H_{acid}(RNH)$.[85, 101, 102]

From these direct measurements, additional important thermochemical quantities can be derived. In particular, by using the expression in Equation 2.27,[101] it is possible to calculate the homolytic bond dissociation energy (BDE) in the RNH radical, D(RN-H).

$$D(R–H) = \Delta H_{acid}(RH) + E_{EA}(R) - IE(H) \qquad (2.27)$$

Consequently, if the enthalpy of formation of RNH is known, then the BDE can be used to determine the absolute enthalpy of formation of the nitrene, $\Delta H_f(RN)$. Currently, only NH and PhN are characterized to this extent. A summary of the measured thermochemical values obtained by studies of nitrene anions is shown in Table 2.1.

Table 2.1 Thermchemical Properties of Nitrenes and Nitrene Anions from Mass Spectrometry Studies

Nitrene Ion (RN⁻)	$E_{EA}(RN)$, eV	$\Delta H_{acid}(RNH)$, kJ/mol	$\Delta E_{ST}(RN)$, kJ/mol	$D(RN-H)$ kJ/mol[a]	References
NH⁻	0.38 ± 0.03				Celotta et al.[70]
	0.381 ± 0.014		152 ± 2		Engelking and Lineberger[60]
	0.370 ± 0.004				Neumark et al.[62]
	0.374362(5)				Al-Za'al et al.[64]
			150.6 ± 0.1		Rohrer and Stuhl[71]
CH₃N⁻	0.022 ± 0.009		130.5 ± 0.1		Travers et al.[19]
PhN⁻	1.46 ± 0.02		18.0 ± 1.7		Drzaic and Brauman[67, 68]
	1.45 ± 0.02		62 ± 2[b]		Travers et al.[66]
	1.43 ± 0.02		76.6 ± 2.9		McDonald and Davidson[69]
	1.45 ± 0.02		62 ± 2		Wijeratne et al.[53]
		1560 ± 8		388 ± 8	McDonald et al.[47]
o-ClPhN⁻	1.79 ± 0.05		58 ± 8		Wijeratne et al.[53]
		1534 ± 16		395 ± 17	Wijeratne et al.[41]
m-ClPhN⁻	1.82 ± 0.05		63 ± 8		Wijeratne et al.[53]
		1535 ± 16		399 ± 17	Wijeratne et al.[41]
p-ClPhN⁻	1.72 ± 0.05		58 ± 8		Wijeratne et al.[53]
		1533 ± 16		387 ± 17	Wijeratne et al.[41]
o-OC₆H₄N⁻	1.715 ± 0.010		149 ± 1[c]		Hossain et al.[80]
p-OC₆H₄N⁻	1.675 ± 0.010				Hossain et al.[80]
C₆H₅CON⁻		1453 ± 10			Wijeratne and Wenthold[94]

[a]Derived from $D(R-H) = \Delta H_{acid}(RH) + E_{EA}(R) - IE(H)$

[b]Although this was originally reported as 75 ± 8 kJ/mol, the original data were re-interpreted in reference by Wijeratne et al.[53] to the value of 62 kJ/mol.

[c]This is technically the doublet-quartet splitting because the neutral nitrene is an odd-electron species; in contrast to the other nitrenes in the table, which are ground-state triplets, the low-spin (doublet) state is the ground state

Additional characterization of the benzoyl nitrene radical anion, BzN⁻, was reported by Wijeratne and Wenthold.[94] Collision-induced dissociation (CID) of BzN⁻ occurs by loss of NCO⁻ to form phenyl anion (Equation 2.28). By using energy-resolved CID, the authors were able to determine the energy for the dissociation reaction in Equation 2.28 which, when combined with the well-known enthalpies of formation of phenyl radical[100] and CNO⁻, [103] could be used to determine the enthalpy of formation of the benzoyl nitrene radical anion.

$$(2.28)$$
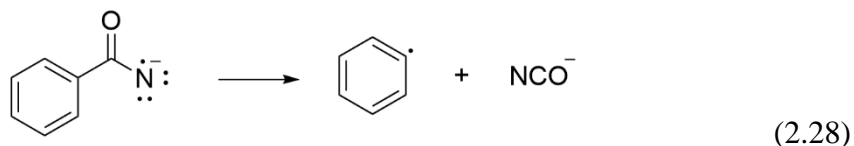
Similarly, bracketing reactions were used to determine the proton affinity of the anion, and, consequently, the gas-phase acidity of the benzamidyl radical (Equation 2.29). Proton transfer was observed with formic acid but not with 1,2,3-triazole, resulting in a proton affinity of 1453 ± 10 kJ/mol.

$$(2.29)$$
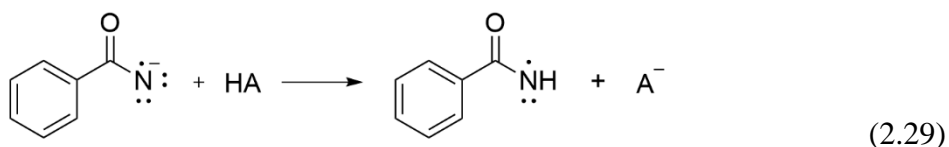
By combining these two measurements, a wealth of thermochemical data could be derived (Figure 10) including the homolytic BDE in benzoylamide (D(PhCONH-H) = 429 ± 14 kJ/mol), the electron affinity of the benzoylamidyl radicl (EA(PhCONH) = 2.70 ± 0.17 eV) and the oxygen anion (O^-) affinity of benzonitrile (D(PhCN-O^-) = 294 ± 9 kJ/mol).
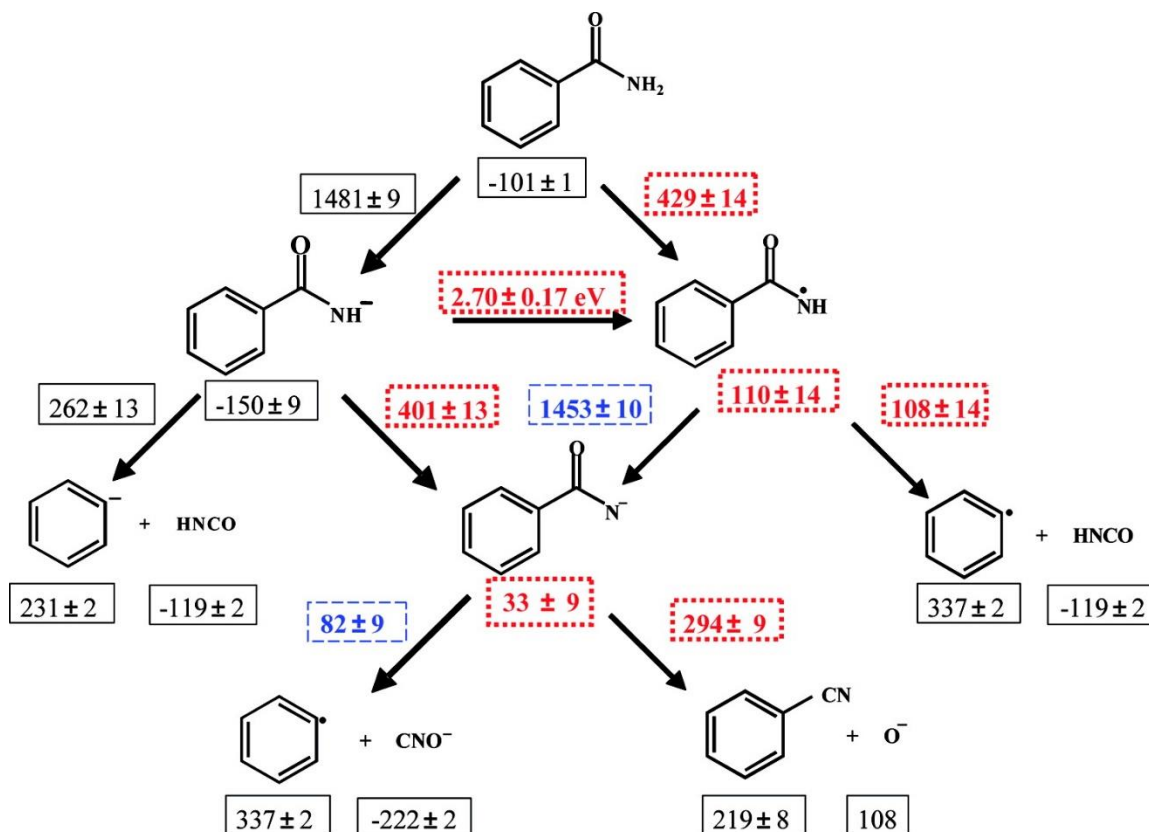
Figure 2.10 Thermochemical properties measured and derived from the studies of benzoylnitrene radical anion. All values are in k/mol. Values in blue dashed-line boxes were measured directly in this work, whereas values in red dotted-line boxes were derived from those measurements and literature values, shown in black. Reprinted with permission from *J. Phys. Chem. A* 2007, 111, 42, 10712–10716.[94] Copyright 2007 American Chemical Society.

2.7   Condensed-phase Nitrene Anions

While nitrene anions are difficult to isolate in solution, they are known to take part in condensed phase chemistry.[104-106] They fall into a category of organic molecules with low-lying high-spin electronic states that have drawn significant interest for many years because of their unique electronic properties.[107] Because of their high reactivity, they are difficult to characterize. However, a few examples have been reported in the literature, which will be discussed below.

In the electrochemical reduction of p-nitrophenyl azide in DMF, acetonitrile, and butyronitrile, Herbranson and Hawley[104] proposed the formation of p-$O_2NC_6H_4N_3^-$ radical anion (Equation 2.30) which decomposes by loss of dinitrogen to give the corresponding phenylnitrene anion as a short-lived, unobserved intermediate (Equation 2.31). The formation of the dimeric

dianion $4,4'\text{-}O_2NC_6H_4N\text{=}NC_6H_4NO_2^{2-}$ is presumed to go through the dimerization of either p-$O_2NC_6H_4N_3^{-}$ (Equation 2.32) or p-$O_2NC_6H_4N^{-}$ (Equation 2.33).

$$p\text{-}O_2NC_6H_4N_3 + e^- \rightleftharpoons p\text{-}O_2NC_6H_4N_3^{\bullet-} \tag{2.30}$$

$$p\text{-}O_2NC_6H_4N_3^{\bullet-} \longrightarrow p\text{-}O_2NC_6H_4N^{\bullet-} + N_2 \tag{2.31}$$

$$2\,p\text{-}O_2NC_6H_4N_3^{\bullet-} \longrightarrow$$

$$4,4'\text{-}O_2NC_6H_4N\text{=}NC_6H_4NO_2^{2-} + 2N_2 \tag{2.32}$$

$$p\text{-}O_2NC_6H_4N^{\bullet-} \longrightarrow$$

$$4,4'\text{-}O_2NC_6H_4N\text{=}NC_6H_4NO_2^{2-} \tag{2.33}$$
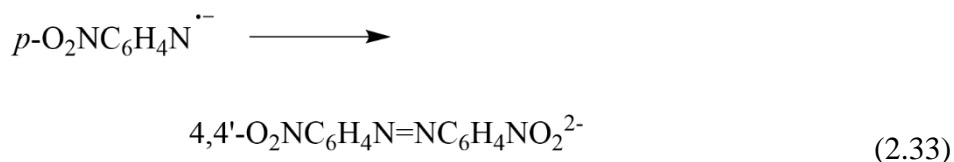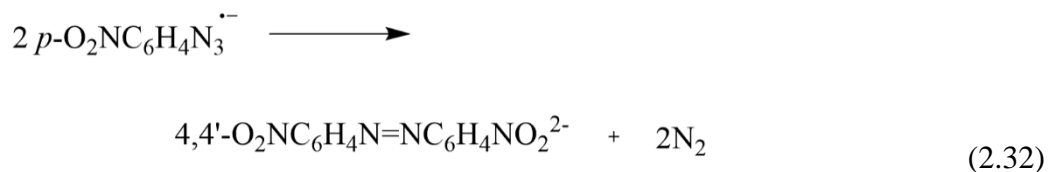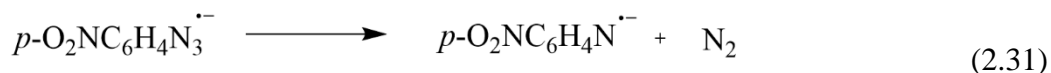
The proclivity of these anion radicals to undergo carbonyl addition/radical β-fragmentation reaction was also tested by controlled-potential electrolysis of p-$O_2NC_6H_4N_3$ in the presence of excess 2,3-butanedione, $(CH_3CO)_2$. The product p-$O_2NC_6H_4N\text{-}COCH_3$ obtained after the electrolysis was again presumed to have formed via one of the two intermediates shown in Equations 2.34 and 2.35.

$$2\,p\text{-}O_2NC_6H_4N_3^{\bullet-} + (CH_3CO)_2 \longrightarrow$$

$$4,4'\text{-}O_2NC_6H_4NCOCH_3^{-} + CH_3CO^{\bullet} + N_2 \tag{2.34}$$

$$2\,p\text{-}O_2NC_6H_4N^{\bullet-} + (CH_3CO)_2 \longrightarrow$$

$$4,4'\text{-}O_2NC_6H_4NCOCH_3^{-} + CH_3CO^{\bullet} \tag{2.35}$$

70
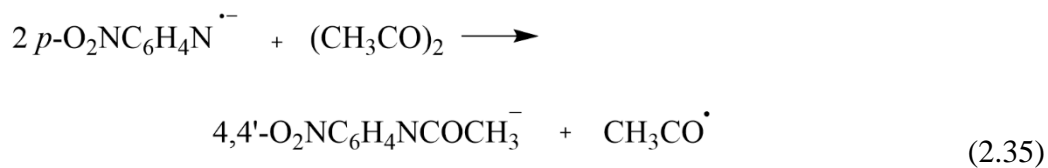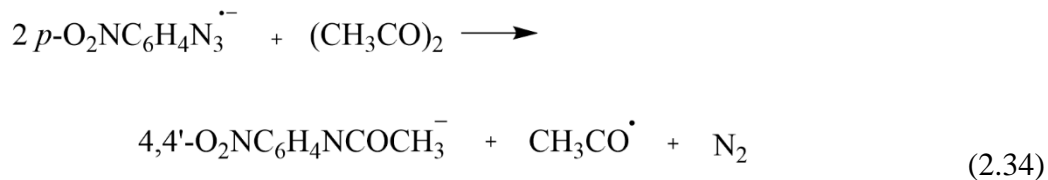
Some other experimental evidence provided by the authors for the formation of the radical anions $p\text{-}O_2NC_6H_4N_3^-$ and $p\text{-}O_2NC_6H_4N^-$ were observed during diazo transfer reactions with diethyl malonate and the formation of $p\text{-}O_2NC_6H_4N\text{-}CON(CO_3)_2$ in DMF.

Van Galen, Barnes, and Hawley[105] also observed evidence for the formation of tosylnitrene dianion radical $Fl=NNTs^{2-}$ during the electrochemical reduction of fluorenone tosylhydrazone anion ($Fl=NNTs^-$). The dianion radical was found to be stable on the cyclic voltammetry timescale ($ip,a/ip,c = 1.0$) in DMF-0.1 F $(n\text{-}Bu)_4NClO_4$, and could be readily protonated in the coulometric time scale or in the presence of proton donors with $pKa < 29$. Furthermore, the reduction of $Fl=NNTs^-$ yielded the expected product $F1=NH$ which further reduced reversibly to $Fl=NH^-$ radical anion on the cyclic voltammetric time scale in the absence of added proton donors.

The product studies of the decomposition reaction of $Fl=NNTs^{2-}$ on the coulometric scale, afforded the products $F1NH_2$ and $TsNH_2$, and the pathway for their formation was proposed to go through the TsN^- radical anion species. Although attempts to capture TsN^- were unsuccessful, the data was consistent with the formation of TsN^- which was presumed to rapidly undergo hydrogen atom abstraction, proton abstraction or other types of reactions in the condensed phase.

Formation of nitrene radical anion intermediates was also proposed by Murata, Nakatsuji, and Tomioka[106] during pyrene-sensitized photolysis studies of p-butylphenyl azide in the presence of diethylamine (DEA). The photolysis product p-butylaniline was proposed to form via one electron reduction of the azide to give the azide radical anion which then loses a dinitrogen to produce the nitrene radical anion. The nitrene radical anion would then undergo proton and hydrogen atom abstraction to yield the final aniline. The authors also proposed that the one electron reduction of the p-butylphenyl azide was carried out by the pyrene radical anion (Py^-) formed by electron transfer from DEA to the excited pyrene (Py^*), as shown in Scheme 2.6.

Scheme 2.6
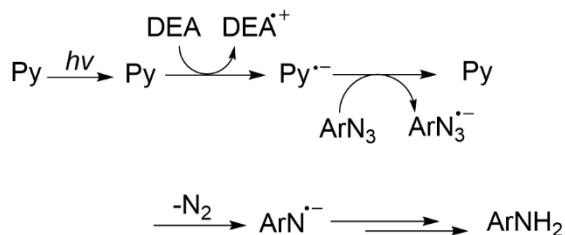
Mudgal et al.[108] studied the formation of an important biomolecule radical, aminyl radical (RNH) in 3′-azidothymidine (3'-AZT) (Figure 2.11), 2′-azido-2′-deoxyuridine (2′-AZdU), 4′-azido-2′-deoxycytidine (4′-AZ-2′-dC), methyl 2-azido-2-deoxy-α-D-lyxofuranoside, and methyl 2-azido-2-deoxy-β-D-ribofuranoside.[109] The sugars were subjected to one electron reduction by radiation-produced prehydrated electrons which resulted in the formation of the corresponding, highly unstable azide anion radicals. Similar to examples discussed earlier, the azide anion radicals then underwent subsequent dinitrogen elimination to yield the corresponding nitrene anion radicals which led to rapid protonation to form RNH.
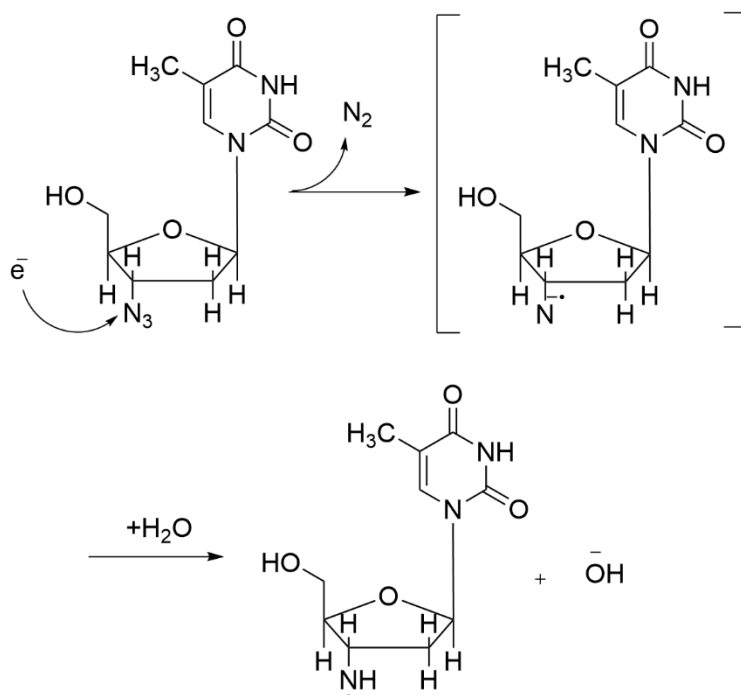
Figure 2.11 Formation of aminyl radical RNH from 3'-AZT via one-electron reduction[108]

Using ultraviolet and 1H NMR experiments, Perrotta and Falvey[107] characterized several ion-diradicals with low energy triplet states. Although not predicted to be the ground state, the authors found that sufficiently strong electron-withdrawing groups could lower the energy of the triplet state enough to create a population of triplet anilide (imide) anions. For example, 3,5-dinitroanilide anion, 4, was found to have paramagnetic behavior indicating a triplet electronic state.
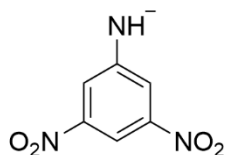
4

2.8 Conclusion

Advancements in techniques such as laser photolysis and flash vacuum pyrolysis with very short contact times and cryomatrices at temperatures of 2-4 K have enabled the generation and isolation of numerous nitrenes and primary radical intermediates. Developments in spectroscopic techniques have helped in their identification and characterization. The electronic states of many nitrenes along with their reactivities have also been identified. However, much work remains to be done to fully understand the factors that govern their energies, correlations, structures, and tunneling reactions that involve intersystem crossing and mixing of electronic states. The biggest challenge associated with these studies is the accessibility to the always decomposing nitrene intermediates.

Nitrene anions serving as protected nitrene intermediates offer easy access to spectroscopically probe their neutral counterparts because of their reluctance to undergo rearrangement reactions. Nitrene anions also exhibit their own unique reactivity. Thus, investigations into nitrene anions should go hand in hand with the development of nitrene chemistry.

2.9 References

1. Dequirez, G.; Pons, V.; Dauban, P., Nitrene Chemistry in Organic Synthesis: Still in Its Infancy? Angewandte Chemie International Edition 2012, 51 (30), 7384-7395.

2. Iddon, B.; Meth-Cohn, O.; Scriven, E. F. V.; Suschitzky, H.; Gallagher, P. T., Developments in Arylnitrene Chemistry: Syntheses and Mechanisms [New synthetic methods (31)]. Angewandte Chemie International Edition in English 1979, 18 (12), 900-917.

3. Wang, Y.-C.; Lai, X.-J.; Huang, K.; Yadav, S.; Qiu, G.; Zhang, L.; Zhou, H., Unravelling nitrene chemistry from acyclic precursors: recent advances and challenges. Organic Chemistry Frontiers 2021, 8 (7), 1677-1693.

4. Fleming, S., Chemical reagents in photoaffinity labeling. Tetrahedron 1995, 51 (46), 12479-12520.

5. Kotzyba-Hibert, F.; Kapfer, I.; Goeldner, M., Recent Trends in Photoaffinity Labeling. Angewandte Chemie International Edition in English 1995, 34 (12), 1296-1312.

6. Schock, M.; Bräse, S., Reactive & Efficient: Organic Azides as Cross-Linkers in Material Sciences. Molecules 2020, 25 (4), 1009.

7. Meyer, D. M.; Roth, K. C., Discovery of Interstellar NH. The Astrophysical Journal 1991, 376, L49.

8. Bach, R. D.; Su, M. D.; Aldabbagh, E.; Andres, J. L.; Schlegel, H. B., A theoretical model for the orientation of carbene insertion into saturated hydrocarbons and the origin of the activation barrier. Journal of the American Chemical Society 1993, 115 (22), 10237-10246.

9. Closs, G. L.; Closs, L. E., Induced dynamic nuclear spin polarization in reactions of photochemically and thermally generated triplet diphenylmethylene. Journal of the American Chemical Society 1969, 91 (16), 4549-4550.

10. Hirai, K.; Komatsu, K.; Tomioka, H., Reactions and Kinetics of (2,4,6-Tri-tert-butylphenyl)phenylcarbene. Chemistry Letters 1994, 23 (3), 503-506.

11. Sander, W.; Kirschfeld, A.; Kappert, W.; Muthusamy, S.; Kiselewsky, M., Dimesitylketone O-Oxide: First NMR Spectroscopic Characterization of a Carbonyl O-Oxide. Journal of the American Chemical Society 1996, 118 (27), 6508-6509.

12. Meijer, E. W.; Nijhuis, S.; Van Vroonhoven, F. C. B. M., Poly-1,2-azepines by the photopolymerization of phenyl azides. Precursors for conducting polymer films. Journal of the American Chemical Society 1988, 110 (21), 7209-7210.

13. Platz, M. S., Comparison of Phenylcarbene and Phenylnitrene. Acc. Chem. Res. 1995, 28 (12), 487-492.

14. Wang, J.; Burdzinski, G.; Platz, M. S., Ultrafast Time-Resolved Studies of the Photochemistry of Aryl Azides. In Nitrenes and Nitrenium Ions, Falvey, D. E.; Gudmundsdottir, A. D., Eds. John Wiley & Sons, Inc.: Hoboken, New Jersey, 2013; pp 1-31.

15. Gritsan, N. P.; Platz, M. S., Kinetics and spectroscopy of substituted phenylnitrenes. In Advances in Physical Organic Chemistry, Richard, J. P.; Tidwell, T. T., Eds. Academic Press: 2001; Vol. 36, pp 255-304.

16. Cullin, D. W.; Soundararajan, N.; Platz, M. S.; Miller, T. A., Laser-induced fluorescence spectrum of the cyanocyclopentadienyl radical: a band system long attributed to triplet phenylnitrene. J. Phys. Chem. 1990, 94 (26), 8890-8896.

17. Wentrup, C., Thermochemistry of carbene and nitrene rearrangements. Tetrahedron 1974, 30 (10), 1301-1311.

18. Wentrup, C.; Crow, W. D., Pyrolysis of 1(H)-triazoloarenes: Ring contraction to 5-ring nitriles, and CN-group migration. Tetrahedron 1970, 26 (16), 3965-3981.

19. Travers, M. J.; Cowles, D. C.; Clifford, E. P.; Ellison, G. B.; Engelking, P. C., Photoelectron spectroscopy of the CH3N− ion. J. Chem. Phys. 1999, 111 (12), 5349-5360.

20. Wentrup, C., Matrix Studies on Aromatic and Heteroaromatic Nitrenes and their Rearrangements. In Nitrenes and Nitrenium Ions, Falvey, D. E.; Gudmundsdottir, A. D., Eds. John Wiley & Sons, Inc.: Hoboken, New Jersey, 2013; pp 273-315.

21. Nunes, C. M.; Knezz, S. N.; Reva, I.; Fausto, R.; McMahon, R. J., Evidence of a Nitrene Tunneling Reaction: Spontaneous Rearrangement of 2-Formyl Phenylnitrene to an Imino Ketene in Low-Temperature Matrixes. J. Am. Chem. Soc. 2016, 138 (47), 15287-15290.

22. Chapyshev, S. V.; Wentrup, C., Properties of Triplet Tetrachloro-4-pyridylnitrene Isolated in Inert Matrices. Chem. Heterocycl. Compd. (N. Y., NY, U. S.) 2001, 37 (9), 1119-1129.

23. Maltsev, A.; Bally, T.; Tsao, M.-L.; Platz, M. S.; Kuhn, A.; Vosswinkel, M.; Wentrup, C., The Rearrangements of Naphthylnitrenes: UV/Vis and IR Spectra of Azirines, Cyclic Ketenimines, and Cyclic Nitrile Ylides. J. Am. Chem. Soc. 2004, 126 (1), 237-249.

24. Inui, H.; Irisawa, M.; Oishi, S., Reaction of (4-Nitorophenyl)nitrene with Molecular Oxygen in Low-temperature Matrices: First IR Detection and Photochemistry of Aryl Nitroso Oxide. Chem. Lett. 2005, 34 (4), 478-479.

25. Gritsan, N. P.; Platz, M. S., Kinetics, Spectroscopy, and Computational Chemistry of Arylnitrenes. Chem. Rev. (Washington, DC, U. S.) 2006, 106 (9), 3844-3867.

26. Burdzinski, G. T.; Gustafson, T. L.; Hackett, J. C.; Hadad, C. M.; Platz, M. S., The Direct Detection of an Aryl Azide Excited State: An Ultrafast Study of the Photochemistry of para- and ortho-Biphenyl Azide. J. Am. Chem. Soc. 2005, 127 (40), 13764-13765.

27. Burdzinski, G.; Hackett, J. C.; Wang, J.; Gustafson, T. L.; Hadad, C. M.; Platz, M. S., Early Events in the Photochemistry of Aryl Azides from Femtosecond UV/Vis Spectroscopy and Quantum Chemical Calculations. J. Am. Chem. Soc. 2006, 128 (41), 13402-13411.

28. Broadus, K. M.; Kass, S. R., The Electron as a Protecting Group. 3. Generation of Acenaphthyne Radical Anion and the Determination of the Heat of Formation of a Strained Cycloalkyne. J. Am. Chem. Soc. 2001, 123 (18), 4189-4196.

29. Broadus, K. M.; Kass, S. R., The Electron as a Protecting Group. 2. Generation of Benzocyclobutadiene Radical Anion in the Gas Phase and an Experimental Determination of the Heat of Formation of Benzocyclobutadiene. J. Am. Chem. Soc. 2000, 122 (43), 10697-10703.

30. Reed, D. R.; Hare, M.; Kass, S. R., Formation of Gas-Phase Dianions and Distonic Ions as a General Method for the Synthesis of Protected Reactive Intermediates. Energetics of 2,3- and 2,6-Dehydronaphthalene. J. Am. Chem. Soc. 2000, 122 (43), 10689-10696.

31. Wenthold, P. G.; Hu, J.; Squires, R. R., Regioselective Synthesis of Biradical Negative Ions in the Gas Phase. Generation of Trimethylenemethane, m-Benzyne, and p-Benzyne Anions. J. Am. Chem. Soc. 1994, 116 (15), 6961-6962.

32. Wenthold, P. G.; Kim, J. B.; Lineberger, W. C., Photoelectron Spectroscopy of m-Xylylene Anion. J. Am. Chem. Soc. 1997, 119 (6), 1354-1359.

33. Wenthold, P. G.; Squires, R. R.; Lineberger, W. C., Ultraviolet Photoelectron Spectroscopy of the o-, m-, and p-Benzyne Negative Ions. Electron Affinities and Singlet−Triplet Splittings for o-, m-, and p-Benzyne. Journal of the American Chemical Society 1998, 120 (21), 5279-5290.

34. Wenthold, P. G.; Hu, J.; Squires, R. R.; Lineberger, W. C., Photoelectron Spectroscopy of the Trimethylene- methane Negative Ion. The Singlet−Triplet Splitting of Trimethylenemethane. J. Am. Chem. Soc. 1996, 118 (2), 475-476.

35. Wenthold, P. G.; Polak, M. L.; Lineberger, W. C., Photoelectron Spectroscopy of the Allyl and 2-Methylallyl Anions. J. Phys. Chem. 1996, 100 (17), 6920-6926.

36. Hare, M.; Emrick, T.; Eaton, P. E.; Kass, S. R., Cubyl Anion Formation and an Experimental Determination of the Acidity and C−H Bond Dissociation Energy of Cubane. J. Am. Chem. Soc. 1997, 119 (1), 237-238.

37. Ervin, K. M.; Gronert, S.; Barlow, S. E.; Gilles, M. K.; Harrison, A. G.; Bierbaum, V. M.; DePuy, C. H.; Lineberger, W. C.; Ellison, G. B., Bond strengths of ethylene and acetylene. J. Am. Chem. Soc. 1990, 112 (15), 5750-5759.

38. Davico, G. E.; Bierbaum, V. M.; DePuy, C. H.; Ellison, G. B.; Squires, R. R., The C-H Bond Energy of Benzene. J. Am. Chem. Soc. 1995, 117 (9), 2590-2599.

39. P. Clifford, E.; G. Wenthold, P.; Carl Lineberger, W.; Barney Ellison, G.; X. Wang, C.; J. Grabowski, J.; Vila, F.; D. Jordan, K., Properties of tetramethyleneethane (TME) as revealed by ion chemistry and ion photoelectron spectroscopy. J. Chem. Soc., Perkin Trans. 2 1998, (5), 1015-1022.

40. McDonald, R. N.; Chowdhury, A. K., Hypovalent radicals. 7. Gas-phase generation of phenylnitrene anion radical and its reaction with phenyl azide. J. Am. Chem. Soc. 1980a, 102 (15), 5118-5119.

41. Wijeratne, N. R.; Munsch, T. E.; Haupert, L. J.; Wenthold, P. G., Thermochemical studies of substituted phenylnitrenes: Enthalpies of formation of chlorophenylnitrenes. J. Chem. Thermodyn. 2014, 73, 213-217.

42. Rau, N. J.; Wenthold, P. G., The low-lying triplet state in p-nitrobenzaldimide. Int. J. Mass Spectrom. 2015, 377, 496-501.

43. McDonald, R. N.; Chowdhury, A. K., Hypovalent radical. Part 12. Gas-phase ion-molecule reactions of phenylnitrene anion radical with certain .alpha.,.beta.-unsaturated molecules. A study of 1,2- vs. 1,4-addition mechanisms. J. Phys. Chem. 1982, 86 (18), 3641-3645.

44. McDonald, R. N.; Chowdhury, A. K., Gas-phase nucleophilic addition reactions of phenylnitrene anion radical with certain carbonyl-containing molecules. J. Am. Chem. Soc. 1981, 103 (3), 674-676.

45. Wijeratne, N. R.; Wenthold, P. G., Benzoylnitrene Radical Anion: A New Reagent for the Generation of M-2H Anions. J. Am. Soc. Mass Spectrom. 2007a, 18 (11), 2014-2016.

46. Pellerite, M. J.; Brauman, J. I., Gas-phase ion-molecule reactions of phenylnitrene anion. J. Am. Chem. Soc. 1981, 103 (3), 676-677.

47. McDonald, R. N.; Chowdhury, A. K.; Setser, D. W., Gas-phase generation of phenylnitrene anion radical – proton affinity and $\Delta H°f$ of PhN-• and its clustering with ROH molecules. J. Am. Chem. Soc. 1981, 103 (22), 6599-6603.

48. McDonald, R. N.; Chowdhury, A. K., Hypovalent radicals. 8. Identification of nucleophilic 1,2- and 1,4-addition processes with .alpha.,.beta.-unsaturated molecules in the gas phase. J. Am. Chem. Soc. 1980b, 102 (19), 6146-6147.

49. McDonald, R. N.; Chowdhury, A. K., Hypovalent radicals. 13. Gas-phase nucleophilic reactivities of phenylnitrene (PhN-•) and sulfur anion radicals (S-•) at sp3 and carbonyl carbon. J. Am. Chem. Soc. 1983, 105 (2), 198-207.

50. Borden, W. T.; Gritsan, N. P.; Hadad, C. M.; Karney, W. L.; Kemnitz, C. R.; Platz, M. S., The Interplay of Theory and Experiment in the Study of Phenylnitrene. Acc. Chem. Res. 2000, 33 (11), 765-771.

51. Johnson, W. T. G.; Sullivan, M. B.; Cramer, C. J., meta and para substitution effects on the electronic state energies and ring-expansion reactivities of phenylnitrenes. Int. J. Quantum Chem. 2001, 85 (4-5), 492-508.

52. Salem, L.; Rowland, C., The Electronic Properties of Diradicals. Angew. Chem., Int. Ed. Engl. 1972, 11 (2), 92-111.

53. Wijeratne, N. R.; Fonte, M. D.; Ronemus, A.; Wyss, P. J.; Tahmassebi, D.; Wenthold, P. G., Photoelectron Spectroscopy of Chloro-Substituted Phenylnitrene Anions. J. Phys. Chem. A 2009, 113 (34), 9467-9473.

54. Falvey, D. E., Nitrenium Ions. React. Intermed. Chem. 2003, 593-650.

55. Albini, A.; Bettinetti, G.; Minoli, G., Photodecomposition of Some Para-Substituted 2-Pyrazolylphenyl Azides. Substituents Affect the Phenylnitrene S−T Gap More Than the Barrier to Ring Expansion. J. Am. Chem. Soc. 1999, 121 (13), 3104-3113.

56. Rau, N. J.; Welles, E. A.; Wenthold, P. G., Anionic Substituent Control of the Electronic Structure of Aromatic Nitrenes. J. Am. Chem. Soc. 2013, 135 (2), 683-690.

57. Koirala, D.; Poole, J. S.; Wenthold, P. G., Reactivity of 3- and 4-pyridinylnitrene-n-oxide radical anions. Int. J. Mass Spectrom. 2015, 378, 69-75.

58. Mazeau, J.; Gresteau, F.; Hall, R. I.; Huetz, A., Energy and width of N-(3P) from observation of its formation by dissociative attachment to N2 and NO. Journal of Physics B: Atomic and Molecular Physics 1978, 11 (18), L557-L560.

59. Al-Za'al, M.;   Miller, H. C.; Farley, J. W., Observation of metastable states in the autodetachment continuum of the negative molecular ion NH−. Chem. Phys. Lett. 1986, 131 (1), 56-59.

60. Engelking, P. C.; Lineberger, W. C., Laser photoelectron spectrometry of NH−: Electron affinity and intercombination energy difference in NH. J. Chem. Phys. 1976, 65 (10), 4323-4324.

61. Lykke, K. R.; Murray, K. K.; Neumark, D. M.; Lineberger, W. C., High-Resolution Studies of Autodetachment in Negative Ions. Philos. Trans. R. Soc., A 1988, 324 (1578), 179-196.

62. Neumark, D. M.; Lykke, K. R.; Andersen, T.; Lineberger, W. C., Infrared spectrum and autodetachment dynamics of NH−. J. Chem. Phys. 1985, 83 (9), 4364-4373.

63. Srivastava, S.; Sathyamurthy, N., Ab Initio Potential Energy Curves for the Ground and Low Lying Excited States of NH– and the Effect of 2Σ± States on Λ-Doubling of the Ground State X2Π. J. Phys. Chem. A 2013, 117 (36), 8623-8631.

64. Al-Za'al, M.;   Miller, H. C.; Farley, J. W., High-resolution measurement of the infrared rotation-vibration spectrum of the negative molecular ion 14NH-. Physical Review A 1987, 35 (3), 1099-1112.

65. Miller, H. C.; Al-Za'al, M.; Farley, J. W., Measurement of Hyperfine Structure in the Infrared Rotation-Vibration Spectrum of NH-. Phys. Rev. Lett. 1987, 58 (20), 2031-2034.

66. Travers, M. J.; Cowles, D. C.; Clifford, E. P.; Ellison, G. B., Photoelectron spectroscopy of the phenylnitrene anion. J. Am. Chem. Soc. 1992, 114 (22), 8699-8701.

67. Drzaic, P. S.; Brauman, J. I., A determination of the triplet-singlet splitting in phenylnitrene via photodetachment spectroscopy. J. Am. Chem. Soc. 1984a, 106 (12), 3443-3446.

68. Drzaic, P. S.; Brauman, J. I., Electron photodetachment from phenylnitrene, anilide, and benzyl anions. Electron affinities of the anilino and benzyl radicals and phenyl nitrene. J. Phys. Chem. 1984b, 88 (22), 5285-5290.

69. McDonald, R. N.; Davidson, S. J., Electron photodetachment of the phenylnitrene anion radical: EA, ΔH°f , and the singlet-triplet splitting for phenylnitrene. J. Am. Chem. Soc. 1993, 115 (23), 10857-10862.

70. Celotta, R. J.; Bennett, R. A.; Hall, J. L., Laser photodetachment determination of the electron affinities of OH, NH2, NH, SO2, and S2. J. Chem. Phys. 1974, 60 (5), 1740-1745.

71. Rohrer, F.; Stuhl, F., The 193 (and 248) nm photolysis of HN3: Formation and internal energy distributions of the NH (a 1Δ, b 1∑+, A 3Π, and c 1Π) states. J. Chem. Phys. 1988, 88 (8), 4788-4799.

72. Sadygov, R. G.; Yarkony, D. R., Electronic structure aspects of the spin-forbidden reaction CH3(X 2A2″)+N(4S)→HCN(X 1Σ+)+H2(X 1Σg+). J. Chem. Phys. 1997, 107 (13), 4994-4999.

73. Leermakers, J. A., The Thermal Decomposition of Methyl Azide. A Homogeneous Unimolecular Reaction. J. Am. Chem. Soc. 1933, 55 (8), 3098-3105.

74. Bock, H.; Dammel, R., The Pyrolysis of Azides in the Gas Phase. Angew. Chem., Int. Ed. Engl. 1987, 26 (6), 504-526.

75. Winkler, M., Singlet−Triplet Energy Splitting and Excited States of Phenylnitrene. J. Phys. Chem. A 2008, 112 (37), 8649-8653.

76. Alexander, M. L.; Johnson, M. A.; Levinger, N. E.; Lineberger, W. C., Photodissociation of Mass-Selected (CO2)n- Clusters: Evaporation Leading to Magic Numbers in Fragment-Ion Distributions. Phys. Rev. Lett. 1986, 57 (8), 976-979.

77. Weber, J. M.; Robertson, W. H.; Johnson, M. A., Argon predissociation and electron autodetachment spectroscopy of size-selected CH3NO2−·Arn clusters. J. Chem. Phys. 2001, 115 (23), 10718-10723.

78. Metz, R. B.; Weaver, A.; Bradforth, S. E.; Kitsopoulos, T. N.; Neumark, D. M., Probing the transition state with negative ion photodetachment: the chlorine atom + hydrogen chloride and bromine atom + hydrogen bromide reactions. J. Phys. Chem. 1990, 94 (4), 1377-1388.

79. Karney, W. L.; Borden, W. T., Ab Initio Study of the Ring Expansion of Phenylnitrene and Comparison with the Ring Expansion of Phenylcarbene. J. Am. Chem. Soc. 1997, 119 (6), 1378-1387.

80. Hossain, E.; Deng, S. M.; Gozem, S.; Krylov, A. I.; Wang, X.-B.; Wenthold, P. G., Photoelectron Spectroscopy Study of Quinonimides. J. Am. Chem. Soc. 2017, 139 (32), 11138-11148.

81. Ferreira, K. N.; Iverson, T. M.; Maghlaoui, K.; Barber, J.; Iwata, S., Architecture of the Photosynthetic Oxygen-Evolving Center. Science (Washington, DC, U. S.) 2004, 303 (5665), 1831-1838.

82. Srinivasan, N.; Golbeck, J. H., Protein–cofactor interactions in bioenergetic complexes: The role of the A1A and A1B phylloquinones in Photosystem I. Biochim. Biophys. Acta, Bioenerg. 2009, 1787 (9), 1057-1088.

83. Barrès, A.-L.; Geng, J.; Bonnard, G.; Renault, S.; Gottis, S.; Mentré, O.; Frayret, C.; Dolhem, F.; Poizot, P., High-Potential Reversible Li Deintercalation in a Substituted Tetrahydroxy-p-benzoquinone Dilithium Salt: An Experimental and Theoretical Study. Chem. - Eur. J. 2012, 18 (28), 8800-8812.

84. Popp, B. V.; Stahl, S. S., Palladium-Catalyzed Oxidation Reactions: Comparison of Benzoquinone and MolecularOxygen as Stoichiometric Oxidants. In Organometallic Oxidation Catalysis, Meyer, F.; Limberg, C., Eds. Springer: Berlin, Heidelberg, 2007; pp 149-189.

85. Bartmess, J. E.; McIver, R. T., Chapter 11 - The gas-phase acidity scale. In Gas Phase Ion Chemistry, Bowers, M. T., Ed. Academic Press: 1979; pp 87-121.

86. Chacko, S. A.; Wenthold, P. G., The negative ion chemistry of nitric oxide in the gas phase. Mass Spectrom. Rev. 2006, 25 (1), 112-126.

87. Creary, X., Super Radical Stabilizers. Acc. Chem. Res. 2006, 39 (10), 761-771.

88. Hossain, E.; Wenthold, P. G., Singlet stabilization of oxazole- and isoxazolenitrene-n-oxides by radical delocalization. Comput. Theor. Chem. 2013, 1020, 180-186.

89. Wenthold, P. G., Spin-State Dependent Radical Stabilization in Nitrenes: The Unusually Small Singlet–Triplet Splitting in 2-Furanylnitrene. J. Org. Chem. 2012, 77 (1), 208-214.

90. Yoshimura, T.; Asada, K.; Oae, S., Deoxygenation of Tertiary Amine Oxides with Carbon Bisulfide. Bull. Chem. Soc. Jpn. 1982, 55 (9), 3000-3003.

91. Wenthold, P. G.; Squires, R. R., Gas-Phase Properties and Reactivity of the Acetate Radical Anion. Determination of the C-H Bond Strengths in Acetic Acid and Acetate Ion. J. Am. Chem. Soc. 1994, 116 (26), 11890-11897.

92. Hammad, L. A.; Wenthold, P. G., An Electron-Catalyzed Cope Cyclization. The Structure of the 2,5-Dicyano-1,5-hexadiene Radical Anion in the Gas Phase. J. Am. Chem. Soc. 2003, 125 (36), 10796-10797.

93. Wijeratne, N. R.; Wenthold, P. G., Structure and Reactivity of Benzoylnitrene Radical Anion in the Gas Phase. J. Org. Chem. 2007b, 72 (25), 9518-9522.

94. Wijeratne, N. R.; Wenthold, P. G., Thermochemical Studies of Benzoylnitrene Radical Anion: The N−H Bond Dissociation Energy in Benzamide in the Gas Phase. J. Phys. Chem. A 2007c, 111 (42), 10712-10716.

95. Pritchina, E. A.; Gritsan, N. P.; Bally, T., Ground state multiplicity of acylnitrenes: computational and experimental studies. Russ. Chem. Bull. 2005, 54 (3), 525-532.

96. Autrey, T.; Schuster, G. B., Are aroylnitrenes ground-state singlets? Photochemistry of .beta.-naphthoyl azide. J. Am. Chem. Soc. 1987, 109 (19), 5814-5820.

97. Gritsan, N. P.; Pritchina, E. A., Are aroylnitrenes species with a singlet ground state? Mendeleev Commun. 2001, 11 (3), 94-95.

98. Pritchina, E. A.; Gritsan, N. P.; Maltsev, A.; Bally, T.; Autrey, T.; Liu, Y.; Wang, Y.; Toscano, J. P., Matrix isolation, time-resolved IR, and computational study of the photochemistry of benzoyl azide. Phys. Chem. Chem. Phys. 2003, 5 (6), 1010-1018.

99. Lee, J.; Grabowski, J. J., Reactions of the atomic oxygen radical anion and the synthesis of organic reactive intermediates. Chem. Rev. (Washington, DC, U. S.) 1992, 92 (7), 1611-1647.

100. Ervin, K. M., Experimental Techniques in Gas-Phase Ion Thermochemistry. Chem. Rev. (Washington, DC, U. S.) 2001, 101 (2), 391-444.

101. Berkowitz, J.; Ellison, G. B.; Gutman, D., Three methods to measure RH bond energies. J. Phys. Chem. 1994, 98 (11), 2744-2765.

102. Blanksby, S. J.; Ellison, G. B., Bond Dissociation Energies of Organic Molecules. Acc. Chem. Res. 2003, 36 (4), 255-263.

103. Linstrom, P. J.; Mallard, W. G., NIST Chemistry WebBook. National Institute of Standards and Technology: Gaithersburg, MD, 2018.

104. Herbranson, D. E.; Hawley, M. D., Electrochemical reduction of p-nitrophenyl azide: evidence consistent with the formation of p-nitrophenylnitrene anion radical as a short-lived intermediate. J. Org. Chem. 1990, 55 (14), 4297-4303.

105. Van Galen, D. A.; Barnes, J. H.; Hawley, M. D., The electrochemical reduction of fluorenone tosylhydrazone. Evidence consistent with the formation to the tosyl nitrene anion radical. J. Org. Chem. 1986, 51 (13), 2544-2550.

106. Murata, S.; Nakatsuji, R.; Tomioka, H., Mechanistic studies of pyrene-sensitized decomposition of p-butylphenyl azide: generation of nitrene radical anion through a sensitizer-mediated electron transfer from amines to the azide. J. Chem. Soc., Perkin Trans. 2 1995, (4), 793-799.

107. Perrotta, R. R.; Falvey, D. E., The 3,5-dinitroanilide anion: a singlet anilide anion with evidence for a thermally accessible triplet state. J. Phys. Org. Chem. 2013, 26 (9), 699-706.

108. Mudgal, M.; Rishi, S.; Lumpuy, D. A.; Curran, K. A.; Verley, K. L.; Sobczak, A. J.; Dang, T. P.; Sulimoff, N.; Kumar, A.; Sevilla, M. D.; Wnuk, S. F.; Adhikary, A., Prehydrated One-Electron Attachment to Azido-Modified Pentofuranoses: Aminyl Radical Formation, Rapid H-Atom Transfer, and Subsequent Ring Opening. J. Phys. Chem. B 2017, 121 (19), 4968-4980.

109. Adhikary, A.; Khanduri, D.; Pottiboyina, V.; Rice, C. T.; Sevilla, M. D., Formation of Aminyl Radicals on Electron Attachment to AZT: Abstraction from the Sugar Phosphate Backbone versus One-Electron Oxidation of Guanine. J. Phys. Chem. B 2010, 114 (28), 9289-9299.

CHAPTER 3. GAS-PHASE PYROLYSIS OF ANISOLE, GUAIACOL, AND DIMETHOXYBENZENE BY COLLISION-INDUCED DISSOCIATION CHARGE-REMOTE FRAGMENTATION MASS SPECTROMETRY

3.1 Introduction

Lignin is a plant biopolymer that can be converted into bio-oil under high temperatures and in the absence of oxygen through a process called fast pyrolysis, and the bio-oil can be catalytically upgraded into second-generation renewable fuel or used as chemical building blocks. [1-5] However, polycyclic aromatic hydrocarbons (PAHs) also form during lignin pyrolysis, which poison catalysts and make upgrading bio-oil difficult.[6-8] PAHs are thought to grow from a high concentration of radical precursors present during fast pyrolysis.[9] Identifying the thermolytic mechanisms by which these radical intermediates form is key to making fast pyrolysis a viable chemical and energy source.

Radical formation is commonly thought to begin with cleavage of the etheric β-O-4 bond that composes 60 percent of the total bonds in some hardwood lignin.[10-12] Thermolysis of the β-O-4 bond is thought to occur through direct bond dissociation to form phenoxy radical (Scheme 3.1). Under fast pyrolysis conditions, phenoxy radical then continues to dissociate via routes that are dependent on the substituents present around the aromatic ring.

Scheme 3.1
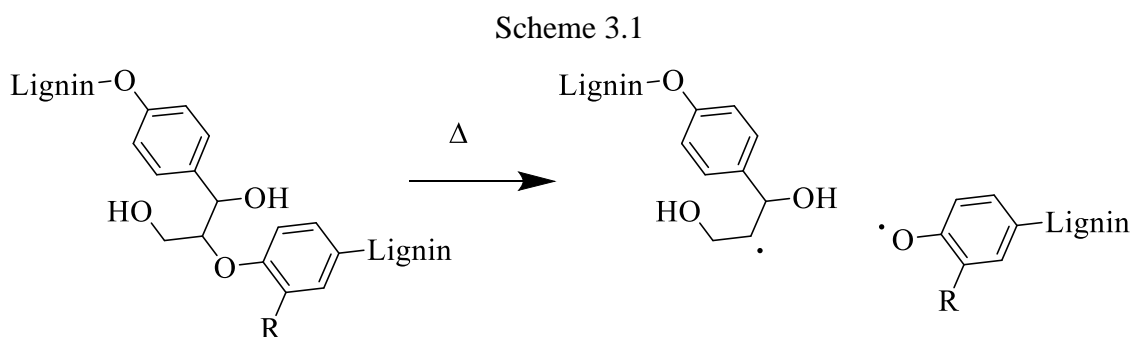
Smaller model compounds containing the same moieties and linkages as lignin can be used to study how lignin breaks down in the gas phase.[13-16] Therefore, anisole (**A1**), guaiacol (**G1**), and *ortho*-dimethoxybenzene (**O1**), and *meta*-dimethoxybenzene (**M1)** are commonly used for

modeling lignin because they dissociate into phenoxy radicals (**A2-M2**) when heated and contain common functional groups (H, OH and OCH$_3$) that are found throughout lignin (Scheme 3.2).[9, 10]

Scheme 3.2
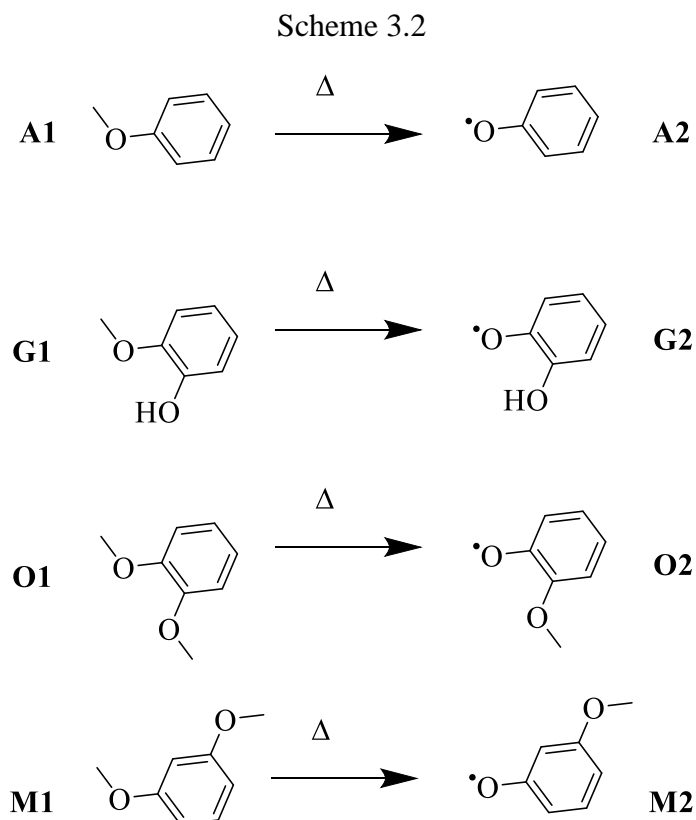
Many methods have been used to study the behavior of lignin pyrolysis products in the gas phase.[7, 8, 17] However, the occurrence of bimolecular reactions often creates a problem because they interfere with the detection of primary pyrolysis products. Minimizing bimolecular reactions is usually done by decreasing the concentration of the sample, but this has a negative effect on sensitivity. Other ways of preventing product recombination include the laser ablation of samples with short pulses to shorten heating times, and the cooling of primary products using supersonic expansion.[6,18] Alternatively, collision-induced dissociation mass spectrometry (CID-MS) can be used to monitor the step-by-step unimolecular decomposition of lignin model compounds in the gas phase.

Although nominally, CID-MS requires ions for activation and detection, it can be used to examine the dissociation of *neutral* moieties within molecules through "charge-remote" fragmentation, where an inert charge site is separated from the dissociation region. This is in

contrast to generating deprotonated or protonated lignin-like ions, which mainly undergo charge-driven fragmentation patterns.[5] Charge-remote fragmentation (CRF) has been used previously to study fatty acids, steroids, lipids, oligosaccharides, and other biological molecules.[19-22] Now, with the advent of electrospray ionization mass spectrometry for ion generation, it is possible to generate very large ions with ion tags, such that CID-CRF can offer structural information on the degradation of even large neutral compounds without the need of high temperatures and without interference of secondary reactions. In this work, we applied CID-CRF to a series of methoxy-substituted aromatic compounds tagged with SO_3^- to determine their unimolecular routes of decomposition.

3.2   Methods

3.2.1   Materials

Starting materials and solvents were purchased from commercially available sources and used as received. 1,2-dimethoxy-D6-benzene was purchased from CDN Isotopes, Quebec, Canada. Synthetic procedures are given in Chapter 2 of this dissertation.

General Heck Olefination: The synthetic route for attaching a sulfonated styrene tag to the molecules in this work was a Heck reaction using palladium(II) acetate catalyst in DMF/water as described by Khemaïs and coworkers.[14] A 100 mL round bottom flask with a magnetic stir bar was charged with the 4-bromo substrate analog (5 mmol), sodium p-styrenesulfonate hydrate (0.93 g, 4.5 mmol), potassium carbonate (7.5 mmol), palladium(II) acetate (1 mol %, 11.2 mg), Aliquat 336 (1.14 mL, 2.5 mmol), DMF (2 mL), and water (2 mL). The reaction mixture was stirred at 95 °C for 2 hr. After the reaction was completed, 40 mL chloroform was added and the solid was filtered. The solid was rinsed with methanol (100 mL), and the filtrate was collected. The methanol was removed under reduced pressure to give a solid product. The solid was rinsed multiple times with methanol/ethyl acetate (1:10) to remove unreacted p-styrenesulfonate, which was slightly less polar than the target molecule.

^{1}H-NMR spectroscopic data were collected with a Bruker AV-III-400-HD.

A1-$C_8H_6SO_3^-$: ^{1}H-NMR (400 MHz, DMSO-d_6) δ: 7.54 (2H, d, J = 8.4 Hz), 7.53 (2H, d, J = 8.4 Hz), 7.48 (2H, d, J = 8.4 Hz), 7.20 (1H, d, J = 16.4 Hz), 7.07 (1H, d, J = 16.4 Hz), 6.93 (2H, d, J = 8.4 Hz), 3.75 (3H, s).

G1-C$_8$H$_6$SO$_3$$^-$: ^{1}H-NMR (400 MHz, DMSO-d_6) δ: 7.55 (2H, d, J = 8.4 Hz), 7.47 (2H, d, J = 8.4 Hz), 7.19 (1H, d, J = 1.6 Hz), 7.14 (1H, d, J = 16.4 Hz), 7.04 (1H, d, J = 16.4 Hz), 6.97 (1H, dd, J = 8.4, 1.6 Hz), 6.76 (1H, d, J = 8.4 Hz), 3.81 (3H, s).

O1-C$_8$H$_6$SO$_3$$^-$: ^{1}H-NMR (400 MHz, DMSO-d_6) δ: 7.57 (2H, d, J = 8.4 Hz) 7.49 (2H, d, J = 8.4 Hz), 7.24 (1H, d, J = 1.6 Hz), 7.20 (1H, d, J = 16.4 Hz), 7.10 (1H, d, J = 16.4 Hz), 7.09 (1H, dd, J = 8.4, 1.6 Hz), 6.93 (1H, d, J = 8.4 Hz), 3.80 (3H, s), 3.75 (3H, s).

M1-C$_8$H$_6$SO$_3$$^-$: ^{1}H-NMR (400 MHz, DMSO-d_6) δ: 7.58 (2H, d, J = 8.4 Hz) 7.53 (2H, d, 8.4 Hz), 7.27 (1H, d, J = 16.4 Hz), 7.18 (1H, d, J = 16.4 Hz), 6.78 (2H, d, J = 2.0 Hz), 6.40 (1 H, t, J = 2.0 Hz), 3.76 (6H, s).

3.2.2 Instrumentation

Mass spectra were collected on a commercial LCQ-DECA (Thermo Electron Corporation, San Jose, CA, USA) quadrupole ion trap mass spectrometer. Samples were diluted in 50:50 water/methanol and then injected into the mass spectrometer by using electrospray ionization (ESI). CID experiments were done using helium as the collision target. The collisional energy was given by the normalized collision energy (NCE) which ranges from 0% to 100%.

3.2.3 Quantum Chemical Calculations

Geometry optimizations and frequency calculations for both ground states and transition states were performed using density functional theory (DFT) with the M06-2X functional[23] and the 6-31++G(d,p) basis set. Calculations were done using Gaussian16.[24]

3.3 Results

3.3.1 Anisole

The first system investigated by CID-CRF was sulfonated anisole, **A1-C$_8$H$_6$SO$_3$$^-$**. As will be discussed in more detail in Chapter 5, a styrene linker was used to separate the inert charge site from the labile portion of anisole. The full scan and subsequent CID spectra of **A1-C$_8$H$_6$SO$_3$$^-$** (m/z 289) are shown in Figure 3.1. As expected, the first dissociation was loss of methyl radical to form phenoxy radical, **A2-C$_8$H$_6$SO$_3$$^-$**. In addition to loss of methyl radical, subsequent CO loss also

occurred in competition with loss of SO_2, as shown in Scheme 3.3. The peaks at m/z 273 and m/z 245 are likely artifacts due to a low ion count and high collision energy. Although weak in intensity, the appearance of cyclopentadienyl radical, **A3-C$_8$H$_6$SO$_3^-$** (m/z 246) showed that it was possible to isolate multiple product ions in the dissociation of lignin model compounds using CID-CRF.
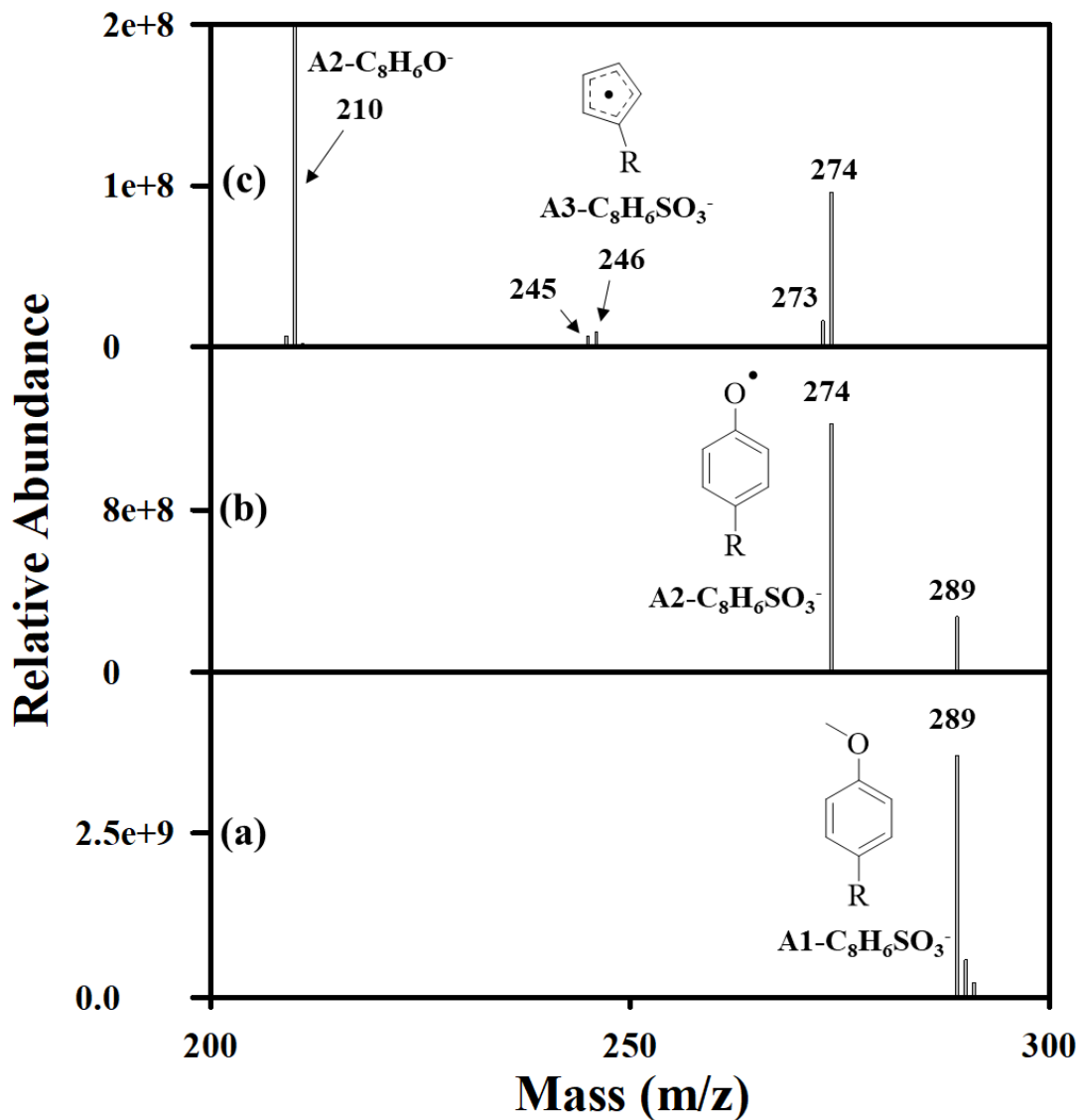
Figure 3.1 The unimolecular decomposition of sulfonated anisole (R=C$_8$H$_6$SO$_3^-$). The full mass spectrum (a) shows the molecular ion, **A1-C$_8$H$_6$SO$_3^-$**. Subsequent CID spectra show loss of methyl radical (b) and CO (c) to form **A2-C$_8$H$_6$SO$_3^-$** and **A3-C$_8$H$_6$SO$_3^-$**, respectively.

Scheme 3.3 Dissociation of sulfonated anisole

$-CH_3^{\cdot}$

$-SO_2$

$-CO$

A1-C$_8$H$_6$SO$^-$

m/z 210

CPDR-C$_8$H$_6$SO$_3^-$

m/z 246

A1-C$_8$H$_6$SO$_3^-$

m/z 289

A2-C$_8$H$_6$SO$_3^-$

m/z 274
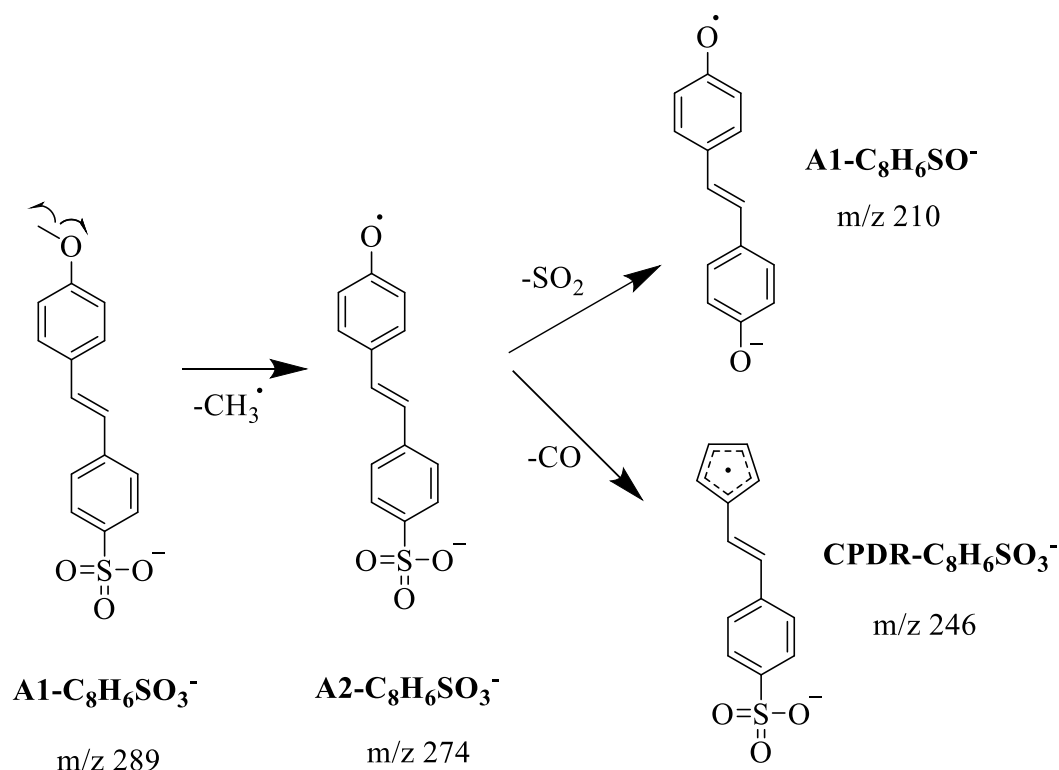
3.3.2 Guaiacol

The next system investigated by CID-CRF was guaiacol, **G1-C$_8$H$_6$SO$_3^-$**. The full scan and subsequent CID spectra of **G1-C$_8$H$_6$SO$_3^-$** (m/z 305) are shown in Figure 3.2. The two product ions in Figure 2c were assigned as *ortho*-benzoquinone, **OBQ-C$_8$H$_6$SO$_3^-$** (m/z 289) and cyclopentadienone, **CPD-C$_8$H$_6$SO$_3^-$** (m/z 261). CID of the m/z 289 peak revealed the m/z 261 peak as its own product ion, showing that stepwise loss of H and CO is a possible pathway for **CPD-C$_8$H$_6$SO$_3^-$** formation, as shown in Scheme 3.4; however, direct formation of **CPD-C$_8$H$_6$SO$_3^-$** from **G2-C$_8$H$_6$SO$_3^-$** cannot be ruled out. Lastly, CID of the m/z 261 peak showed loss of CO and a product peak at m/z 233.
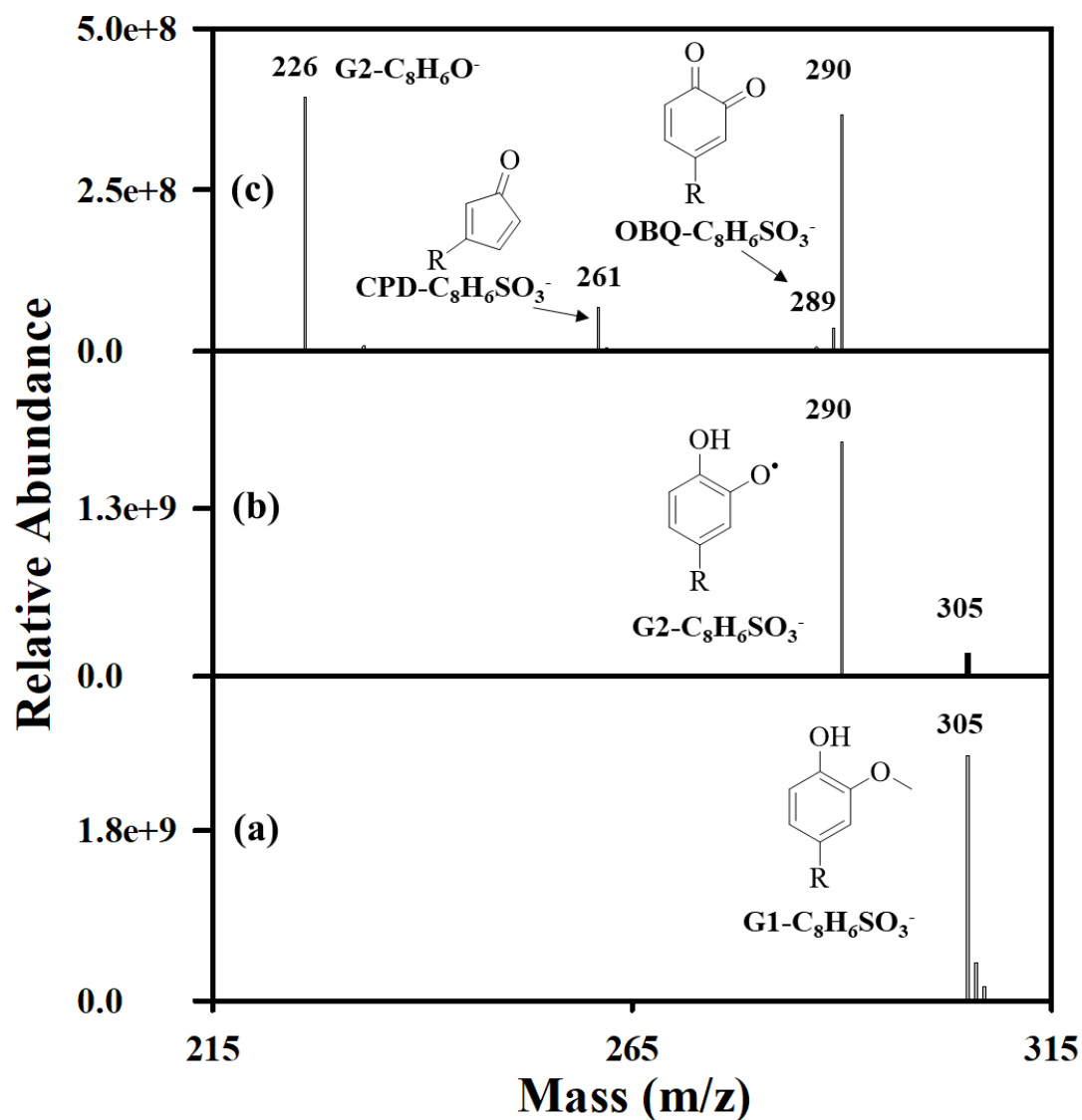
Figure 3.2 The unimolecular decomposition of sulfonated guaiacol. (a) The full mass spectrum shows the molecular ion, **G1-C₈H₆SO₃⁻**. (b) Subsequent CID revealed loss of methyl radical to form **G2-C₈H₆SO₃⁻**, and (c) further dissociation of H and COH to form **OBQ-C₈H₆SO₃⁻** and **CPD-C₈H₆SO₃⁻**, respectively.

Scheme 3.4 Dissociation of sulfonated guaiacol

OBQ-C$_8$H$_6$SO$_3^-$

m/z 289

-H$^\bullet$

-CO

-CH$_3^\bullet$

-CO

-H$^\bullet$

G1-C$_8$H$_6$SO$_3^-$

m/z 305

G2-C$_8$H$_6$SO$_3^-$

m/z 290

CPD-C$_8$H$_6$SO$_3^-$

m/z 261
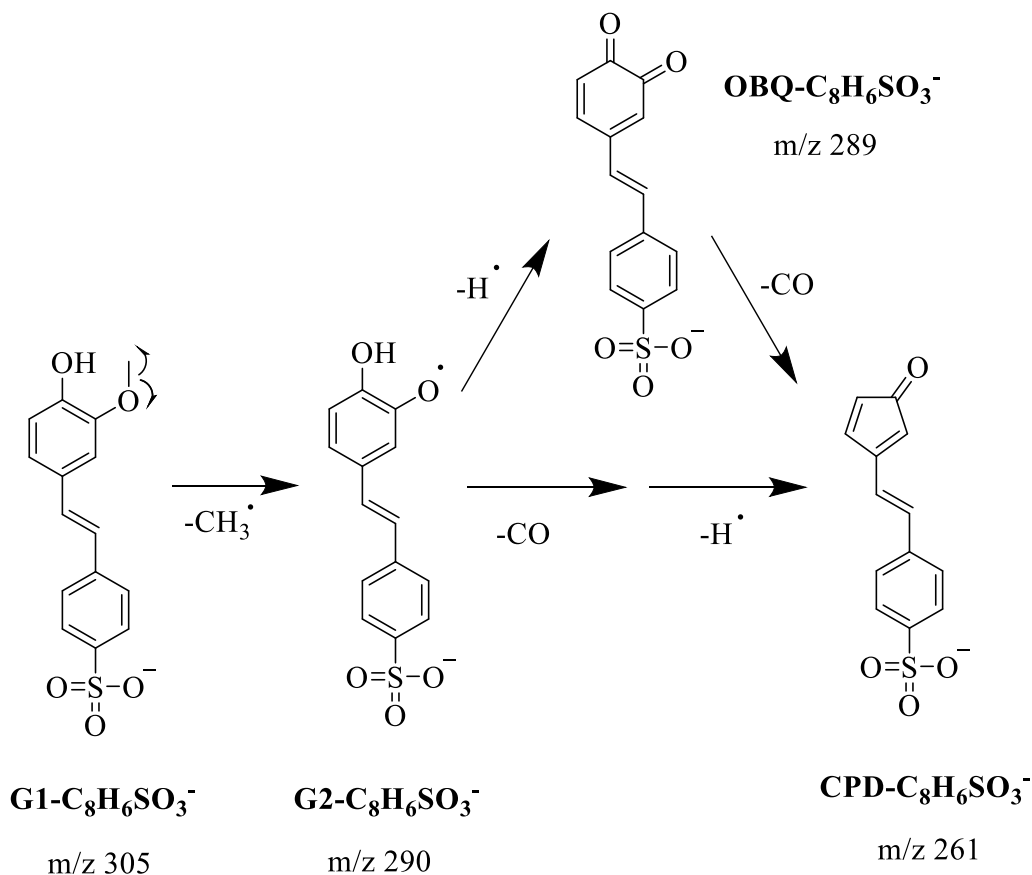
3.3.3 *Ortho*-dimethoxybenzene

We next investigated the dissociation of *ortho*-dimethoxybenzene, **O1**. The full MS scan and subsequent CID spectra of **O1-C$_8$H$_6$SO$_3^-$** (m/z 319) are shown in Figure 3.3. The first step, as expected, is loss of methyl radical. CID-CRF of the methoxy phenoxy radical, **O2-C$_8$H$_6$SO$_3^-$** (m/z 304), occurred by loss of H to form *ortho*-hydroxybenzaldehyde, **OHBA-C$_8$H$_6$SO$_3^-$** (m/z 303). Additional product ions are m/z 289 and m/z 275.

Figure 3.3 The unimolecular decomposition of sulfonated *ortho*-dimethoxybenzene. (a) The full mass spectrum shows the molecular ion, **O1-C₈H₆SO₃⁻**. (b-d) Subsequent CID spectra show multiple product ions.

A peak at m/z 289 is evidence that **O2-C₈H₆SO₃⁻** (m/z 304) can undergo a second methoxy scission to form *ortho*-benzoquinone, **OBQ-C₈H₆SO₃⁻**. This product ion then loses CO to form **CPD-C₈H₆SO₃⁻**, as shown in Scheme 3.5.

91

Scheme 3.5
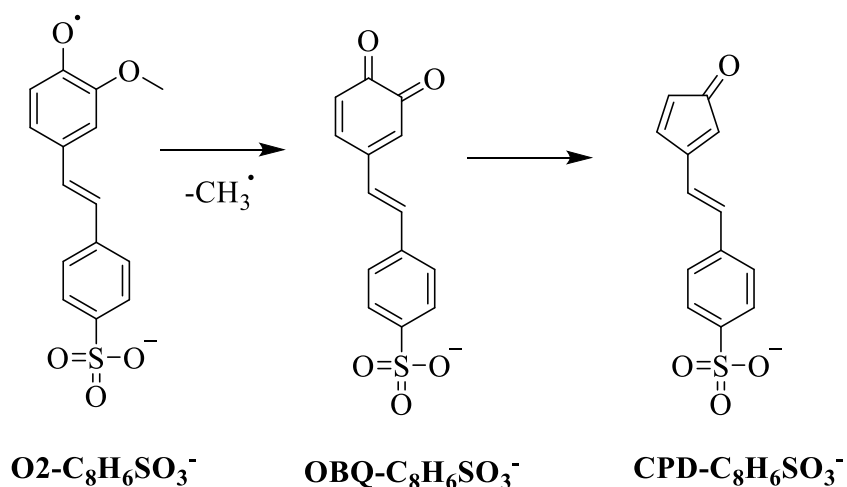
O2-C$_8$H$_6$SO$_3$$^-$ **OBQ-C$_8$H$_6$SO$_3$$^-$**   **CPD-C$_8H_6SO_3$$^-$**

To investigate whether **O2-C$_8$H$_6$SO$_3$$^-$** was losing an H atom from one of the methoxy groups or from the ring, we sulfonated deuterated *ortho*-dimethoxy-d6-benzene and performed CID. The CID spectrum showed loss of CD$_3$ followed by deuterium elimination and confirmed that the source of H loss was one of the methoxy hydrogens, which is consistent with the mechanism proposed by Robichaud (Scheme 3.6).[10]

Scheme 3.6
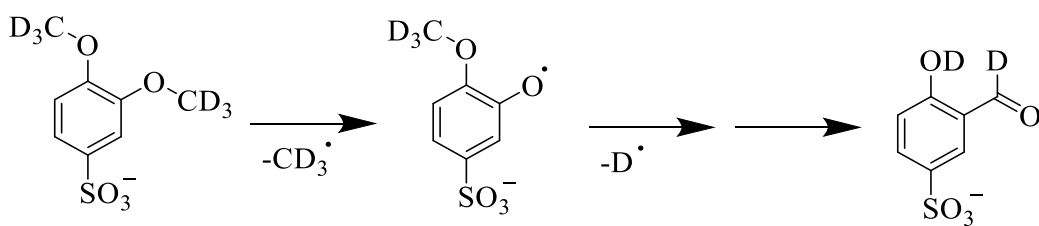
The product at m/z 275 (**PHE-C$_8$H$_6$SO$_3$$^-$**) can be attributed to CO loss from **OHBA-C$_8$H$_6$SO$_3$$^-$**. The ion **OHBA-C$_8H_6SO_3$$^-$** also dissociates by loss of CO and H$_2$ leading to a product **O3-C$_8$H$_6$SO$_3$$^-$** (Scheme 3.7).

Scheme 3.7
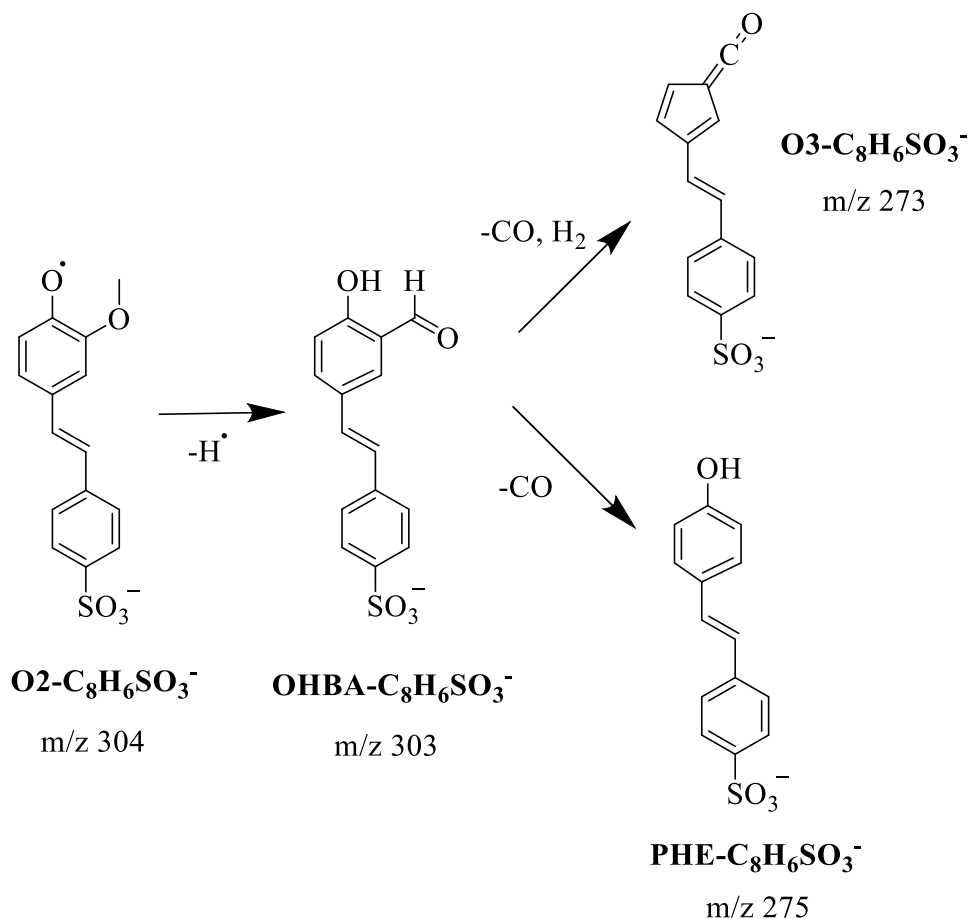
To confirm the structure of **OHBA-C₈H₆SO₃⁻**, we examined CID of authentic sulfonated 2-hydroxybenzaldehyde and found that it produced a matching spectrum to **OHBA-C₈H₆SO₃⁻**. There is no evidence for **O2-C₈H₆SO₃⁻** undergoing CO elimination and ring reduction to give a peak at m/z 276.

3.3.4 *Meta*-dimethoxybenzene

Finally, we wanted to see how increasing the distance between the methoxy groups in dimethoxybenzene would alter the dissociation, so we investigated *meta*-dimethoxybenzene, **M1**. The full MS scan and CID spectra of **M1-C₈H₆SO₃⁻** are shown in Figure 3.4.
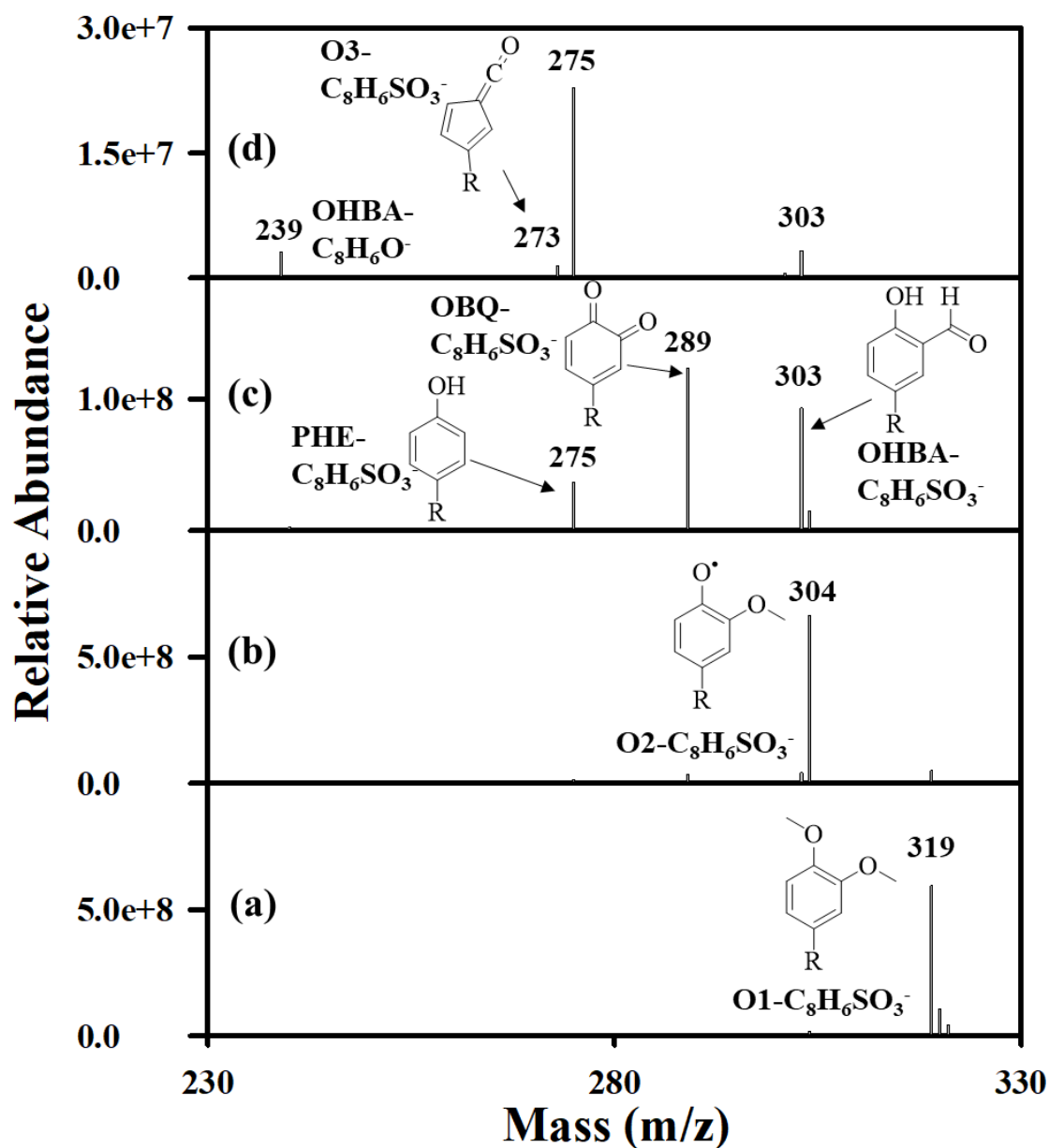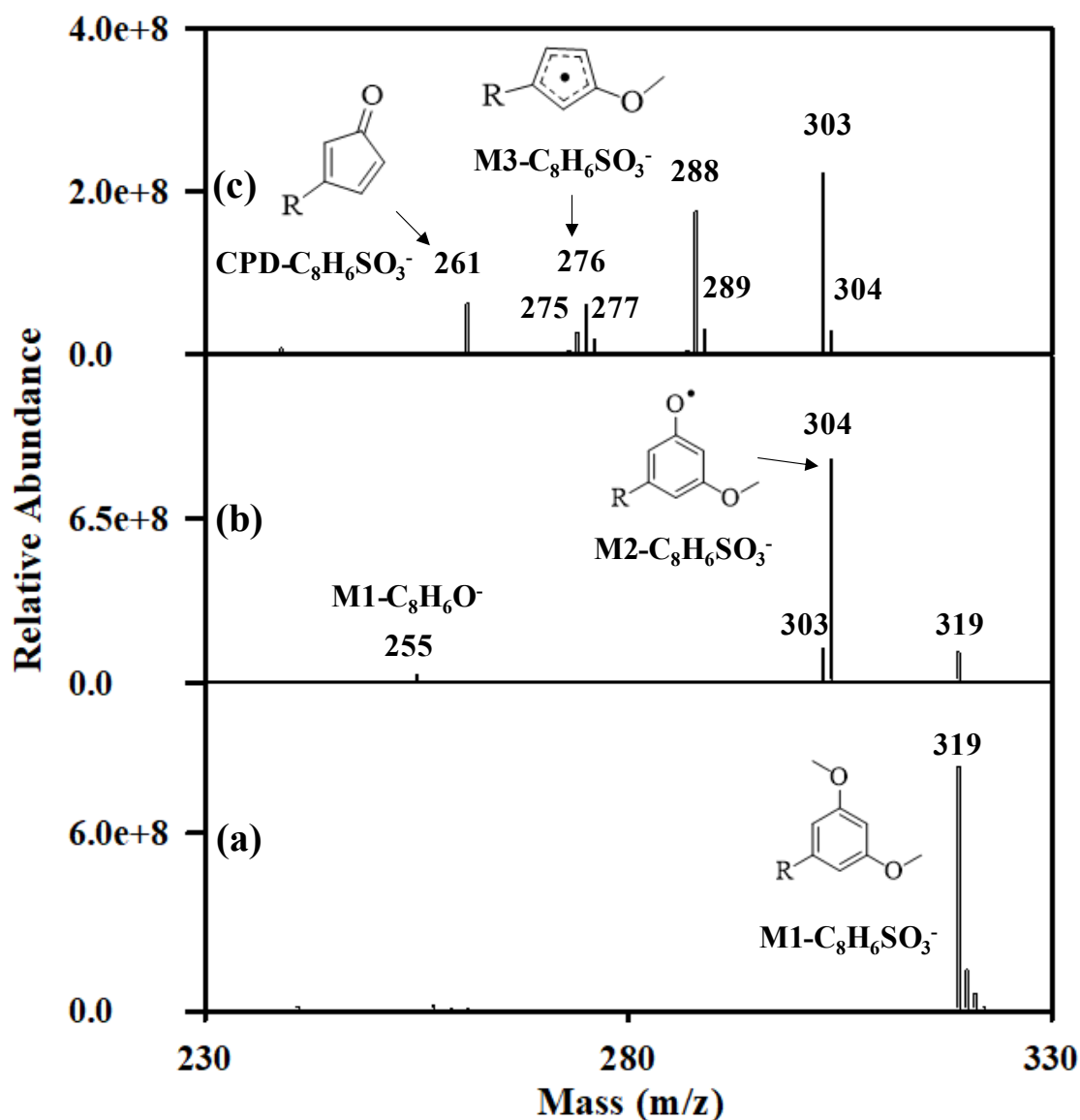
Figure 3.4 The unimolecular decomposition of sulfonated *meta*-dimethoxybenzene. (a) The full mass spectrum shows the molecular ion, **M1-C$_8$H$_6$SO$_3$**. (b-c) Subsequent CID spectra show its dissociation products.

After the initial loss of methyl radical, the methoxy phenoxy radical **M2-C$_8$H$_6$SO$_3$** (m/z 304) dissociates by loss of CO to form **M3-C$_8$H$_6$SO$_3$** (m/z 276), unlike what was found for the *ortho* isomer. Upon CID, the m/z 276 peak loses methyl radical to form **CPD-C$_8$H$_6$SO$_3$** (m/z 261), as shown in Scheme 3.8.

Scheme 3.8

M1-C$_8$H$_6$SO$_3$$^-$

m/z 319

M2-C$_8$H$_6$SO$_3$$^-$

m/z 304

M3-C$_8$H$_6$SO$_3$$^-$

m/z 276

CPD-C$_8$H$_6$SO$_3$$^-$

m/z 261
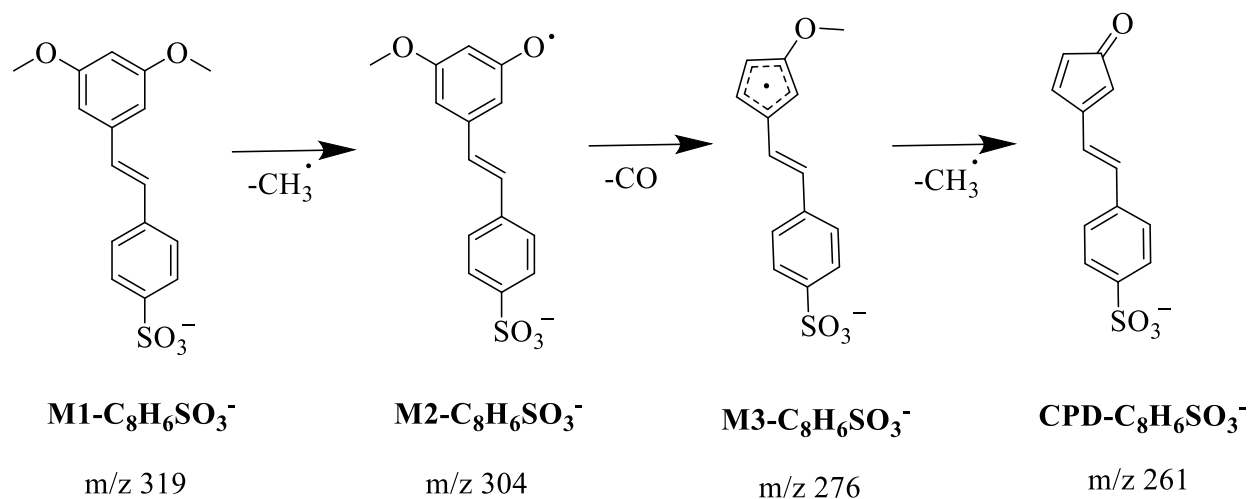
Despite the increased distance between the two methoxy groups, dissociation of **M2-C$_8$H$_6$SO$_3$$^-$** still occurred by H elimination, forming a peak at m/z 303. Because m/z 275 is also present, which is most likely phenol, a possible structure for m/z 303 is 3-hydroxybenzaldehyde, **MHBA-C$_8$H$_6$SO$_3$$^-$**, which can form on the same route to phenol, as shown in Scheme 3.9.

Scheme 3.9

MHBA-C$_8$H$_6$SO$_3$$^-$

m/z 303

-H$^\bullet$

M2-C$_8$H$_6$SO$_3$$^-$

m/z 304

-CH$_3$O$^\bullet$
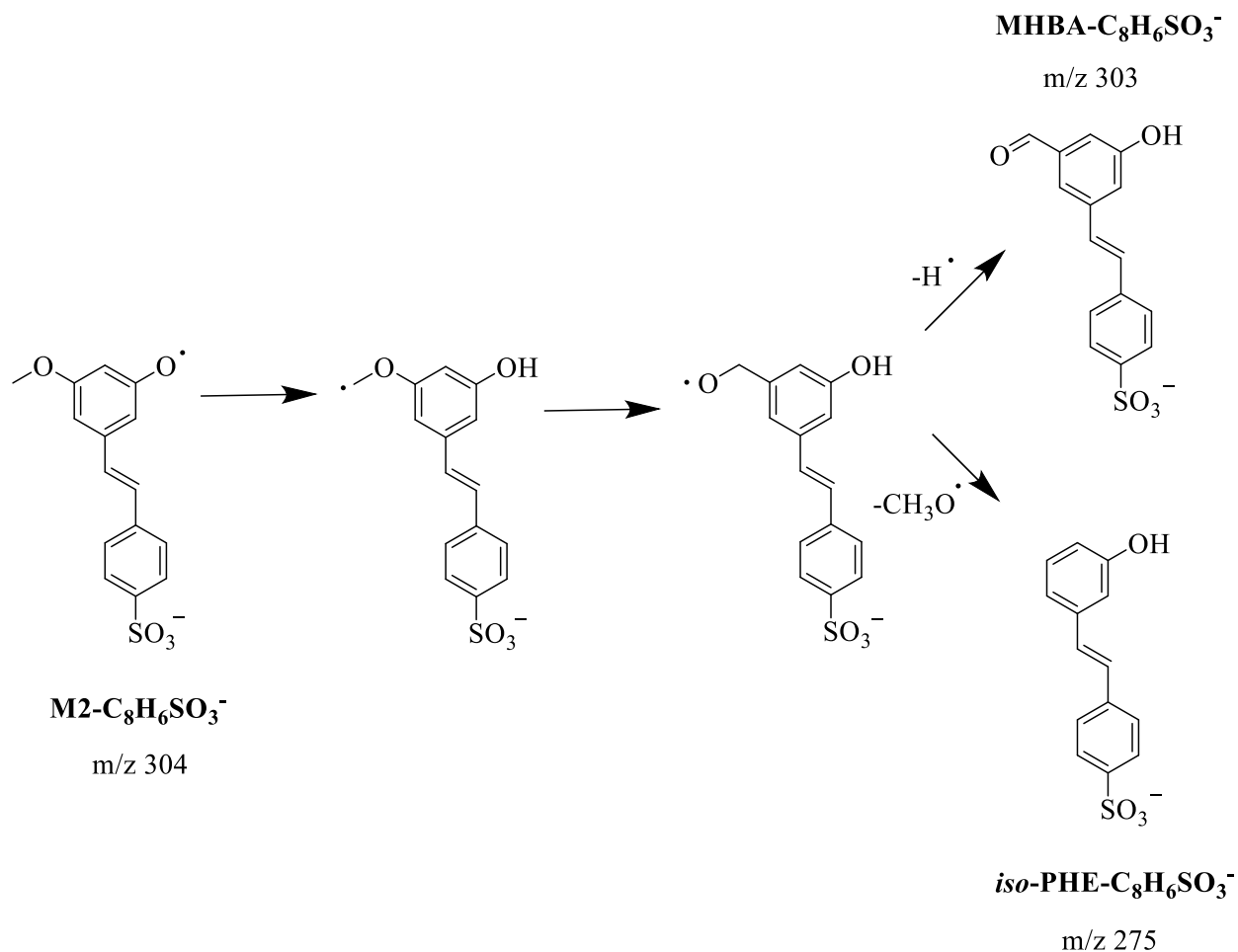
iso-**PHE-C$_8$H$_6$SO$_3$$^-$**

m/z 275

CID of the m/z 303 peak leads to loss of methyl radical to form a peak at m/z 288 peak, followed by loss of CO to form a peak at m/z 260. However, CID-CRF of the authentic 3-hydroxybenzaldehyde structure did not occur by methyl radical loss, ruling out **MHBA-C$_8$H$_6$SO$_3$$^-$** as the structure of m/z 303. Therefore, the structure is not assigned.

Finally, loss of a second methyl radical from **M2-C$_8$H$_6$SO$_3$$^-$** leads to a peak at m/z 289. A possible structure for this product ion is *meta*-benzoquinone, **MBQ-C$_8$H$_6$SO$_3$$^-$**, or an isomer resulting from rearrangement, as shown in Scheme 3.10.

Scheme 3.10

| M2-C8H6SO3⁻ | MBQ-C8H6SO3⁻ |
| m/z 304 | m/z 289 |
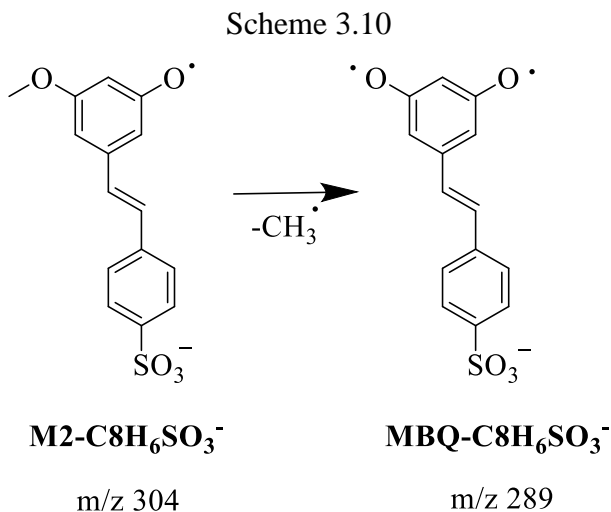
3.4 Discussion

As mentioned in the introduction, the most common motif in lignin is the β-O-4 linkage. During pyrolysis, this etheric C-O bond undergoes bond homolysis leading to the formation of substituted phenoxy radicals, as shown in Scheme 3.1. Some convenient models for studying the pyrolysis of this lignin linkage are anisole, guaiacol, and dimethoxybenzene, which also generate phenoxy radicals upon pyrolysis.[9, 10, 25] In this work, we observed the CID-CRF of sulfonated analogs of these compounds and compared our results to the product ions formed during pyrolysis of authentic compounds. A benchmark for isolating primary pyrolysis products is photoionization mass spectrometry (pyrolysis-PIMS).

We found that the first dissociation step for each of the sulfonated compounds by CID-CRF is methyl radical loss as was also observed by pyrolysis-PIMS. However, one difference between pyrolysis-PIMS and CID-CRF is that the charge tag lowers the BDE of the first methyl radical loss between 3 to 12 kcal mol⁻¹ (Table 5.3) This is due to the stability of the phenoxy radical resulting from interaction between the charge and the radical center. As a result, the resulting phenoxy radical can be isolated in high abundance. For example, Figure 3.3 shows an intense signal for **O2-C8H6SO3⁻**, which contrasts with the weak signal observed in the pyrolysis-PIMS spectrum of the corresponding non-sulfonated structure, **O2**.[10] This is one advantage of the CID-CRF approach because it is effective at isolating short-lived radical intermediates involved in pyrolysis.

3.4.1 Anisole

Anisole, **A1**, has been widely studied for constructing kinetic models of the thermochemical decomposition of lignin.[26] Anisole is a simple aromatic compound containing the O-Me bond which is ubiquitous in lignin. Despite its simplicity, a combination of unimolecular and bimolecular reactions during pyrolysis leads to dozens of anisole pyrolysis products, including benzene, naphthalene, and other PAHs.[27] These compounds are thought to stem from radical intermediates such as cyclopentadienyl radical, **CPDR**, that form during the pyrolysis of anisole (Scheme 3.11) and then undergo molecular weight growth.[9, 28-31]

Scheme 3.11
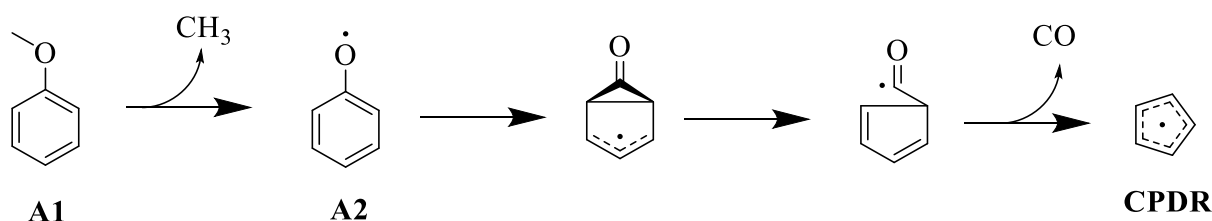
By attaching an SO_3^- group to **A1** and subjecting it to CID-CRF, the reactive intermediates could be isolated and detected by MS. The CID-CRF spectra of sulfonated anisole, **A1-C₈H₆SO₃⁻**, are shown in Figure 3.1. The decomposition of this anisole derivative followed the same route that was observed for authentic anisole during pyrolysis-PIMS. One difference, however, was that bimolecular reactions were eliminated leading to simpler spectra. This is in contrast to pyrolysis-PIMS that included compounds that had undergone molecular weight growth, such as benzene, from smaller dissociation products.[9] Thus, CID-CRF can simplify the study of primary pyrolysis products.

We carried out calculations to construct a potential energy surface (PES) for this reaction so that we could know how the charge tag influenced the overall process. Geometry optimizations and frequency calculations for both ground states and transition states were done using the M06-2X and the 6-31++G(d,p) basis set. The PES of the decomposition of **A1** and **A1-C₈H₆SO₃⁻** are shown in Figure 3.1,which can be compared to that found by Carstensen and Dean.[29] The diagram shows that the charge tag raises the energy of many of the transition states and intermediates after

the initial methyl radical loss. However, because the dissociation is unimolecular, this has little effect on the branching ratios of the observed products.

Figure 3.5 Potential energy surface of the dissociation of anisole. The energies are in kcal/mol and are calculated for R=H and (R=$C_8H_6SO_3^-$). All energies are shown relative to the phenoxy radical, **A2**.

3.4.2 Guaiacol

Guaiacol, **G1**, represents one of the three monolignol monomers that make up lignin. It contains a hydroxy group in addition to the ubiquitous O-Me bond found throughout lignin. Pyrolysis is initiated by loss of methyl radical to form hydroxyphenoxy radical, **G2**, followed by decarbonylation to form hydroxycyclopentadienyl radical, **G3**, as is shown in Scheme 3.12.[25, 32]

Scheme 3.12
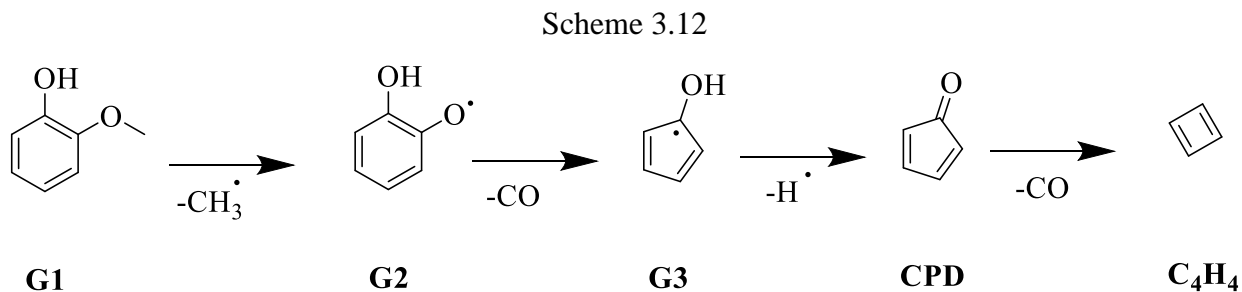
In this work, decomposition of the sulfonated guaiacol derivative followed a similar route that was observed by pyrolysis-PIMS. However, one difference between pyrolysis-PIMS and CID-CRF is whether **G2** undergoes H radical loss to form *ortho*-benzoquinone, **OBQ** (Scheme 3.13).

Scheme 3.13

G2

$-CH_3^{\bullet}$

OBQ
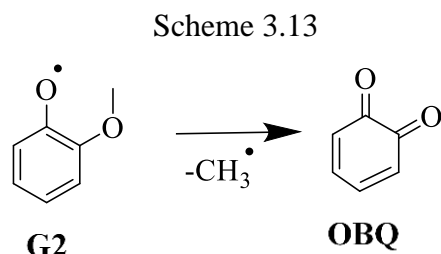
O*rtho*-benzoquinone had not been detected previously, although Scheer et al.[25] did observe methane loss during the pyrolysis of guaiacol based on a $v_4(CH_4)$ transition present in an IR spectrum during; thus, they concluded **G1** may undergo methane loss to form **OBQ** (Scheme 3.14).

Scheme 3.14

G1

$-CH_4$

OBQ
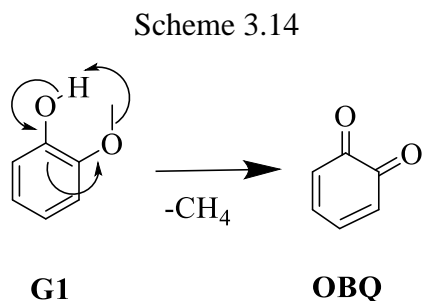
However, CID-CRF of **G2-C$_8$H$_6$SO$_3^-$**, showed a peak at m/z 289 which we assigned to **OBQ-C$_8$H$_6$SO$_3^-$**, showing that this method is effective at isolating reactive intermediates that may be missed using other method.

Another difference between pyrolysis and CID-CRF in the decomposition of guaiacol is the appearance of **G3** in the pyrolysis-PIMS spectra[25], but there was no evidence for **G3-C$_8$H$_6$SO$_3^-$** (m/z 262) upon CID-CRF (Figure 3.2). Because the subsequent product is visible by both pyrolysis-PIMS (**CPD**) and CID-CRF (**CPD-C$_8$H$_6$SO$_3^-$**), it is possible that **G3-C$_8$H$_6$SO$_3^-$** either immediately dissociates upon formation or an alternate route is taken to **CPD-C$_8$H$_6$SO$_3^-$** that does not involve **G3-C$_8$H$_6$SO$_3^-$**. For example, **OBQ-C$_8$H$_6$SO$_3^-$** can undergo CO loss to form **CPD-C$_8$H$_6$SO$_3^-$** (Scheme 3.4).

Calculations were again carried out to construct a potential energy surface (PES) for the decomposition of guaiacol so that we could know how the charge tag was influencing the overall process. The PES for guaiacol decomposition is shown in Figure 3.6.
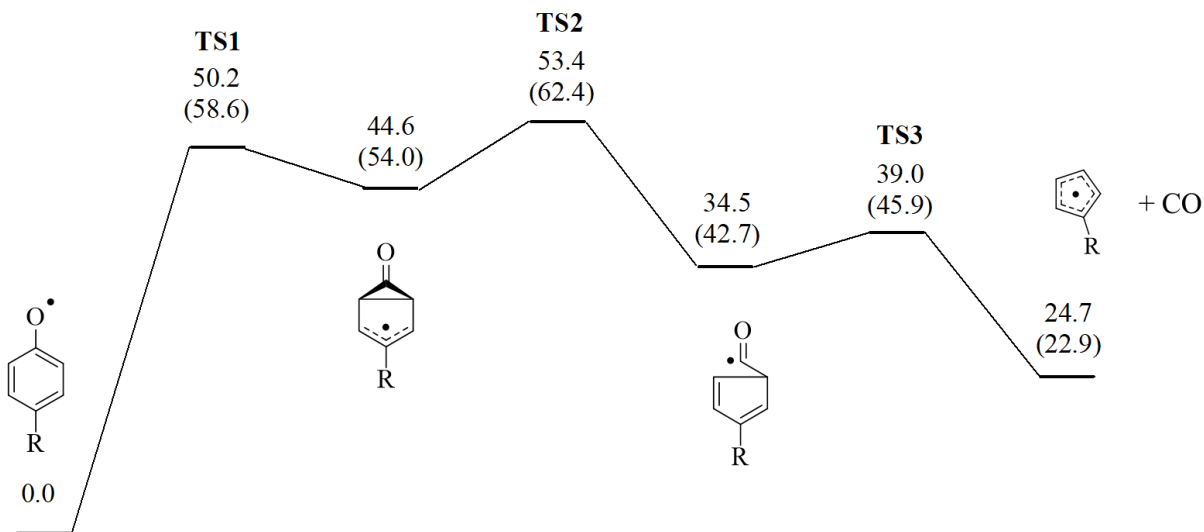

Figure 3.6 Potential energy surface for the decomposition of guaiacol. The energies are in kcal/mol and are calculated for R=H and (R=$C_8H_6SO_3^-$) using the M06-2X/6-31++G(d,p) level of theory. All energies are shown relative to phenoxy radical, **G2**.

The diagram shows both stabilizing and destabilizing effects of the transition states and pyrolysis products relative to the authentic structures. In some cases, the effect is as small as 2 kcal/mol, but in other cases the effect is as large as 9 kcal/mol. However, these effects do not explain the lack of **G3-$C_8H_6SO_3^-$** in Figure 2c, which should be stable according to the PES of guaiacol. Thus, in addition to energetics, entropy may need to be considered when interpreting the branching ratios of the CID-CRF products.

3.4.3 *Ortho*-dimethoxybenzene

Gas-phase pyrolysis of *ortho*-dimethoxybenzene, **O1-C₈H₆SO₃⁻**, has been proposed to undergo methyl radical loss followed by one of three possible pathways, although only evidence for the H-transfer pathway has previously been observed (Scheme 3.15).[10]
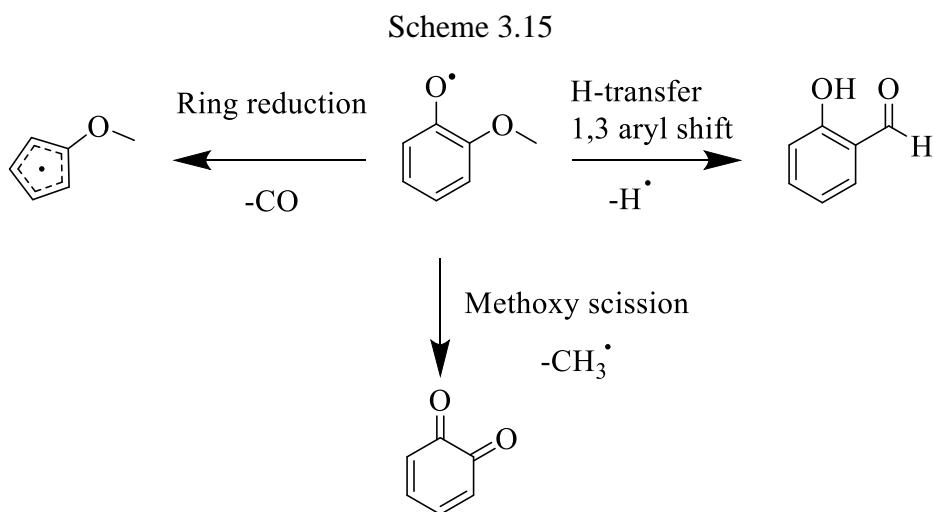
Scheme 3.15

The H-transfer and a 1,3 aryl shift are thought to occur because of the proximity of the two methoxy groups, as shown in Scheme 3.16.[10] Because of how quickly **O2** decomposed into **OHBA**, Robichaud et al.[10] were not able to detect **O2** using pyrolysis-PIMS. In contrast, we were able to observe a very intense **O2-C₈H₆SO₃⁻** (m/z 304) peak without immediate decomposition (Figure 3.3).
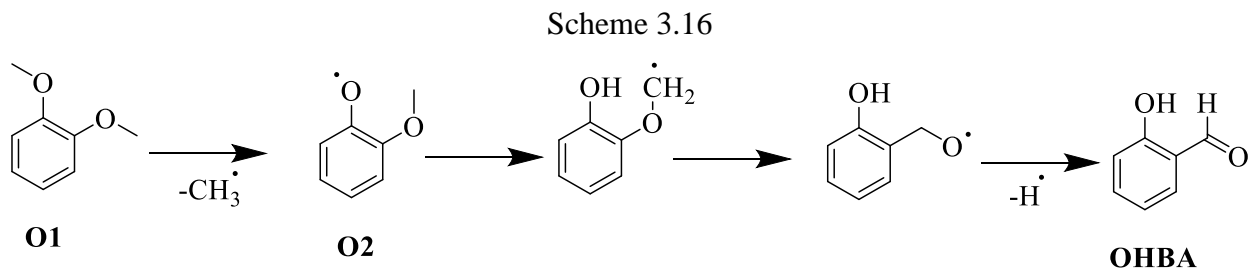
Scheme 3.16

Next, phenol (**PHE**) appeared in the pyrolysis-PIMS spectra. Robichaud et al.[10] proposed that the source of **PHE** was **O2** undergoing COH loss, as shown in Scheme 3.17. However, CID-CRF revealed an alternative route where **OBA-C₈H₆SO₃⁻** undergoes CO loss to produce **PHE-**

C₈H₆SO₃⁻ (Figure 3.3). Thus, CID-CRF can reveal the step-by-step unimolecular decomposition of model compounds.

Scheme 3.17
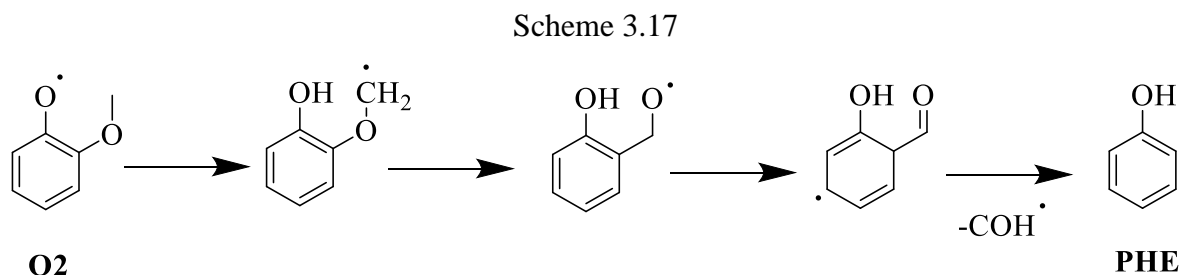
Another difference is the appearance of *ortho*-benzoquinone, **OBQ-C₈H₆SO₃⁻** (m/z 289), by CID-CRF, whereas **OBQ** was not present in the pyrolysis-PIMS spectra.[10] Based on the PES diagram in Figure 3.7, the charge tag does not appear to be responsible for **OBQ-C₈H₆SO₃⁻** formation because it is a higher energy pathway; thus, we think it is a valid pyrolysis product of **O1-C₈H₆SO₃⁻**.
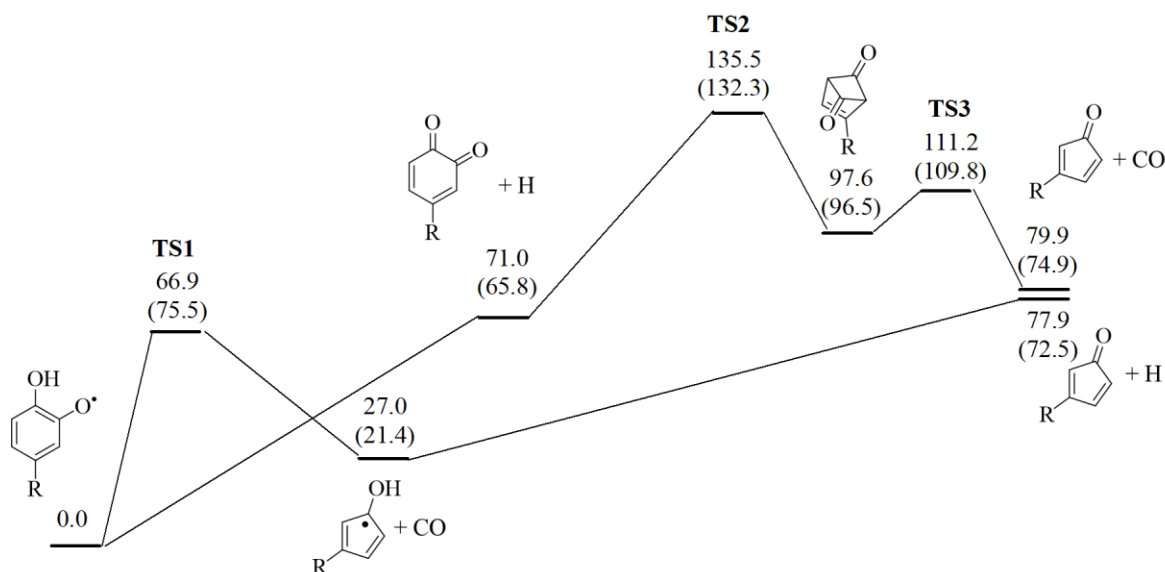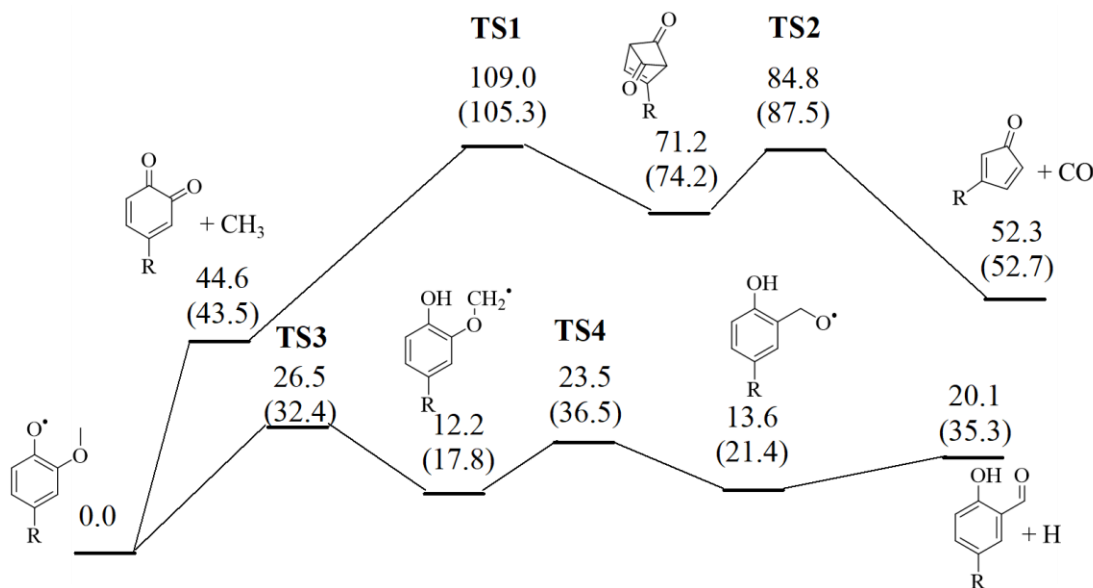

Figure 3.7 Potential energy surface for the decomposition of ortho-dimethoxybenzene. The energies are in kcal/mol and are calculated for R=H and (R=C₈H₆SO₃⁻) using the M06-2X/6-31++G(d,p) level of theory. All energies are shown relative to phenoxy radical, **O2**.

3.4.4 *Meta*-dimethoxybenzene

The degradation of *meta*-dimethoxybenzene, **M1**, is different from the *ortho* isomer because the two methoxy substituents are in less proximity to each other. As a result, the H transfer pathway is hindered during pyrolysis, and the CO elimination ring reduction pathway dominates (Scheme 3.18).[10]

Scheme 3.18
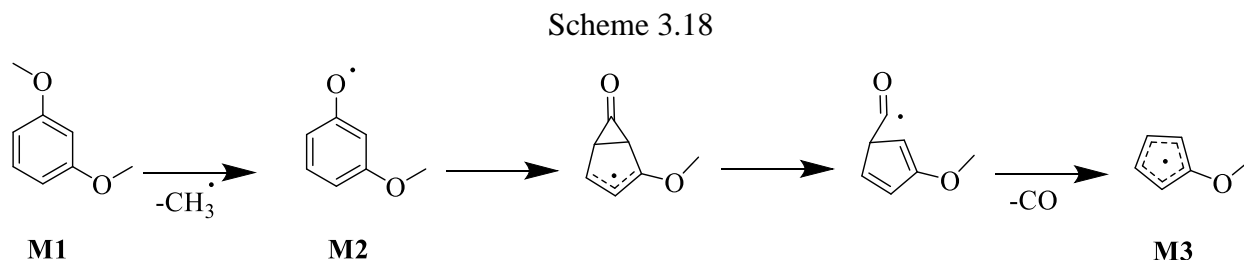
Using CID-CRF, we likewise found evidence for the ring reduction pathway. Starting with CID of *meta*-dimethoxybenzene, **M1-C$_8$H$_6$SO$_3^-$** (m/z 319), methyl radical was lost to form **M2-C$_8$H$_6$SO$_3^-$** (m/z 304), as shown in Figure 3.4. This was followed by loss of CO to form **M3-C$_8$H$_6$SO$_3^-$** (m/z 276). **M3-C$_8$H$_6$SO$_3^-$** then goes on to lose methyl radical to form **CPD-C$_8$H$_6$SO$_3^-$** (m/z 261).

Robichaud and coworkers[10] found that pyrolysis of **M1** also produced phenol, **PHE**, which was difficult to explain because the H transfer pathway has a high energy barrier. They proposed that the most likely pathway to **PHE** formation involves shuffling the H through the ring, as is shown in Scheme 3.19. However, very little *meta*-hydroxybenzaldehyde, **MHBA**, was co-produced by pyrolysis-PIMS despite **PHE** and **MHBA** having similar energy barriers..

Scheme 3.19
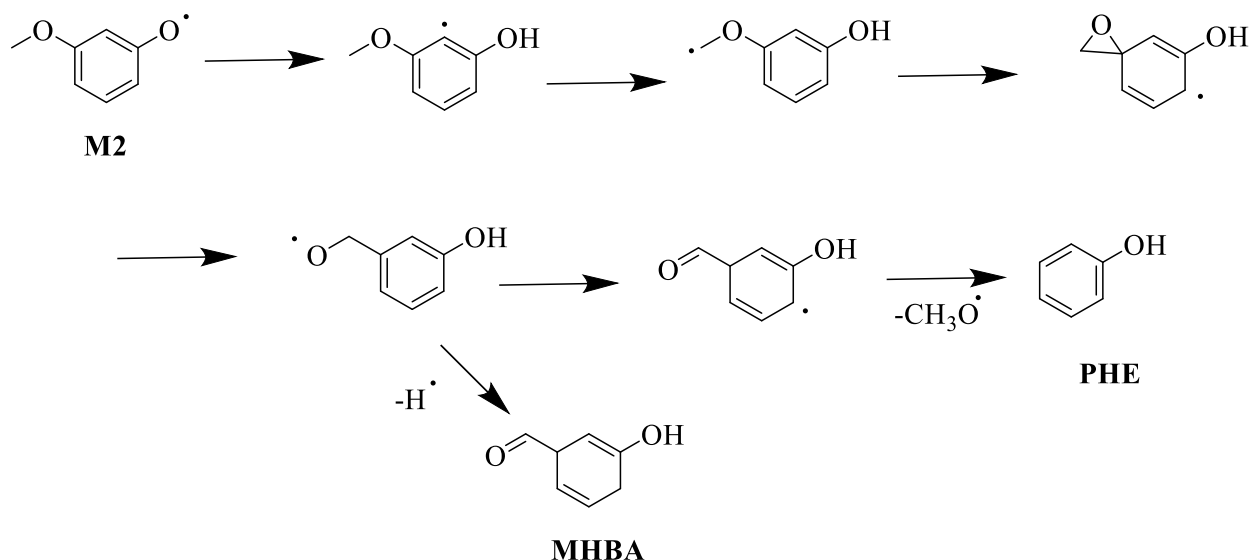
We also observed phenol, *iso*-**PHE-C$_8$H$_6$SO$_3^-$** (m/z 275), in the CID spectra as expected. However, loss of H from **M2-C$_8$H$_6$SO$_3^-$** (m/z 304) to form a peak at m/z 303 is the dominant pathway. We are unsure of the structure of the m/z 303 peak. CID of a potential candidate, 3-hydroxybenzaldehyde, resulted in a CID spectrum that was different from the CID spectrum of the compound at m/z 303. The m/z 303 compound further dissociates by loss of methyl radical to form a peak at m/z 288 followed by loss of CO to form a peak at m/z 260.

Additionally, we also observed **M2-C$_8$H$_6$SO$_3^-$** undergoing a second methoxy loss and forming *meta*-benzoquinone, **MBQ-C$_8$H$_6$SO$_3^-$** (289 m/z), despite it being a highly reactive diradical (Scheme 3.10).

3.5   Conclusion

CID-CRF proved to be an efficient method for isolating reactive intermediates involved in lignin pyrolysis. Some differences were observed between this method and pyrolysis-PIMS, such as the formation of *ortho-* and *meta*-benzoquionone during the pyrolysis of *ortho-* and *meta*-dimethoxybenzene. CID-CRF also made the study the gas-phase unimolecular decomposition of model compounds easier by eliminating bimolecular reactions that normally convolute these studies. The ease of attaching a charge tag to model compounds makes the scope of this method very broad. These insights provide valuable information in the study of lignin pyrolysis.

105

3.6 References

1. Fan, L.; Zhang, Y.; Liu, S.; Zhou, N.; Chen, P.; Cheng, Y.; Addy, M.; Lu, Q.; Omar, M. M.; Liu, Y.; Wang, Y.; Dai, L.; Anderson, E.; Peng, P.; Lei, H.; Ruan, R., Bio-oil from fast pyrolysis of lignin: Effects of process and upgrading parameters. *Bioresource Technology* **2017,** *241*, 1118-1126.

2. Anex, R. P.; Aden, A.; Kazi, F. K.; Fortman, J.; Swanson, R. M.; Wright, M. M.; Satrio, J. A.; Brown, R. C.; Daugaard, D. E.; Platon, A.; Kothandaraman, G.; Hsu, D. D.; Dutta, A., Techno-economic comparison of biomass-to-transportation fuels via pyrolysis, gasification, and biochemical pathways. *Fuel* **2010,** *89*, S29-S35.

3. Cao, L.; Yu, I. K. M.; Liu, Y.; Ruan, X.; Tsang, D. C. W.; Hunt, A. J.; Ok, Y. S.; Song, H.; Zhang, S., Lignin valorization for the production of renewable chemicals: State-of-the-art review and future prospects. *Bioresource Technology* **2018,** *269*, 465-475.

4. Zakzeski, J.; Bruijnincx, P. C. A.; Jongerius, A. L.; Weckhuysen, B. M., The Catalytic Valorization of Lignin for the Production of Renewable Chemicals. *Chemical Reviews* **2010,** *110* (6), 3552-3599.

5. Marcum, C. L.; Jarrell, T. M.; Zhu, H.; Owen, B. C.; Haupert, L. J.; Easton, M.; Hosseinaei, O.; Bozell, J.; Nash, J. J.; Kenttämaa, H. I., A Fundamental Tandem Mass Spectrometry Study of the Collision-Activated Dissociation of Small Deprotonated Molecules Related to Lignin. *ChemSusChem* **2016,** *9* (24), 3513-3526.

6. Xu, L.; Zhang, Y.; Fu, Y., Advances in Upgrading Lignin Pyrolysis Vapors by Ex Situ Catalytic Fast Pyrolysis. *Energy Technology* **2017,** *5* (1), 30-51.

7. Mukarakate, C.; Scheer, A. M.; Robichaud, D. J.; Jarvis, M. W.; David, D. E.; Ellison, G. B.; Nimlos, M. R.; Davis, M. F., Laser ablation with resonance-enhanced multiphoton ionization time-of-flight mass spectrometry for determining aromatic lignin volatilization products from biomass. *Review of Scientific Instruments* **2011,** *82* (3), 033104.

8. Cheng, H.; Wu, S.; Huang, J.; Zhang, X., Direct evidence from in situ FTIR spectroscopy that o-quinonemethide is a key intermediate during the pyrolysis of guaiacol. *Analytical and Bioanalytical Chemistry* **2017,** *409* (10), 2531-2537.

9. Scheer, A. M.; Mukarakate, C.; Robichaud, D. J.; Ellison, G. B.; Nimlos, M. R., Radical Chemistry in the Thermal Decomposition of Anisole and Deuterated Anisoles: An Investigation of Aromatic Growth. *The Journal of Physical Chemistry A* **2010,** *114* (34), 9043-9056.

10. Robichaud, D. J.; Scheer, A. M.; Mukarakate, C.; Ormond, T. K.; Buckingham, G. T.; Ellison, G. B.; Nimlos, M. R., Unimolecular thermal decomposition of dimethoxybenzenes. *The Journal of Chemical Physics* **2014,** *140* (23), 234302.

11. Lu, J.; Wang, M.; Zhang, X.; Heyden, A.; Wang, F., β-O-4 Bond Cleavage Mechanism for Lignin Model Compounds over Pd Catalysts Identified by Combination of First-Principles Calculations and Experiments. *ACS Catalysis* **2016,** *6* (8), 5589-5598.

12. Kawamoto, H., Lignin pyrolysis reactions. *Journal of Wood Science* **2017,** *63* (2), 117-132.

13. Tolbert, A.; Akinosho, H.; Khunsupat, R.; Naskar, A. K.; Ragauskas, A. J., Characterization and analysis of the molecular weight of lignin for biorefining studies. *Biofuels, Bioproducts and Biorefining* **2014,** *8* (6), 836-856.

14. Parthasarathi, R.; Romero, R. A.; Redondo, A.; Gnanakaran, S., Theoretical Study of the Remarkably Diverse Linkages in Lignin. *The Journal of Physical Chemistry Letters* **2011,** *2* (20), 2660-2666.

15. Huaming Sheng, W. T., Jinshan Gao, James S. Riedeman, Guannan Li,; Tiffany M. Jarrell, M. R. H., Linan Yang, Priya Murria, Xin Ma,; John J. Nash, a. H. I. K., (−)ESI/CAD MSn Procedure for Sequencing Lignin Oligomers Based on a Study of Synthetic Model Compounds with β-O-4 and 5-5 Linkages. *Analytical Chemistry 89* (24), 13089–13096.

16. Vanholme, R., Demedts, B., Morreel, K., Ralph, J., & Boerjan, W., Lignin biosynthesis and Structure. *Plant Physiology* **2010,** *155* (3), 895-905.

17. Bahng, M.-K.; Mukarakate, C.; Robichaud, D. J.; Nimlos, M. R., Current technologies for analysis of biomass thermochemical processing: A review. *Analytica Chimica Acta* **2009,** *651* (2), 117-138.

18. Kidwell, N. M.; Vaquero-Vara, V.; Ormond, T. K.; Buckingham, G. T.; Zhang, D.; Mehta-Hurt, D. N.; McCaslin, L.; Nimlos, M. R.; Daily, J. W.; Dian, B. C.; Stanton, J. F.; Ellison, G. B.; Zwier, a. T. S., Chirped-Pulse Fourier Transform Microwave Spectroscopy Coupled with a Flash Pyrolysis Microreactor: Structural Determination of the Reactive Intermediate Cyclopentadienone. *The Journal of Physical Chemistry Letters* **2014,** *5* (13), 2201-2207.

19. Cheng, C.; Giblin, D.; Gross, M. L., Structural determination of oxofatty acids by charge-remote fragmentations. *Journal of the American Society for Mass Spectrometry* **1998,** *9* (3), 216-224.

20. Adams, J.; Gross, M. L., Charge-remote fragmentations of closed-shell ions. A thermolytic analogy. *Journal of the American Chemical Society 111* (2), 435-440.

21. Chen, G.; Pramanik, B. N.; Bartner, P. L.; Saksena, A. K.; Gross, M. L., Multiple-stage mass spectrometric analysis of complex oligosaccharide antibiotics (everninomicins) in a quadrupole ion trap. *Journal of the American Society for Mass Spectrometry* **2002,** *13* (11), 1313-1321.

22. Gross, M. L., Charge-remote fragmentation: an account of research on mechanisms and applications. *International Journal of Mass Spectrometry* **2000,** *200* (1), 611-624.

23. Zhao, Y.; Truhlar, D. G., The M06 suite of density functionals for main group thermochemistry, thermochemical kinetics, noncovalent interactions, excited states, and transition elements: two new functionals and systematic testing of four M06-class functionals and 12 other functionals. *Theoretical chemistry accounts* **2008,** *120* (1-3), 215-241.

24. Frisch, M. J.; Trucks, G. W.; Schlegel, H. B.; Scuseria, G. E.; Robb, M. A.; Cheeseman, J. R.; Scalmani, G.; Barone, V.; Petersson, G. A.; Nakatsuji, H.; Li, X.; Caricato, M.; Marenich, A. V.; Bloino, J.; Janesko, B. G.; Gomperts, R.; Mennucci, B.; Hratchian, H. P.; Ortiz, J. V.; Izmaylov, A. F.; Sonnenberg, J. L.; Williams; Ding, F.; Lipparini, F.; Egidi, F.; Goings, J.; Peng, B.; Petrone, A.; Henderson, T.; Ranasinghe, D.; Zakrzewski, V. G.; Gao, J.; Rega, N.; Zheng, G.; Liang, W.; Hada, M.; Ehara, M.; Toyota, K.; Fukuda, R.; Hasegawa, J.; Ishida, M.; Nakajima, T.; Honda, Y.; Kitao, O.; Nakai, H.; Vreven, T.; Throssell, K.; Montgomery Jr., J. A.; Peralta, J. E.; Ogliaro, F.; Bearpark, M. J.; Heyd, J. J.; Brothers, E. N.; Kudin, K. N.; Staroverov, V. N.; Keith, T. A.; Kobayashi, R.; Normand, J.; Raghavachari, K.; Rendell, A. P.; Burant, J. C.; Iyengar, S. S.; Tomasi, J.; Cossi, M.; Millam, J. M.; Klene, M.; Adamo, C.; Cammi, R.; Ochterski, J. W.; Martin, R. L.; Morokuma, K.; Farkas, O.; Foresman, J. B.; Fox, D. J. *Gaussian 16 Rev. C.01*, Wallingford, CT, 2016.

25. Scheer, A. M.; Mukarakate, C.; , D. J. R.; Nimlos, M. R.; Ellison, a. G. B., Thermal Decomposition Mechanisms of the Methoxyphenols: Formation of Phenol, Cyclopentadienone, Vinylacetylene, and Acetylene. *The Journal of Physical Chemistry A* **2011,** *115* (46), 13381-13389.

26. Koirala, Y. Investigating the kinetics of anisole : a simple lignin model compound. Colorado School of Mines, 2015.

27. Yuan, W.; Li, T.; Li, Y.; Zeng, M.; Zhang, Y.; Zou, J.; Cao, C.; Li, W.; Yang, J.; Qi, F., Experimental and kinetic modeling investigation on anisole pyrolysis: Implications on phenoxy and cyclopentadienyl chemistry. *Combustion and Flame* **2019,** *201*, 187-199.

28. Friderichsen, A. V.; Shin, E.-J.; Evans, R. J.; Nimlos, M. R.; Dayton, D. C.; Ellison, G. B., The pyrolysis of anisole (C6H5OCH3) using a hyperthermal nozzle. *Fuel* **2001,** *80* (12), 1747-1755.

29. Carstensen, H.-H.; Dean, A. M., A quantitative kinetic analysis of CO elimination from phenoxy radicals. *International Journal of Chemical Kinetics* **2012,** *44* (1), 75-89.

30. Liu, R.; Morokuma, K.; Mebel, A. M.; Lin, M. C., Ab Initio Study of the Mechanism for the Thermal Decomposition of the Phenoxy Radical. *The Journal of Physical Chemistry* **1996,** *100* (22), 9314-9322.

31. Arends, I. W. C. E.; Louw, R.; Mulder, P., Kinetic study of the thermolysis of anisole in a hydrogen atmosphere. *The Journal of Physical Chemistry* **1993,** *97* (30), 7914-7925.

32. Liu, C.; Ye, L.; Yuan, W.; Zhang, Y.; Zou, J.; Yang, J.; Wang, Y.; Qi, F.; Zhou, Z., Investigation on pyrolysis mechanism of guaiacol as lignin model compound at atmospheric pressure. **2018,** *232*, 632-638.

CHAPTER 4.   GAS-PHASE PYROLYSIS OF PHENETHYL PHENYL ETHER BY COLLISION-INDUCED DISSOCIATION MASS SPECTROMETRY

4.1   Introduction

Lignin is the second most abundant biopolymer on Earth and represents a renewable energy option.[1] Whereas cellulose makes up around 33 percent of all plant matter, lignin contains approximately 30 percent of all non-fossil organic carbon.[2, 3] It is readily available as a byproduct of the pulping process, and when heated can be converted into liquid transportation fuels.[4] The thermochemical conversion of lignin into its products results in both a bio-oil mixture and char formation which vary in amounts depending on the temperature and residence times used.[5, 6] The bio-oil contains useful aromatic molecules that can be separated and purified; however, poor product selectivity associated with pyrolysis results in broad product distributions and high purification costs.[1, 7]

Understanding the factors that control product selectivity is difficult because of the structural diversity of lignin and the many different reactions that occur under pyrolysis conditions.[6] While the exact structure of lignin remains unknown, many of its structural features have been inferred from examining its decomposition products, including over eight kinds of linkages.[4, 8] Thermolysis of these linkages have been proposed to decompose via both concerted reaction pathways as well as through homolytic cleavages.[9-13] In addition to temperature and residence time, methoxy and hydroxy substituents have also been found to accelerate decomposition rates of these linkages and affect the distribution of pyrolysis products.[5, 6, 14, 15]

Insights into the gas-phase decomposition of lignin can be found by studying lignin model compounds. Phenethyl phenyl ether (PPE) is the simplest model compound of the β-O-4 linkage which constitutes nearly 50% of all lignin linkages.[1] While much work has been done to identify how this linkage decomposes under various conditions, a debate still revolves around whether initial fragmentation proceeds through a concerted elimination reaction to form phenol or a homolytic bond dissociation to form phenoxy radical.

Four possible homolytic pathways are shown in Figure 4.1 Possible homolytic cleavages of phenethyl phenyl ether. along with their calculated bond dissociation energies (BDE)[12] in kcal

mol^{-1}. The lowest energy pathway is cleavage of the C_β-O bond (69.9 kcal mol^{-1}), so it is expected to cleave before the other three. However, concerted reactions are thought to compete with C_β-O homolysis during PPE pyrolysis. Two concerted reactions, a retro-ene reaction and a Maccoll elimination, are shown in Scheme 2 along with their calculated activation energies[9] in kcal mol^{-1}.
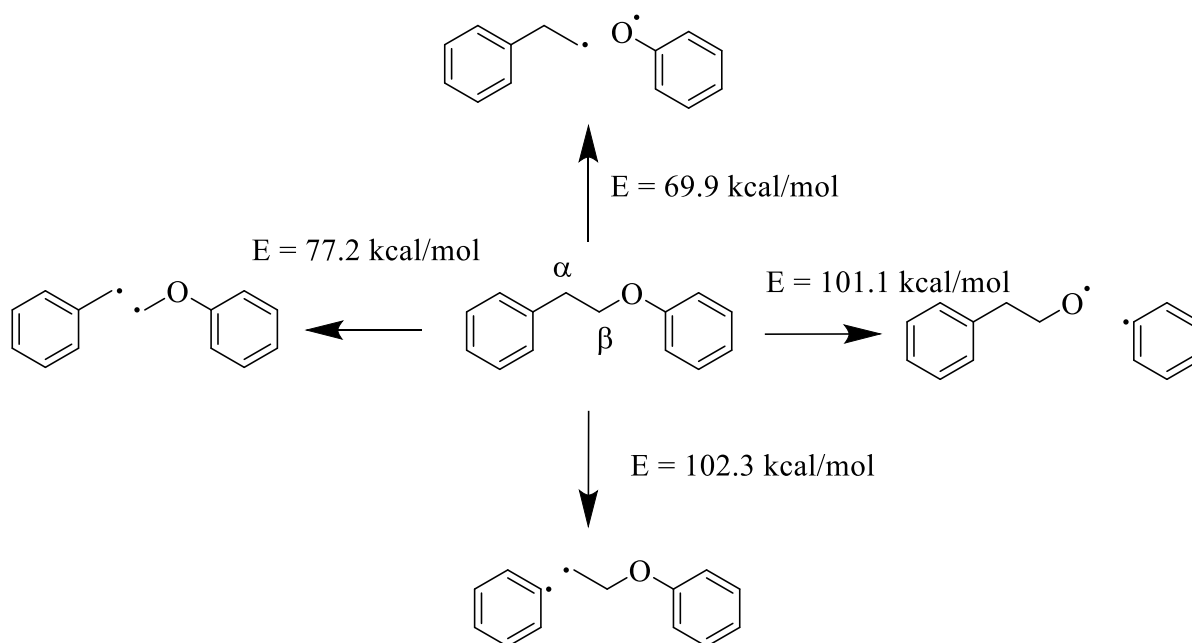
Figure 4.1 Possible homolytic cleavages of phenethyl phenyl ether.

The retro-ene and Macoll elimination reactions proceed through transition states with activation energies of 55.18 kcal mol^{-1} and 62.54 kcal mol^{-1}, respectively. From these activation energies, the retro-ene pathway is expected to dominate over the Macoll elimination reaction, and both the retro-ene and Macoll elimination reactions are lower in energy than all four of the homolytic bond dissociations shown in Figure 4.2.
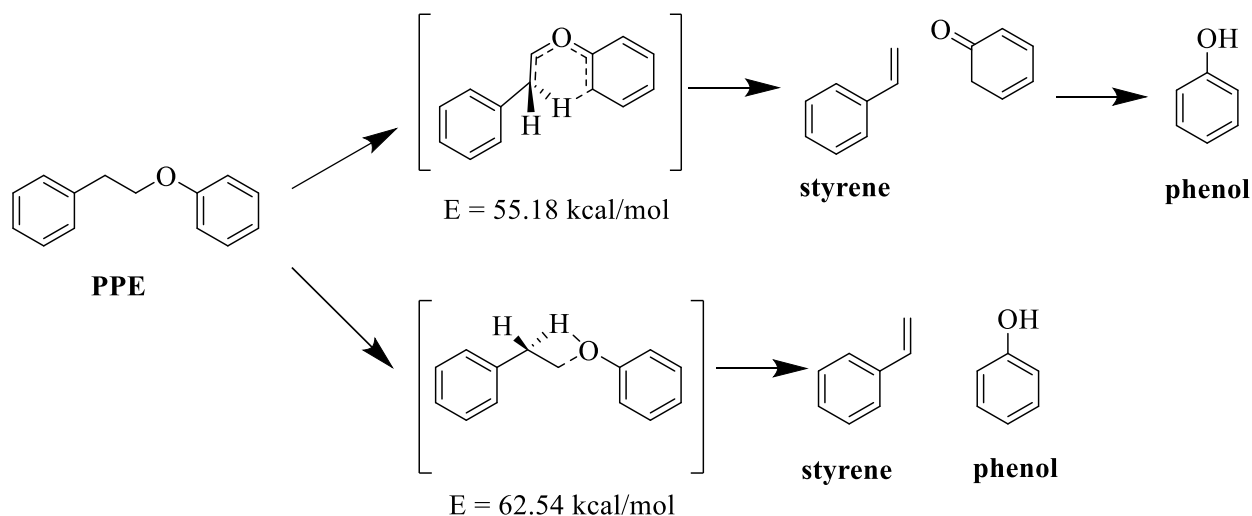
Figure 4.2 Elimination reactions of PPE

However, experimental evidence remains inconclusive about which pathway dominates during pyrolysis. A challenge with discriminating between the concerted pathways and the homolytic bond dissociation is that phenoxy radical can extract an H atom and lead to the same major products as the concerted pathway; namely, phenol and styrene (Scheme 4.1).

Scheme 4.1
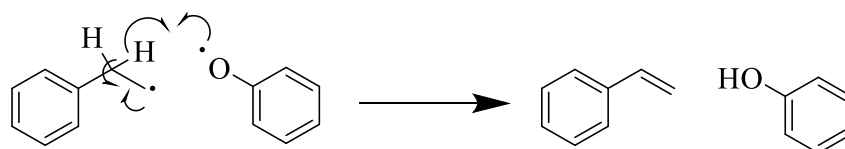
In an attempt to distinguish between the two pathways, Britt et al. placed deuterium in the benzylic position of PPE and observed that the rate of decomposition during flash vacuum pyrolysis at 500 °C was more indicative of a homolytic cleavage.[5, 6] Similarly, Wang et al. found that the product distribution of a synthetic β-O-4 dimer lignin model compound using pyrolysis-GC/MS showed that C_β-O bond homolysis is favored across a wide temperature range (150 °C – 850 °C).[13]

In contrast, by using a hyperthermal nozzle and photoionization time-of-flight mass spectrometry which can detect radicals, Jarvis et al. showed that the C_β-O bond homolysis only becomes significant above 1000 °C whereas the concerted reactions are more significant at lower

temperatures.[11] All of the methods mentioned above suffer from low sensitivity due to dilute samples, which is done to minimize bimolecular reactions.[6] Because of the contrasting results, improving the sensitivity of short-lived radicals during pyrolysis would help solve the question around the initial dissociation of PPE.[11]

In this work, we used collision-induced dissociation charge-remote fragmentation (CID-CRF) mass spectrometry to isolate reactive intermediates involved in the gas-phase degradation of PPE. CID-CRF occurs when a portion of a molecule undergoes fragmentation separate from the location of the charge site. By attaching a charge tag to lignin model compounds, target molecules including reactive intermediates of PPE can be isolated in high concentrations. By varying the collision energy and measuring the branching ratios of the resulting product ions, insights were gained into the transition state of phenol formation.

4.2   Methods

4.2.1   Materials

Starting materials and solvents were purchased from commercially available sources and used as received. All chemicals were used as received. ^{1}H-NMR spectroscopic data were collected with a Bruker AV-III-400-HD.

The synthesis of phenethyl phenyl ether (PPE), 2-methoxy-PPE, 2,6-dimethoxy-PPE, and their brominated analogs was carried out following a method that has been described previously.[16] Dry acetone was obtained by adding 2.5 g calcium sulfate to 100 mL of acetone and stirring for 4 hours. The acetone was then decanted and distilled with another 1 g of fresh calcium sulfate. Approximately 33 mL distilled acetone was collected directly in the 200 mL round bottom reaction flask containing potassium carbonate (6 g, 43 mmol) and a stir bar. Phenol (4 g, 42 mmol), or methoxy-substituted phenol, was added to the reaction, and the round bottom was equipped with a water condenser. The phenol was refluxed for 1 h. After 1 h, (2-bromethyl)-benzene (11 g, 59 mmol) was added, and the reaction continued to reflux for 24 h. After 24 h, water (25 mL) and hexanes (25 mL) were added to the reaction flask. The organic layer was removed, and the aqueous layer was extracted with ethyl acetate, which was combined with the organic layer. The organic layer was then rinsed with 1 M NaOH (3 x 30 mL) and 1 M NaCl (1 x 30 mL). The solvent

was then removed by a rotavapor, and the product was purified by column chromatography using hexanes and ethyl acetate.

PPE ^{1}H-NMR (400 MHz, DMSO-d_6) δ: 7.26 (7H, m), 6.90 (3H, m), 4.15 (2H, t, $J = 6.0$ Hz), 3.01 (2H, t, $J = 8.0$ Hz);

2-methoxy-PPE ^{1}H-NMR (400 MHz, CDCl$_3$) δ: 7.29 (5H, m), 6.90 (4H, m), 4.22 (2H, t, $J = 7.6$ Hz), 3.87 (3H, s), 3.17 (2H, t, $J = 7.6$ Hz)

2,6-dimethoxy-PPE ^{1}H-NMR (400 MHz, DMSO-d_6) δ: 7.27 (4H, m), 7.18 (1H, m), 6.96 (1H, t, $J = 8.0$ Hz), 6.63 (2H, d, $J = 8.0$ Hz), 4.03 (2H, t, $J = 6.0$ Hz), 3.71 (6H, s), 2.93 (2H, t, $J = 6.0$ Hz)

Silica sulfuric acid was synthesized as described by Zolfigol and coworkers.[17] A 25 mL filtering flask was charged with a magnetic stirrer and silica (5 g, 83 mmol) and a gas inlet tube for drawing away HCl gas over an adsorbing solution (water). The filtering flask was fitted with an addition funnel holding chlorosulfuric acid (1.1 mL, 16 mmol). The chlorosulfuric acid was added dropwise at room temperature over 5 min. HCl gas immediately formed in the filtering flask. After the addition was completed, the mixture was stirred for an additional 10 min. The product was a white solid of silica sulfuric acid.

Direct Sulfonation: The synthetic route to the sulfonated products used in this work was an electrophilic aromatic substitution reaction using silica sulfuric acid in excess of substrate without any solvent as reported by Hajipour and coworkers.[18] A 10 mL round bottom flask with a magnetic stirrer was charged with silica sulfuric acid (38 mg, 0.1 mmol) and also the substrate (0.5 mmol). The reaction mixture was stirred at 80 °C for 30 min, then filtered and washed with 10 mL of ethyl acetate. The solvent was removed under reduced pressure. The remaining liquid was washed with 40 mL of hexanes to form a semi-solid substance and dried under vacuum for several hours to obtain the desired solid product.

General Heck Olefination: The synthetic route for attaching a sulfonated styrene tag to the molecules in this work was a Heck reaction using palladium(II) acetate catalyst in DMF/water as described by Khemaïs and coworkers.[19] A 100 mL round bottom flask with a magnetic stir bar was charged with the 4-bromo substrate analog (5 mmol), sodium p-styrenesulfonate hydrate (0.93 g, 4.5 mmol), potassium carbonate (7.5 mmol), palladium(II) acetate (1 mol %, 11.2 mg), Aliquat 336 (1.14 mL, 2.5 mmol), DMF (2 mL), and water (2 mL). The reaction mixture was stirred at 95 °C for 2 hr. After the reaction was completed, 40 mL chloroform was added and the solid was

114

filtered. The solid was rinsed with methanol (100 mL), and the filtrate was collected. The methanol was removed under reduced pressure to give a solid product. The solid was rinsed multiple times with methanol/ethyl acetate (1:10) to remove unreacted p-styrenesulfonate, which was slightly less polar than the target molecule.

4.2.2   Instrumentation

Mass spectra were collected on a commercial LCQ-DECA (Thermo Electron Corporation, San Jose, CA, USA) quadrupole ion trap mass spectrometer. Samples were diluted in 50:50 water/methanol and then injected into the mass spectrometer using electrospray ionization (ESI). CID experiments were done using helium as the collision target. The collisional energy was given by the normalized collision energy (NCE) which ranges from 0% to 100%.

4.2.3   Quantum Chemical Calculations

Geometry optimizations and frequency calculations for both ground states and transition states were performed using density functional theory (DFT) with the M06-2X functional[20] and the 6-31++G(d,p) basis set. Calculations were done using Gaussian16 suite of programs.[21]

4.3   Results

4.3.1   PPE

PPE was the first system investigated using CID-CRF. The SO_3 group was attached directly to the aryloxy ring. The CID-CRF spectrum of this sulfonated compound, **A1SO$_3^-$** (m/z 277), is shown in Figure 4.3. The dissociation occurs via three competing pathways. The first is loss of SO_2, which is observed at m/z 197 (**A1O$^-$**).
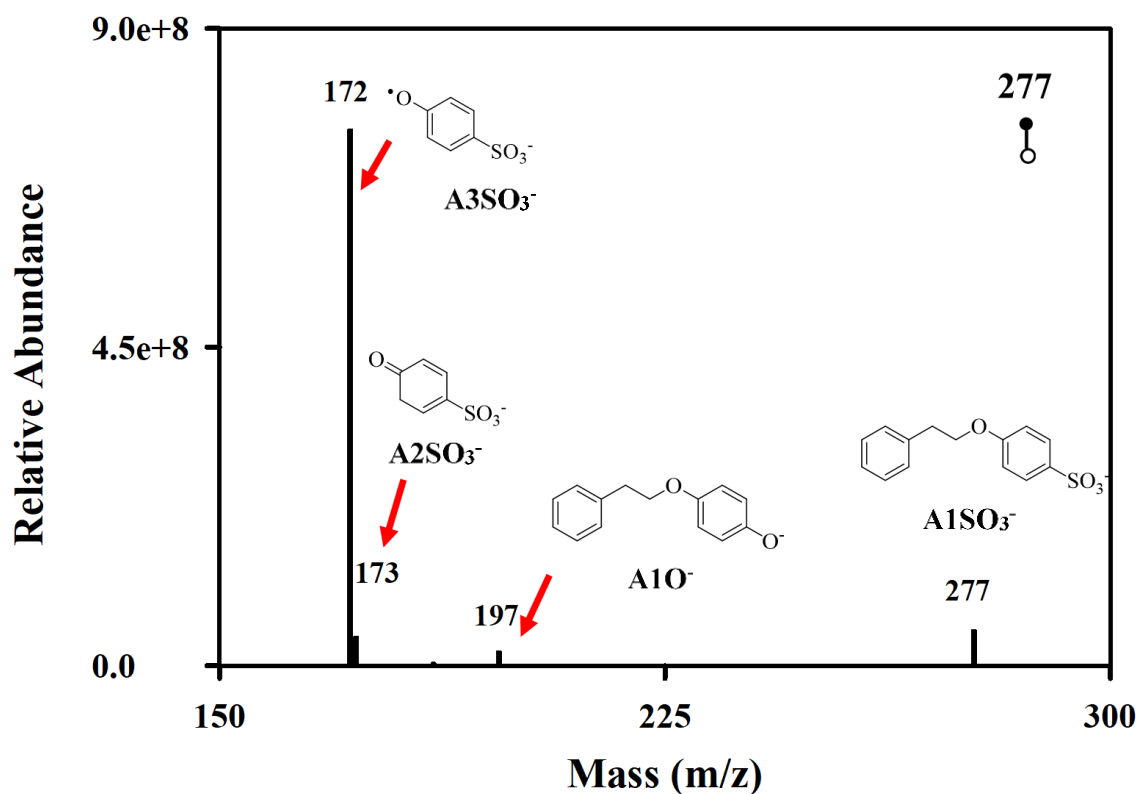
Figure 4.3 CID-CRF of **A1SO₃⁻** (m/z 277)

The second competing pathway is a rearrangement reaction leading to elimination of styrene and **A2SO₃⁻** (m/z 173) or its isomer **iso-A2SO₃⁻** (m/z 173), as shown in Scheme 4.2. The two isomers **A2SO₃⁻** and **iso-A2SO₃⁻** could not be distinguished by CID.

Scheme 4.2

A1SO₃⁻

m/z 277

iso-A2SO₃⁻

m/z 173

A2SO₃⁻
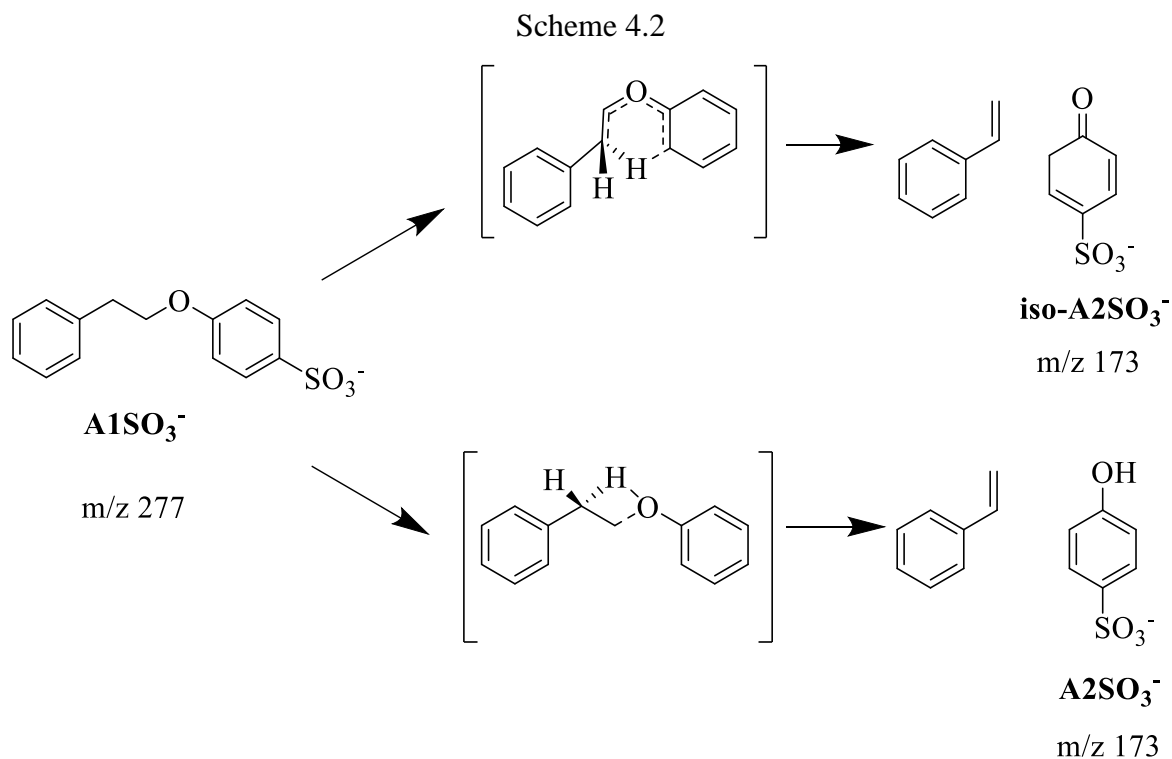
m/z 173

The third competing pathway is homolytic cleavage of the β-O-4 linkage leading to phenethyl radical and phenoxy radical, **A3SO₃⁻** (m/z 172), as shown in Scheme 4.3. To make sure that m/z 172 was a primary product of m/z 277 and not of m/z 173, we carried out CID of the m/z 173 peak. As expected, the O-H bond did not cleave under the experimental conditions. Thus, **A2SO₃⁻** (m/z 172) is a primary product of **A1SO₃⁻** (m/z 277).

Scheme 4.3

A1SO₃⁻

m/z 277

phenethyl

A2SO₃⁻

m/z 172
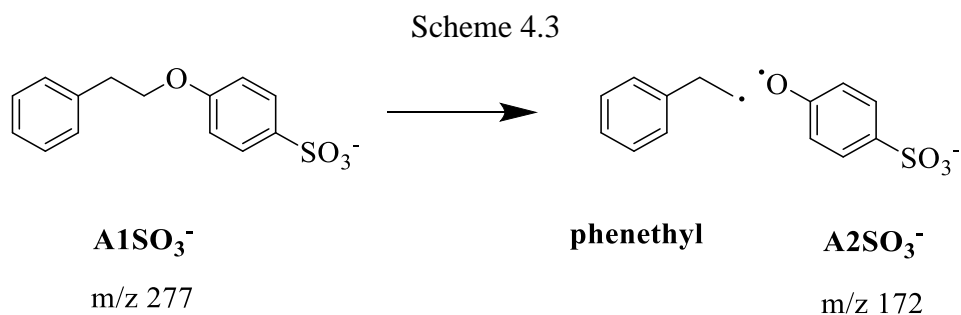
Unfortunately, because the charge tag is on the aryloxy ring, phenethyl radical is not visible in the spectrum. To detect phenethyl radical, we synthesized PPE with the tag on the opposite ring. For ease of synthesis, we included a styrene linker between the ring and the charge tag and called

this molecule **SO₃C₈H₆-PPE⁻**. The resulting CID-CRF spectrum confirmed the formation of phenethyl radical. Based on the peak intensities in Figure 1, homolytic cleavage appears to be the dominant dissociation pathway.

4.3.2   2-methoxy-PPE

The second system investigated using CID-CRF was 2-methoxy-PPE. The full mass scan and subsequent CID spectra of this ion, **B1SO₃⁻** (m/z 307), are shown in Figure 4.4. Rearrangement reactions that were seen with **A1SO₃⁻** are not visible in the CID spectrum of **B1SO₃⁻**. Panel b shows that loss of methyl radical now competes with cleavage of the β-O-4 bond as the main dissociation pathways for this molecule, as shown in Scheme 4.4.

.
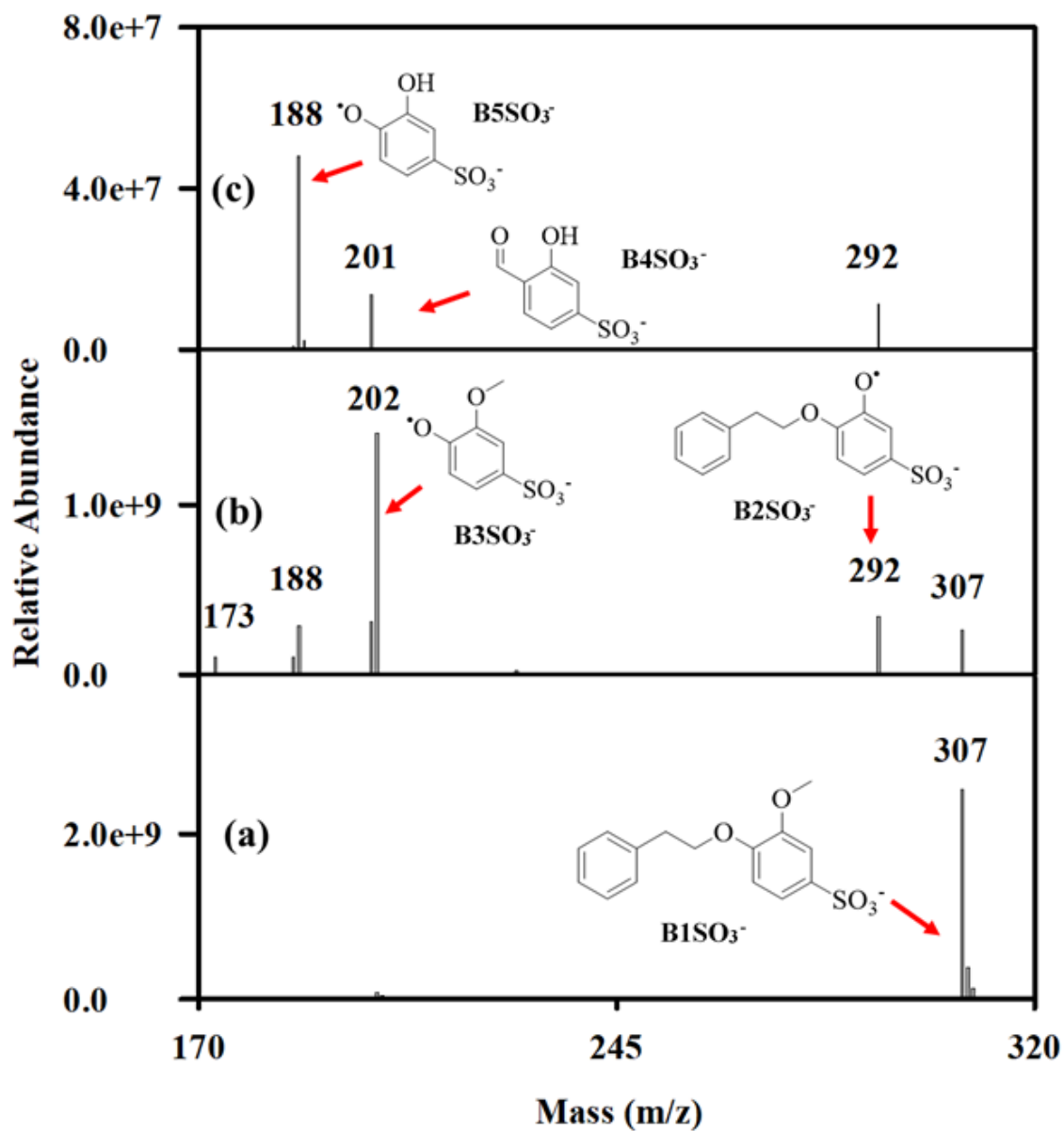
Figure 4.4 (a) The full mass scan of **B1SO$_3^-$** (m/z 307). (b-c) Subsequent CID-CRF.

Scheme 4.4

B1SO₃⁻

m/z 307

-CH₃•

B3SO₃⁻
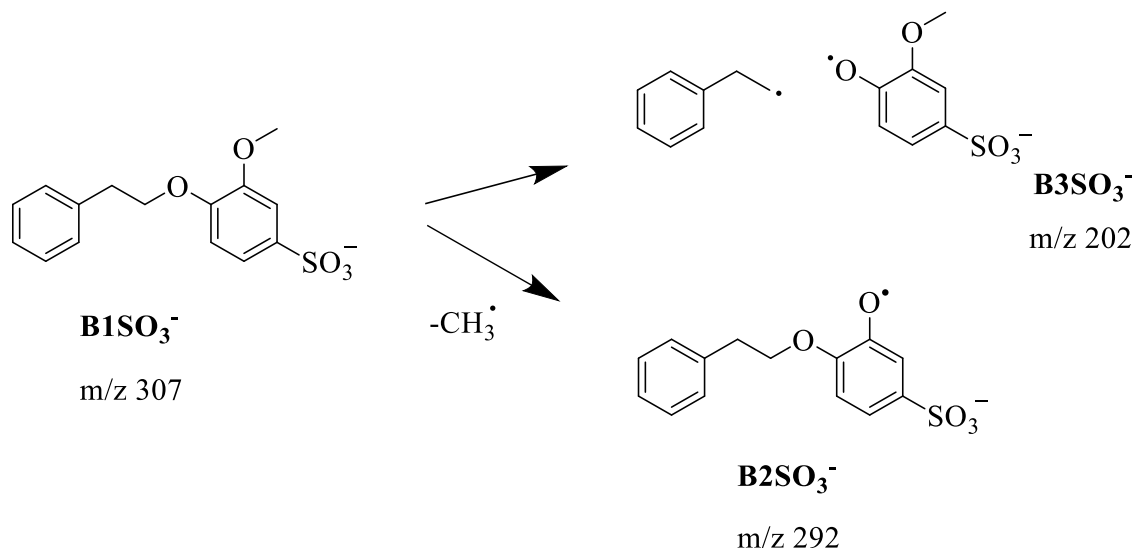
m/z 202

B2SO₃⁻

m/z 292

Upon further CID-CRF, **B2SO₃⁻** (m/z 292) can rearrange via an H transfer involving both the α and β carbons followed by dissociation to form **B4SO₃⁻** (m/z 201) and **B5SO₃⁻** (m/z 188), as shown in Scheme 4.5. Subsequent CID-CRF of **B3SO₃⁻** (m/z 202), **B4SO₃⁻** (m/z 201), and **B5SO₃⁻** (m/z 188), were carried out in Chapter 3 of this work.

Scheme 4.5

B2SO₃⁻

m/z 292

B4SO₃⁻

m/z 201

B5SO₃⁻

m/z 188
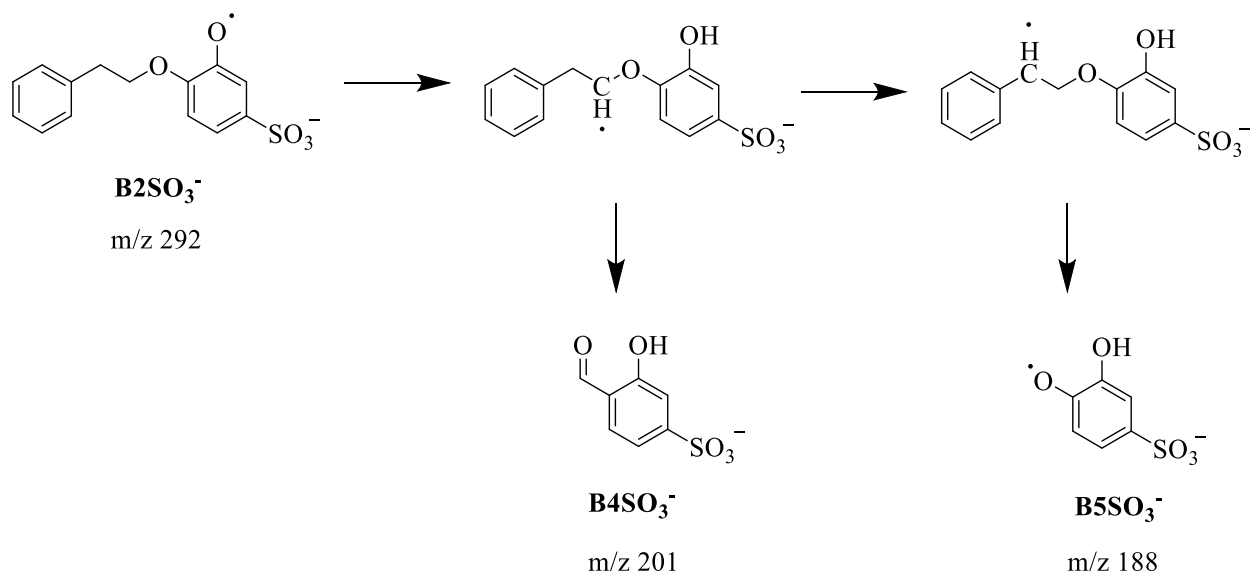
4.3.3   2,6-dimethoxy-PPE

The third system investigated using CID-CRF was 2,6-dimethoxy-PPE. The full mass scan and subsequent CID spectra of this molecule, C1SO3- (m/z 379), are shown in

Figure 4.5. C1SO3- dissociates by two sequential losses of methyl radical to form C2SO3- (m/z 322) and C3SO3- (m/z 307), or by cleavage of the β-O-4 bond to form C4SO3- (m/z 232), as shown in Scheme 4.6.

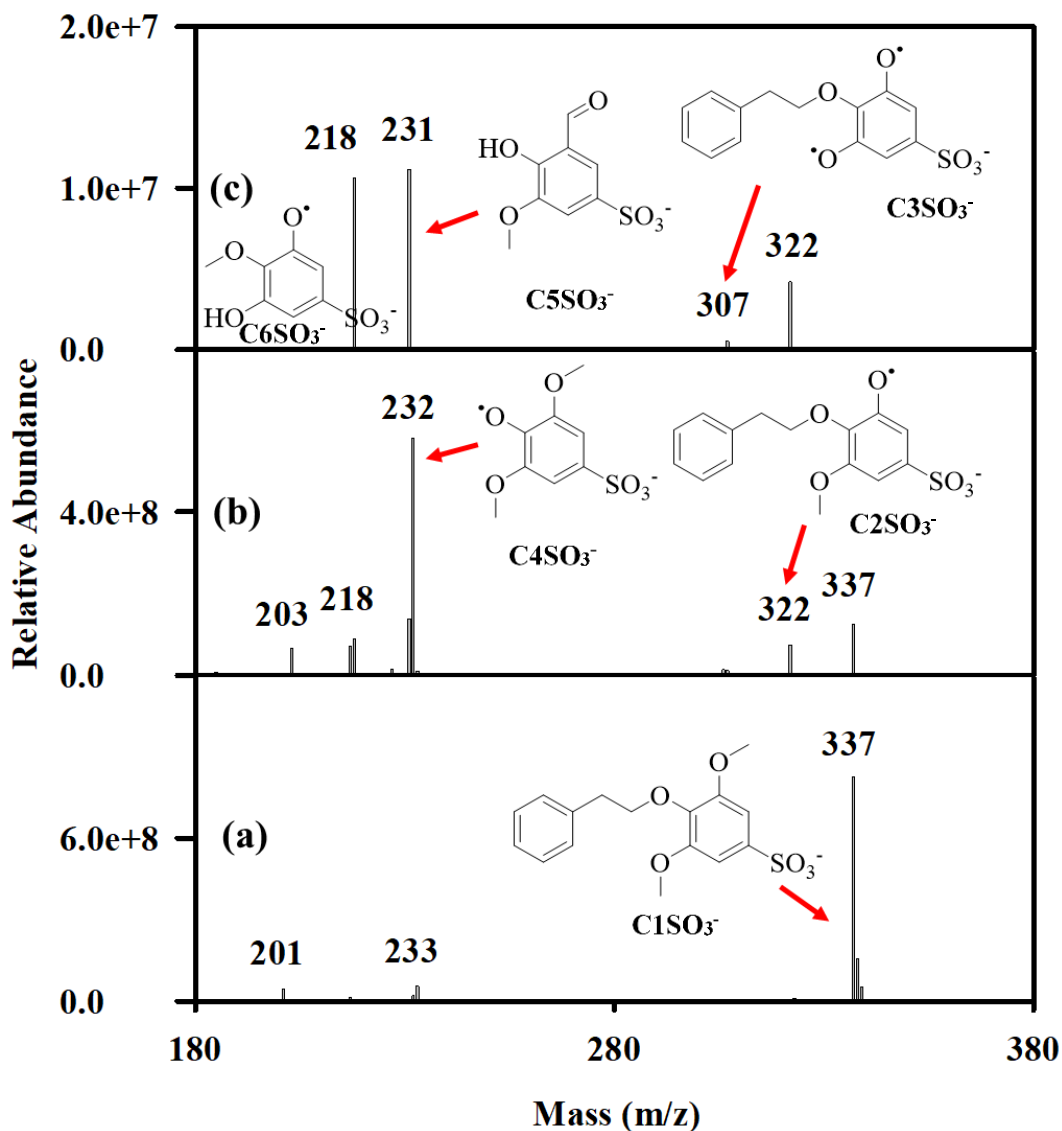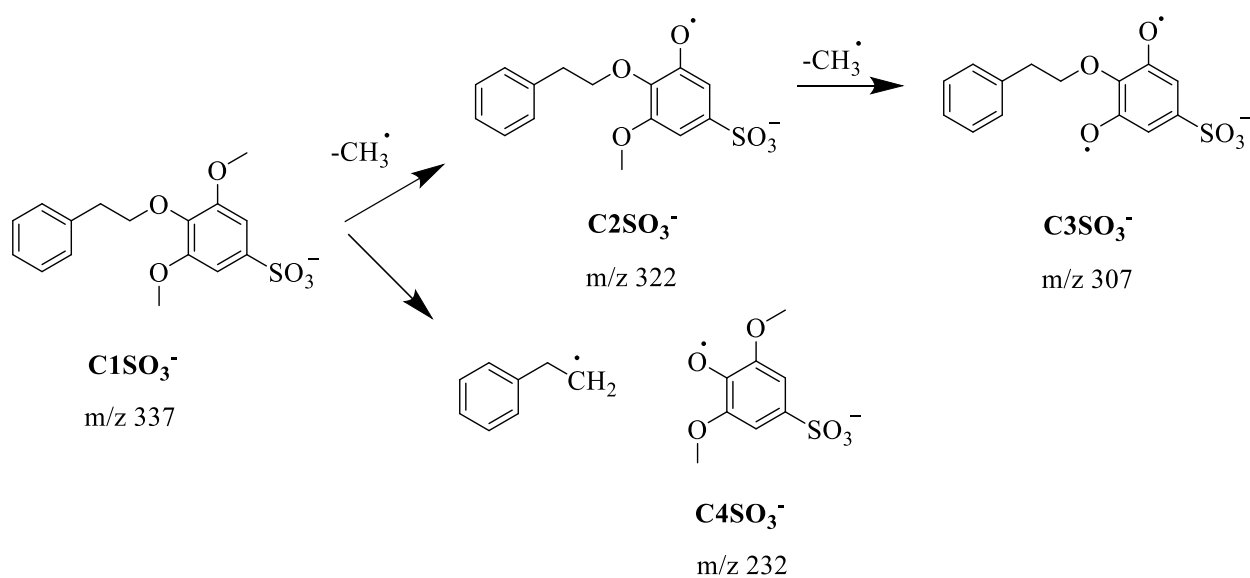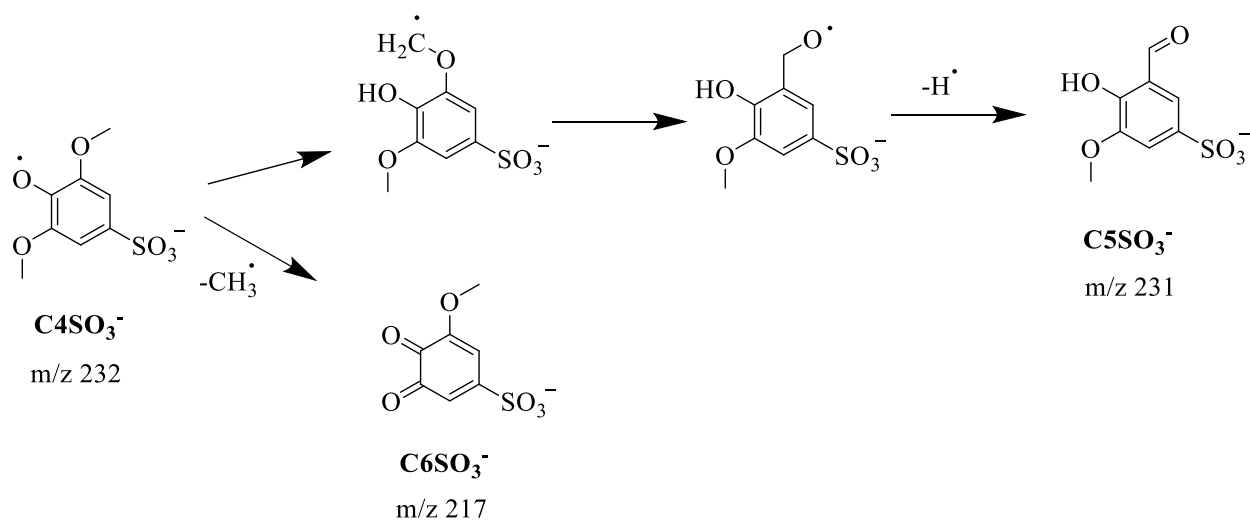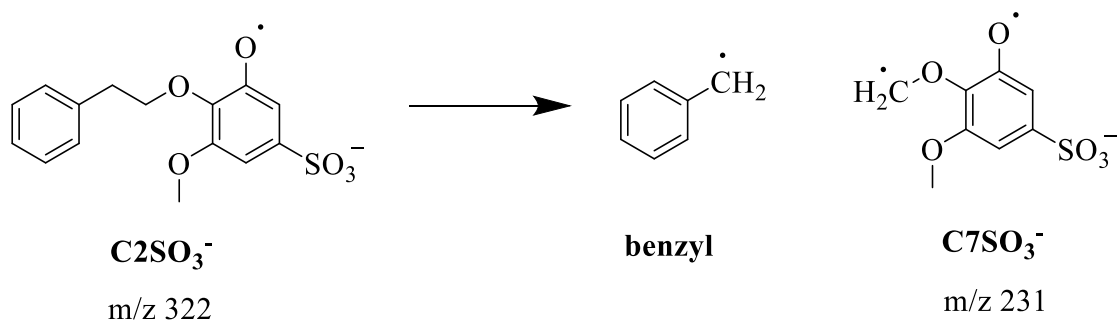Figure 4.5 (a) The full mass scan of **C1SO₃-** (m/z 337). (b-c) Subsequent CID-CRF.

Scheme 4.6

C4SO₃⁻ can dissociate by eliminating H radical to form **C5SO₃⁻** (m/z 231) or by losing a second methyl radical to form **C6SO₃⁻** (m/z 217), as shown in Scheme 4.7.

Scheme 4.7

C2SO₃⁻ contributes to **C7SO₃⁻** (m/z 231) by homolytic cleavage of the α-β C-C bond, as shown in Scheme 4.8.

Scheme 4.8

C2SO$_3^-$

m/z 322

benzyl

C7SO$_3^-$

m/z 231

4.4 Discussion

4.4.1 PPE

CID-CRF has been compared to the thermolysis of compounds in the gas phase.[22] For this reason, we compare the products in our CID-CRF spectra of sulfonated analogs to the products formed from the pyrolysis of authentic PPE. Jarvis and coworkers studied the pyrolysis of PPE using a hyperthermal nozzle and detected the products using photoionization mass spectrometry (pyrolysis-PIMS).[11] Pyrolysis-PIMS showed that PPE dissociated via a concerted retro-ene reaction to eliminate phenol, and the bond homolysis did not become significant until at higher temperatures. In contrast, using CID-CRF, the height of the m/z 172 peak in Figure 4.1 indicates that formation of phenoxy radical via homolytic cleavage is the dominant pathway.

Because computational results also predict the concerted retro-ene reaction to dominate, we wanted to find out the reason why our experimental results were not matching the theoretical predictions. We carried out an energy-resolved CID experiment on **1** to find out how the branching ratio of phenoxy radical to phenol would change as the energy was increased. The plot of the branching ratios of phenoxy to phenol are shown Figure 4.6. The concerted reaction appears to make its greatest contribution at lower energies, which matches what was found by Jarvis et al.[11] Below 1 eV, minimal dissociation was observed, so the branching ratio could not be detected below this point. However, it appears that the homolytic cleavage dominates at all energies.

Branching Ratio (Phenol/Phenoxy radical)
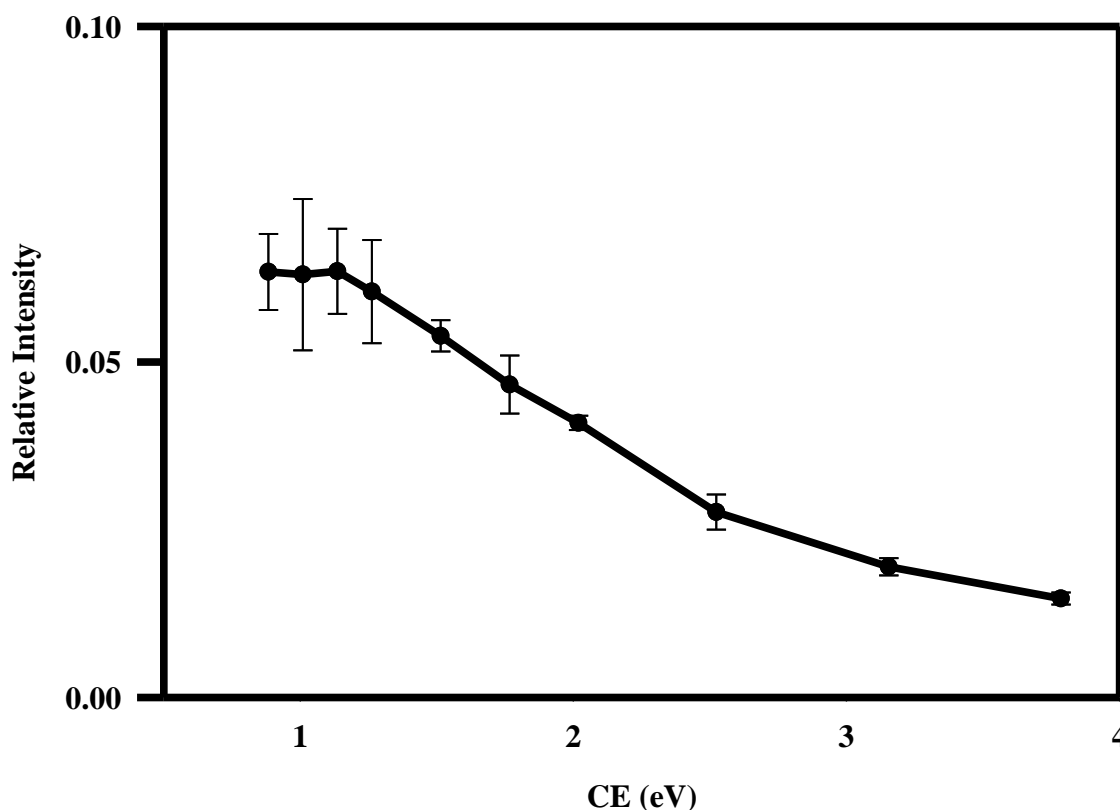
Figure 4.6 Branching ratio of phenol/phenoxy radical.

We wondered whether the addition of the SO_3 charge tag was stabilizing the homolytic bond dissociation over the elimination reaction. In order to see whether this was the case, we carried out quantum mechanial calculations. We found that while addition of the SO_3 did reduce the BDE of the homolytic bond dissocitation by 9 kcal mol^{-1}, it also decreased the activation energy of the rearrangement reaction by 5.4 kcal mol^{-1} keeping it as the lowest energy pathway by 10 kcal mol^{-1} (Table 4.1). Thus, the SO_3 group did not appear to alter the dissociation pathway of PPE.

Table 4.1 The effect of changing the R group on the calculated energy of PPE dissociation using M062X

Pathway	R=H (kcal mol-1)	R=SO$_3^{-1}$ (kcal mol-1)
β-O4 bond dissocation (DH$_{298}$)	69.6	60.8
retro-ene elimination (E$_a$)	56.0	50.6
Macoll elimination (E$_a$)	61.9	59.4

Becaue calculations showed that the order of the energy barriers for the various reactions was not changed by the charge tag (bond homolysis still had the greatest energy barrier), we wondered if a different theory would be better at explaining why bond homolysis was the dominant pathway. Using CRUNCH, a Fortran program written by Armentrout and Ervin, we applied RRKM theory to see how the predicted branching ratios of the unimolecular dissociation products might change as the "tightness" of the retro-ene transition state was adusted, as shown in Figure 4.7. For both curves, the dissociation energy of the direct homolysis was held constant. Using a tight transition state for the retro-ene elimination (blue curve), a best fit curve to the high-energy portion of the experimental data (3-4 eV) shows significant deviation from the experimental data at lower energies. However, when a loose transition state is used for the retro-ene elimination (red curve), a better match with the experimental data is achieved.
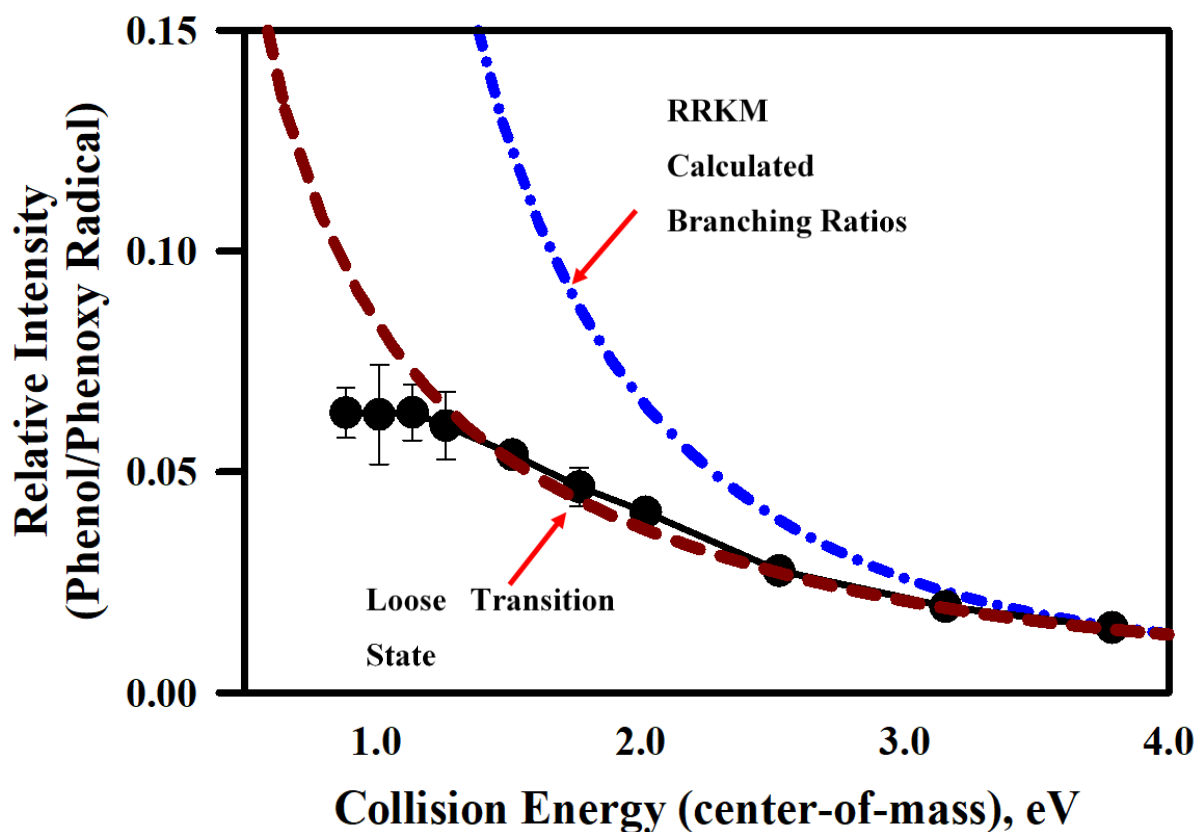
Figure 4.7 RRKM calculated branching ratios of phenol/phenoxy radical using a tight transition state (blue) and a loose transition state (red) for the retro-ene elimination reaction, plotted with the experimental data (black)

Because a loose transition state for phenol formation was a better match of the experimental results, we proposed that phenol formation proceeded via a roaming transition state. A roaming transition state has been described by Townsend and Bowman, where a complex of the dissociation products is held together by electrostatic forces prior to complete separation, and the fragments are free to rotate in all directions.[23, 24] A similar occurrence has been observed for ion-neutral complexes.[25] While the fragments rotate around each other, a hydrogen atom transfer can occur from the phenethyl radical to the phenoxy radical to form phenol.[26] A reaction coordinate diagram indicating this new pathway is shown in Figure 4.8.
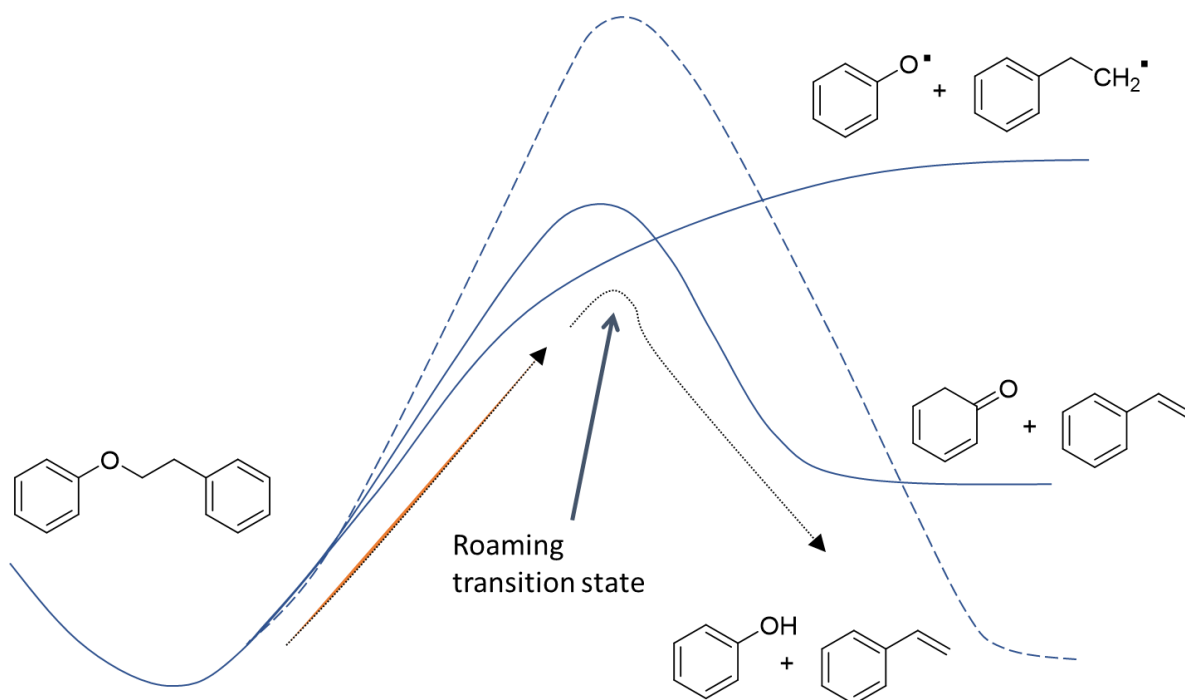
Figure 4.8 Proposed reaction coordinate diagram for PPE dissociation that includes a roaming transition state for phenol formation

4.4.2 2-methoxy-PPE

Previous experimental and computational work on PPE has shown that methoxy substituents can lower the BDE of the C_β-O bond.[5, 6, 14, 15] As a result of the lower BDE as well as the additional methoxy group, the dissociation pathway of PPE can change. This is significant because methoxy groups are common substituents in lignin, so their influence on its dissociation should be understood. We attached an SO_3 charge tag to 2-methoxy-PPE making **B1SO$_3^-$** (m/z 307) so that we could compare CID-CRF of this compound to authentic pyrolysis products.

Radical intermediates have not been isolated for 2-methoxy-PPe before. However, Britt et al. were able to isolate the pyrolysis products of this compound using flash vacuum pyrolysis (FVP). Some of the FVP products are not unimolecular decomposition products because the radical intermediates can abstract H from the walls of the pyrolysis chamber. Nevertheless, we can still compare our results using CID-CRF to those found by FVP.

The major products and percent yield found by Britt et al.[5] for FVP of 2-methoxy-PPE are shown in Figure 4.9. One thing that Britt could not tell from the FVP products is what pathway

was taken when multiple pathways are available. For example, the initial step for formation of 2-hydroxybenzaldehyde, **P1**, can be either methyl loss or β-O-4 bond homolysis (Figure 4.10).

Figure 4.9 Some of the more abundant FVP products of 2-methoxy-PPE found by Britt et al.

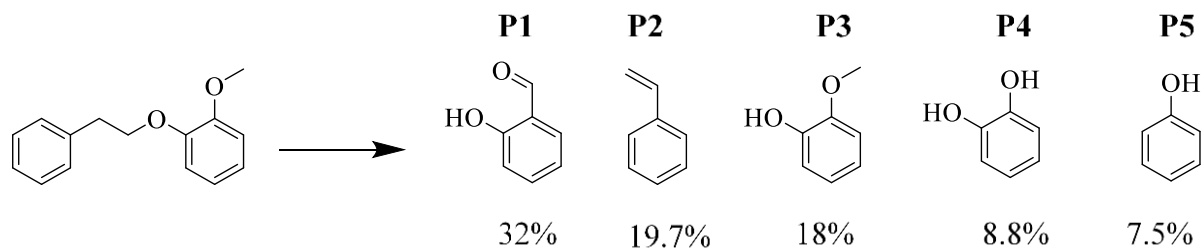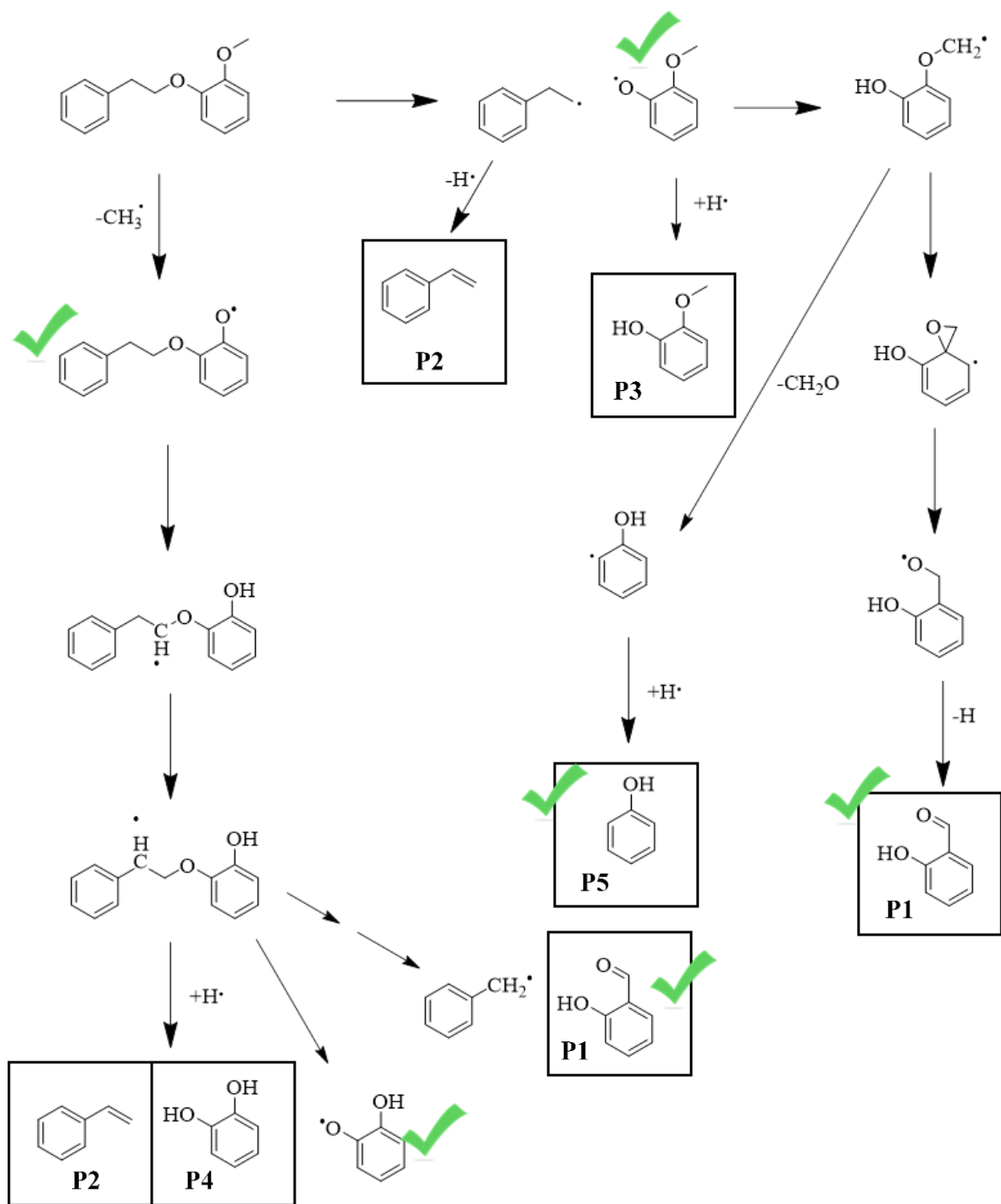Figure 4.10 Proposed degradation mechanism for *ortho*-methoxy-PPE. Products seen by CID-CRF are boxed. Products seen by FVP are circled.

However, using CID-CRF, we can clearly see which of the two pathways are favored because **B3SO₃⁻** has the tallest peak (Figure 4.4b). Thus, most of the 2-hydroxybenzaldehyde must come from **B3SO₃⁻** rather than the **B2SO₃⁻** route.

Because the charge tag is attached to the aryloxy ring, the other ring is lost as a neutral product and not detected by mass spectrometry. For this reason, we were unable to detect neutral styrene. However, an advantage of CID-CRF is that we can detect radical intermediates that are true unimolecular decomposition products of PPE. For example, rather than seeing guaiacol that was observed by Britt et al., we see its precursor 2-methoxyphenoxy radical, **B3SO₃⁻**, which can be isolated and subjected to additional CID. A second example is rather than seeing cresol, we see 2-hydroxyphenoxy radical, **B5SO₃⁻** (Figure 4.4b).

4.4.3 2,6-dimethoxy-PPE

When a second methoxy group is substituted on the aryloxy ring, the model compound is very similar to sinapyl alcohol, an abundant subunit in lignin. Understanding how it decomposes under heat is an important step to understanding the pyrolysis of lignin. Several of the major products and percent yields found by Britt et al.[5] for the FVP of 2,6-dimethoxy-PPE are shown in Figure 4.11.
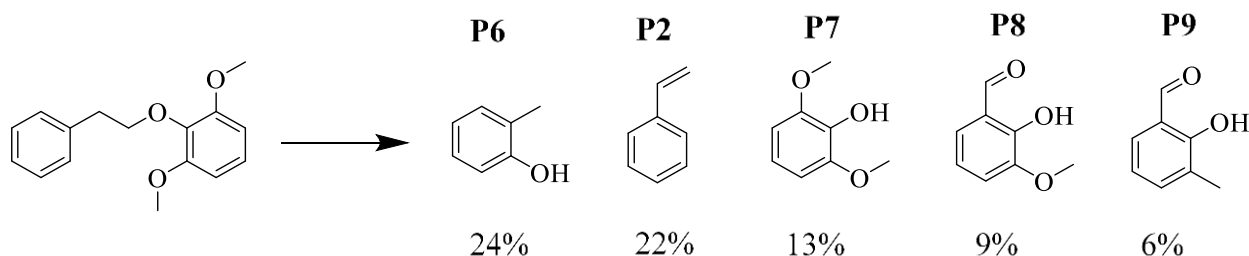
Figure 4.11 Some of the more abundant FVP products of 2,6-dimethoxy-PPE found by Britt et al.[5]

The dissociation pathway proposed by Britt et al., along with the intermediates seen by CID-CRF, are shown below. Once again, while we were unable to detect bimolecular reactions that were seen by Britt et al., we isolated many of their radical precursors. For example, initial

dissociation occurs via homolysis of the β-O-4 linkage to form 2,6-dimethoxyphenoxy radical (Figure 4.12).

Figure 4.12 Dissociation of 2,6-dimethoxyphenoxy radical.

This can undergo H abstraction to form syringol, **P7**, or lose H to form 2-hydroxy-3-methoxybenzaldehyde, **P8**. Alternatively, it can lose CHO to form guaiacol, **P6**. Or it can even lose methyl radical to form a quinone structure, which was not detected by FVP. CID-CRF can then further characterize the structures of these products. For example, the quinone structure was found to undergo a second methy radical loss as well as CO loss upon further CID.

The formation of **P9** was proposed to stem from 2,6-dimethoxyphenoxy radical undergoing multiple rearrangements and then losing H and H_2O followed by the addition of 2H (Figure 4.13).

While we could not see the addition of 2H, we confirmed that this is the likely pathway by detecting three of the intermediates to **P9**.

Figure 4.13 Possible mechanism for the formation of **P9**.

Last, but not least, dissociation of 2,6-dimethoxy-PPE can occur by methyl radical loss (Figure 12).
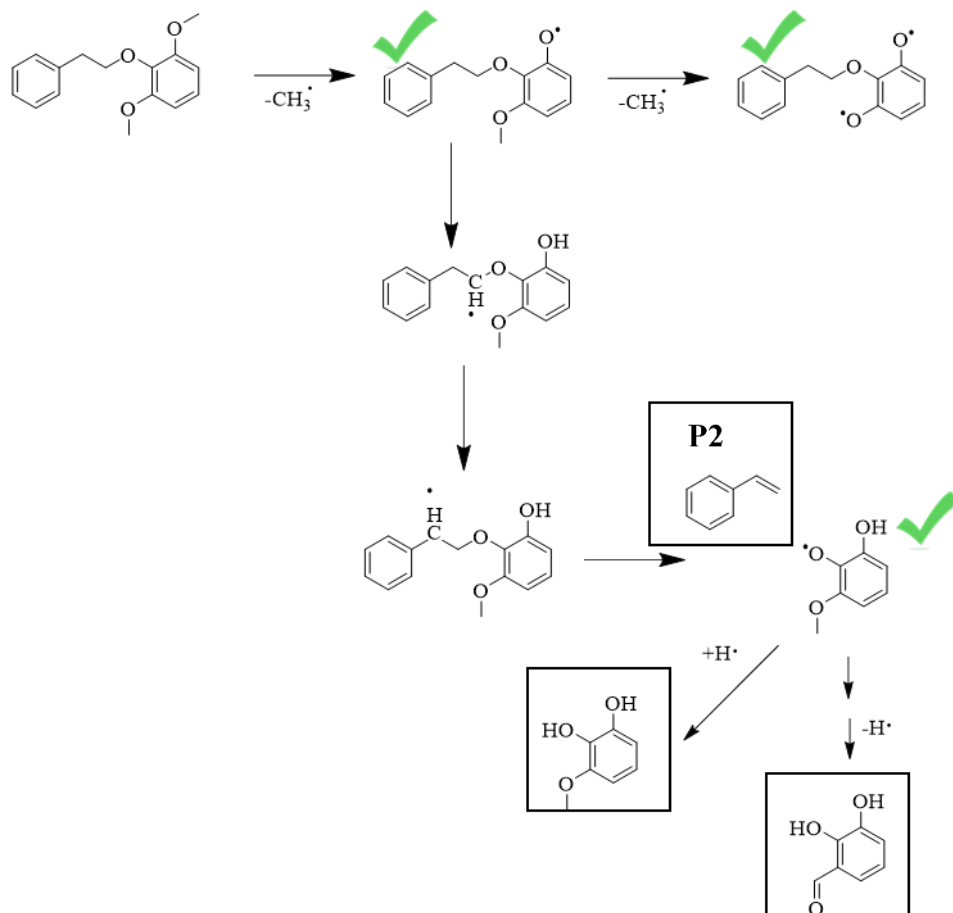
Figure 4.14 Dissociation of 2,6-dimethoxy-PPE by methyl radical loss.

4.5 Conclusion

CID-CRF of phenethyl phenyl ether (PPE) and its methoxy derivatives is an effective way of isolating radical intermediates gen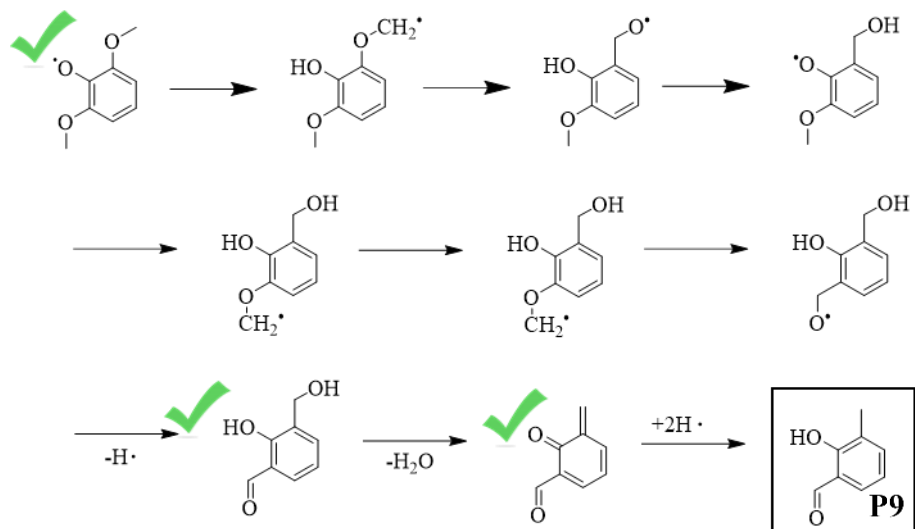erated during the thermal degradation of PPE. Using this method, we observed that the dominant dissociation pathway is β-O-4 bond homolysis rather than a concerted retro-ene elimination to form phenol. The branching ratio of phenol to phenoxide ion indicated that phenol formed via a roaming transition state rather than a concerted elimination reaction. CID-CRF of methoxy-substituted analogs of PPE was consistent with the products observed during FVP. Methoxy-substitution eliminated phenol formation and further favored radical formation. In addition, we identified radical intermediates that had not been isolated before. CID-CRF is an efficient way of tracking the unimolecular decomposition of lignin model compounds in the gas phase and can be used to support other methods.

4.6 References

1. Kawamoto, H., Lignin pyrolysis reactions. *Journal of Wood Science* **2017,** *63* (2), 117-132.

2. Klemm, D.; Heublein, B.; Fink, H.-P.; Bohn, A., Cellulose: Fascinating Biopolymer and Sustainable Raw Material. *Angewandte Chemie International Edition* **2005,** *44* (22), 3358-3393.

3. Boerjan, W.; Ralph, J.; Baucher, M., Lignin Biosynthesis. *Annual Review of Plant Biology* **2003,** *54* (1), 519-546.

4. Chu, S.; Subrahmanyam, A. V.; Huber, G. W., The pyrolysis chemistry of a β-O-4 type oligomeric lignin model compound. *Green Chemistry* **2013,** *15* (1), 125-136.

5. Britt, P. F.; Buchanan, A. C.; Cooney, M. J.; Martineau, D. R., Flash Vacuum Pyrolysis of Methoxy-Substituted Lignin Model Compounds. *The Journal of Organic Chemistry* **2000,** *65* (5), 1376-1389.

6. Britt, P. F.; Buchanan, A. C., III; Martineau, D. R., Flash Vacuum Pyrolysis of Lignin Model Compounds: Reaction Pathways of Aromatic Methoxy Groups. Oak Ridge National Lab., TN (US): United States, 1999.

7. Xu, L.; Zhang, Y.; Fu, Y., Advances in Upgrading Lignin Pyrolysis Vapors by Ex Situ Catalytic Fast Pyrolysis. *Energy Technology* **2017,** *5* (1), 30-51.

8. Chakar, F. S.; Ragauskas, A. J., Review of current and future softwood kraft lignin process chemistry. *Industrial Crops and Products* **2004,** *20* (2), 131-141.

9. Elder, T.; Beste, A., Density Functional Theory Study of the Concerted Pyrolysis Mechanism for Lignin Models. *Energy & Fuels* **2014,** *28* (8), 5229-5235.

10. Klein, M. T.; Virk, P. S., Model pathways in lignin thermolysis. 1. Phenethyl phenyl ether. *Industrial & Engineering Chemistry Fundamentals* **1983,** *22* (1), 35-45.

11. Jarvis, M. W.; Daily, J. W.; Carstensen, H.-H.; Dean, A. M.; Sharma, S.; Dayton, D. C.; Robichaud, D. J.; Nimlos, M. R., Direct Detection of Products from the Pyrolysis of 2-Phenethyl Phenyl Ether. *The Journal of Physical Chemistry A* **2011,** *115* (4), 428-438.

12. Wang, M.; Liu, C., Theoretic studies on decomposition mechanism of o-methoxy phenethyl phenyl ether: Primary and secondary reactions. *Journal of Analytical and Applied Pyrolysis* **2016,** *117*, 325-333.

13. Wang, S.; Ru, B.; Dai, G.; Shi, Z.; Zhou, J.; Luo, Z.; Ni, M.; Cen, K., Mechanism study on the pyrolysis of a synthetic β-O-4 dimer as lignin model compound. *Proceedings of the Combustion Institute* **2017,** *36* (2), 2225-2233.

14. Britt, P. F.; Kidder, M. K.; Buchanan, A. C., Oxygen Substituent Effects in the Pyrolysis of Phenethyl Phenyl Ethers. *Energy & Fuels* **2007,** *21* (6), 3102-3108.

15. Elder, T., A computational study of pyrolysis reactions of lignin model compounds. *Holzforschung* **2010,** *64* (4), 435.

16. Gómez-Monedero, B.; Ruiz, M. P.; Bimbela, F.; Faria, J., Selective hydrogenolysis of αO4, βO4, 4O5 CO bonds of lignin-model compounds and lignin-containing stillage derived from cellulosic bioethanol processing. *Applied Catalysis A: General* **2017,** *541*, 60-76.

17. Zolfigol, M. A.; Madrakian, E.; Ghaemi, E., Silica Sulfuric Acid/ $NaNO_2$ as a Novel Heterogeneous System for the Nitration of Phenols under Mild Conditions. *Molecules* **2002,** *7* (10), 734-742.

18. Hajipour, A. R.; Mirjalili, B. B. F.; Zarei, A.; Khazdooz, L.; Ruoho, A. E., A novel method for sulfonation of aromatic rings with silica sulfuric acid. *Tetrahedron Letters* **2004,** *45* (35), 6607-6609.

19. Khemaïs, S.; Kammoun; Majed; Moussaoui, Y.; Salem; Ben, R., The effect of ultrasound on the yields of Heck reaction using Pd-catalyst in DMF/water. *Mediterranean Journal of Chemistry* **2014,** *1*, 13-18.

20. Zhao, Y.; Truhlar, D. G., The M06 suite of density functionals for main group thermochemistry, thermochemical kinetics, noncovalent interactions, excited states, and transition elements: two new functionals and systematic testing of four M06-class functionals and 12 other functionals. *Theoretical chemistry accounts* **2008,** *120* (1-3), 215-241.

21. Frisch, M. J.; Trucks, G. W.; Schlegel, H. B.; Scuseria, G. E.; Robb, M. A.; Cheeseman, J. R.; Scalmani, G.; Barone, V.; Petersson, G. A.; Nakatsuji, H.; Li, X.; Caricato, M.; Marenich, A. V.; Bloino, J.; Janesko, B. G.; Gomperts, R.; Mennucci, B.; Hratchian, H. P.; Ortiz, J. V.; Izmaylov, A. F.; Sonnenberg, J. L.; Williams; Ding, F.; Lipparini, F.; Egidi, F.; Goings, J.; Peng, B.; Petrone, A.; Henderson, T.; Ranasinghe, D.; Zakrzewski, V. G.; Gao, J.; Rega, N.; Zheng, G.; Liang, W.; Hada, M.; Ehara, M.; Toyota, K.; Fukuda, R.; Hasegawa, J.; Ishida, M.; Nakajima, T.; Honda, Y.; Kitao, O.; Nakai, H.; Vreven, T.; Throssell, K.; Montgomery Jr., J. A.; Peralta, J. E.; Ogliaro, F.; Bearpark, M. J.; Heyd, J. J.; Brothers, E. N.; Kudin, K. N.; Staroverov, V. N.; Keith, T. A.; Kobayashi, R.; Normand, J.; Raghavachari, K.; Rendell, A. P.; Burant, J. C.; Iyengar, S. S.; Tomasi, J.; Cossi, M.; Millam, J. M.; Klene, M.; Adamo, C.; Cammi, R.; Ochterski, J. W.; Martin, R. L.; Morokuma, K.; Farkas, O.; Foresman, J. B.; Fox, D. J. *Gaussian 16 Rev. C.01*, Wallingford, CT, 2016.

22. Adams, J.; Gross, M. L., Charge-remote fragmentations of closed-shell ions. A thermolytic analogy. *Journal of the American Chemical Society* **1989,** *111* (2), 435-440.

23. Townsend, D.; Lahankar, S. A.; Lee, S. K.; Chambreau, S. D.; Suits, A. G.; Zhang, X.; Rheinecker, J.; Harding, L. B.; Bowman, J. M., The roaming atom: straying from the reaction path in formaldehyde decomposition. *Science* **2004,** *306*, 1158+.

24. Bowman, J. M.; Shepler, B. C., Roaming Radicals. *Annual Review of Physical Chemistry* **2011,** *62* (1), 531-553.

25. Morton, T. H., Competition in the formation of ion–neutral complexes. Expulsion of methane from the molecular ion of acetamide. *Organic Mass Spectrometry* **1991,** *26* (1), 18-23.

26. Liu, X.; Gross, M. L.; Wenthold, P. G., Modeling the Competitive Dissociation of Protonated 2,3-Butanedione. The Enthalpy of Formation of Methylhydroxycarbene. *The Journal of Physical Chemistry A* **2005,** *109* (10), 2183-2189.

CHAPTER 5. EXPERIMENTAL AND CALCULATED ENERGY EFFECTS OF VARIOUS CHARGE TAGS ON THE DISSOCIATION PATHWAYS OF LIGNIN MODEL COMPOUNDS

5.1 Introduction

Mass spectrometers use electric and magnetic fields to propel charged molecules entering in at an orifice towards a detector. Neutral molecules entering in at the same orifice will collide with the internal walls of the mass spectrometer because they do not feel the same magnetic pull that would otherwise guide them to the detector. Mass spectrometry thus requires that a molecule be ionized or carry a charge prior to detection. Several ionization methods have been reported for ionizing lignin that include deprotonation and cationization via metalation.[1, 2]

However, we wanted to avoid analyzing deprotonated molecules such as [M - H]⁻ because they are lacking a proton,[3] and collision-induced dissociations (CID) of the [M - H]⁻ ion may not accurately reflect the dissociations of the original neutral molecule. In this work, the primary focus was to observe the fragmentations (or thermolysis) of molecular lignin rather than lignin in a deprotonated state so that the resulting product ions could be compared to primary pyrolysis. To accomplish this, we proposed attaching a charge tag to strike a balance between ionizing lignin and not altering its native structure.

Several examples of naturally occurring charge-carrying groups have been reported that are known to participate in charge-remote fragmentations (CRF) upon CID,[4, 5] which can be applied to ionize lignin. Two examples are steroid sulfate conjugates and sulfonates (Figure 5.1). By attaching a similar charge tag to lignin and subjecting it to CID followed by CRF, insights may be gained into the unimolecular dissociations of *neutral* lignin, which may be compared to the primary pyrolysis of lignin.[6]
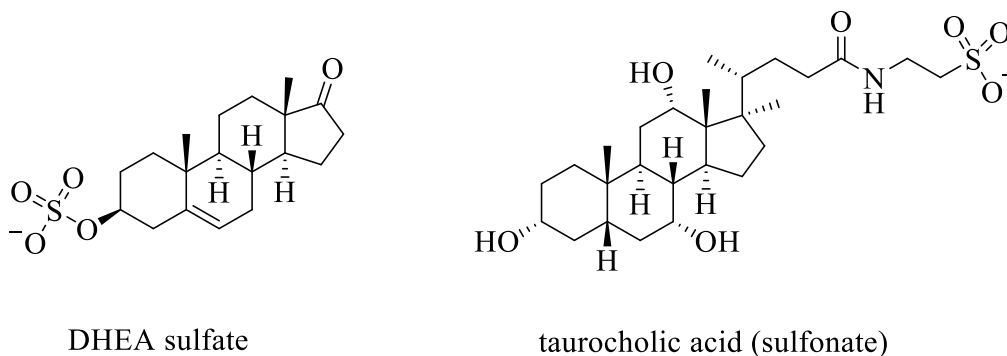
137

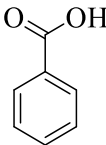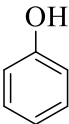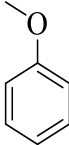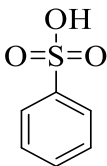DHEA sulfate   taurocholic acid (sulfonate)

Figure 5.1 Examples of negative charge tags in nature

In addition to facilitating CRF, charge tags also have the advantage of giving increased sensitivity to molecules lacking highly ionizable functional groups.[7-9] ESI has two operating modes: positive mode detects molecules carrying a positive charge or protonated molecules, and negative mode detects molecules carrying a negative charge or deprotonated molecules. While lignin contains a variety of functional groups compatible with ESI such as carboxylic acids, other motifs such as the methoxy group are more difficult to ionize. This can be overcome by adding a highly-ionizable charge tag to the molecule.

Although no single factor can predict the ionization efficiency of a molecule, ions that pre-form in solution due to having a low pKa generally have good sensitivity in ESI- (negative mode).[10, 11] Additionally, the stability of the charge in the gas phase is important. Table 5.1 shows the pKa values of several aromatic functional groups. According to the Henderson-Hasselbach equation, only carboxylic acids will dissociate into ions at a neutral pH, so they can be easily detected using ESI-MS. While phenol does not dissociate into ions in solution, it can be deprotonated via another mechanism during ESI and still yield a good signal. However, methoxy groups lack an acidic proton and thus cannot be detected in ESI-.

Table 5.1 Pka's of aromatic functional groups

structure				
functional group	carboxylic acid	hydroxy	methoxy	sulfonate
pKa	4.2	10	N/A	-3

In contrast, by attaching an SO_3^- group to a compound containing only methoxy groups, the molecular ion signal can be greatly enhanced. Furthermore, the sulfonate group is stable in the gas phase, unlike carboxylic acids which quickly undergo decarboxylation. Figure 5.2 compares the MS signal for a 20 mM sample of *ortho*-dimethoxybenzene (**O1**) in 1:1 methanol/water using ESI+ (positive mode) to the MS signal for sulfonated *ortho*-dimethoxybenzene (**O1SO₃⁻**), also in 1:1 methanol/water, using ESI- (negative mode). The improvement in signal is by three orders of magnitude. Thus, the SO_3^- group can greatly improve the sensitivity of lignin model compounds lacking highly ionizable functional groups.
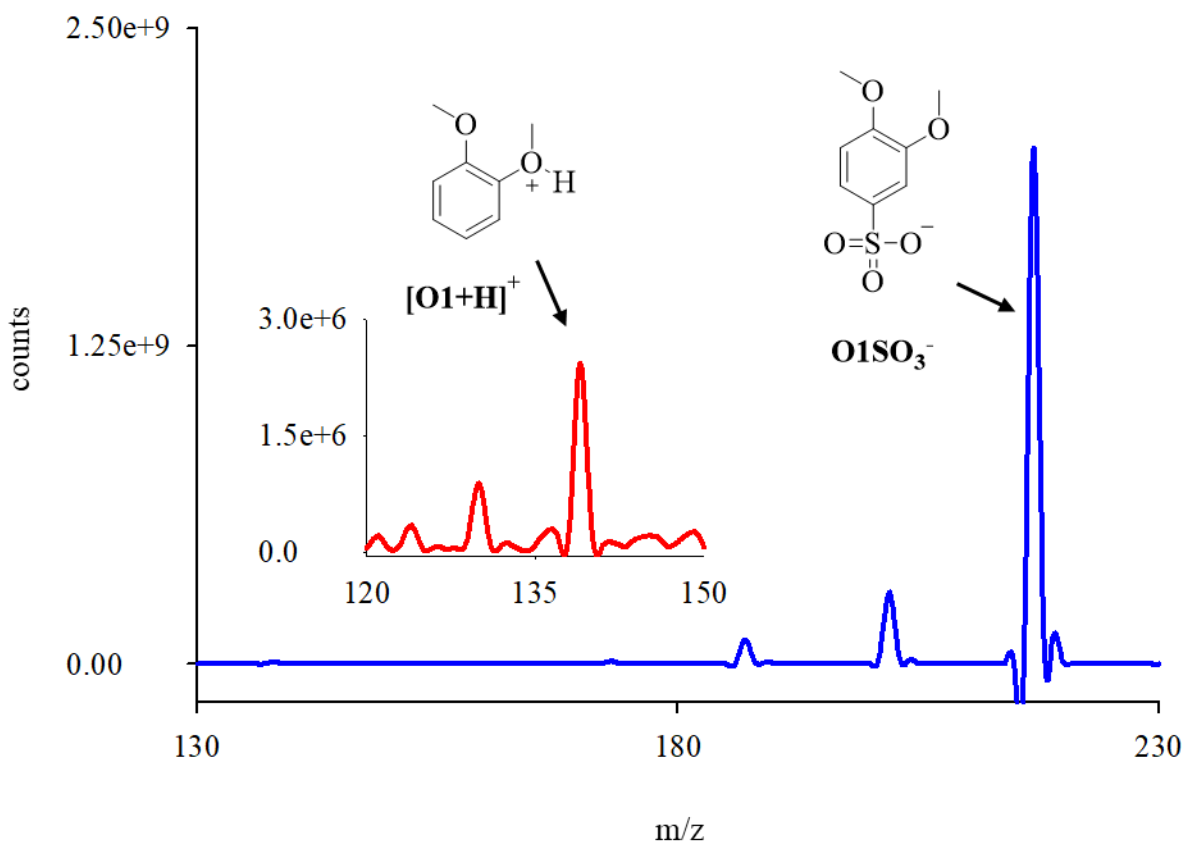
Figure 5.2 Comparison of MS signals for a sulfonated (ESI-) and non-sulfonated (ESI+) methoxy-containing aromatic compound

By attaching a charge tag to lignin model compounds and subjecting them to CID-CRF, the gas-phase dissociation of native lignin may be investigated with improved sensitivity for reactive intermediates. Much must be considered when choosing a suitable charge tag for the mass spectrometric analysis of lignin such as the ESI operating mode (positive vs. negative), whether the tag will promote CRF, and the energy effects of the tag on the transition states and ground states of the product ions. In this chapter, the criteria for selecting SO_3^- as the optimal charge tag for lignin are discussed along with supporting experimental evidence and computational calculations. Future directions for the project are also discussed.

5.2   Methods

5.2.1   Materials

Starting materials and solvents were purchased from commercially available sources and used as received. Silica sulfuric acid was synthesized as described by Zolfigol and coworkers.[12] A 25 mL filtering flask was charged with a magnetic stirrer and silica (5 g, 83 mmol) and a gas inlet tube for drawing away HCl gas over an adsorbing solution (water). The filtering flask was fitted with an addition funnel holding chlorosulfuric acid (1.1 mL, 16 mmol). The chlorosulfuric acid was added dropwise at room temperature over 5 min. HCl gas immediately formed in the filtering flask. After the addition was completed, the mixture was stirred for an additional 10 min. The product was a white solid of silica sulfuric acid.

Direct Sulfonation: The synthetic route to the sulfonated products used in this work was an electrophilic aromatic substitution reaction using silica sulfuric acid in excess of substrate without any solvent as reported by Hajipour and coworkers.[13] A 10 mL round bottom flask with a magnetic stirrer was charged with silica sulfuric acid (38 mg, 0.1 mmol) and also the substrate (0.5 mmol). The reaction mixture was stirred at 80 °C for 30 min, then filtered and washed with 10 mL of ethyl acetate. The solvent was removed under reduced pressure. The remaining liquid was washed with 40 mL of hexanes to form a semi-solid substance and dried under vacuum for several hours to obtain the desired solid product.

General Heck Olefination: The synthetic route for attaching a sulfonated styrene tag to the molecules in this work was a Heck reaction using palladium(II) acetate catalyst in DMF/water as described by Khemaïs and coworkers.[14] A 100 mL round bottom flask with a magnetic stir bar was charged with the 4-bromo substrate analog (5 mmol), sodium p-styrenesulfonate hydrate (0.93 g, 4.5 mmol), potassium carbonate (7.5 mmol), palladium(II) acetate (1 mol %, 11.2 mg), Aliquat 336 (1.14 mL, 2.5 mmol), DMF (2 mL), and water (2 mL). The reaction mixture was stirred at 95 °C for 2 hr. After the reaction was completed, 40 mL chloroform was added and the solid was filtered. The solid was rinsed with methanol (100 mL), and the filtrate was collected. The methanol was removed under reduced pressure to give a solid product. The solid was rinsed multiple times with methanol/ethyl acetate (1:10) to remove unreacted p-styrenesulfonate, which was slightly less polar than the target molecule.

Cholamine derivatization agent: The synthesis of cholamine as a chloride salt been described by Lamos et al.[15] First, boc-protected ethylenediamine (164.9 mg, 1.029 mmol) was stirred into a solution of methanol (20 mL) and $NaHCO_3$ (1.0463 g, 12.454 mmol) at room temperature. The solution was then moved to the dark, and methyl iodide (2.227 g, 15.69 mmol) was added to the solution and stirred for 18 hr. When the reaction was complete, the solution was concentrated by rotavap, then resuspended in $CHCl_3$ (50 mL) and stirred for 1 h before filtering and concentrating into an oil. The boc-protected-cholamine was precipitated upon addition of Et_2O (70 mL). The was washed with Et_2O (40 mL) before drying under reduced pressure to give the boc-protected cholamine intermediate as an iodide salt. The Boc-protected cholamine intermediate (142 mg, 0.4309 mmol) was dissolved in 2 mL of methanol and cooled to 0 °C. Acetyl chloride (173 µL, 2.43 mmol) was then added dropwise and stirred for 3 hr. The reaction was then diluted with 50 mL of Et_2O causing precipitation. The Et_2O was filtered and washed with Et_2O (3×30 mL) before concentrating. Minimal anhydrous acetone was added to dissolve the solid before adding 40 mL of Et_2O, which again caused precipitation. The supernatant was decanted, and the resulting salts were dried in under reduced pressure to give cholamine methyl iodide as a white chloride salt.

The addition of cholamine to the carboxylic acid substrate has been described by Sun et al.[16] To an aliquot (1 mL) of an acetonitrile solution of, 3 µM of substrate was added 100 µL aliquots of acetonitrile solutions of 1 mM N,N-diisopropylethylamine (DIPEA) and 1 mM 1-[bis(dimethylamino)-methylene]-1H-1,2,3-triazolo[4,5-b]pyridinium-3-oxide hexafluorophosphate (HATU), and the mixture was incubated for 15 min at room temperature. A 100-µL aliquot of an aqueous solution of 1 mM derivatization reagent (cholamine) was then added, and the mixture was incubated at room temperature for 1 h to give a nearly quantitative conversion.

5.2.2   Instrumentation

Mass spectra were collected on a commercial LCQ-DECA (Thermo Electron Corporation, San Jose, CA, USA) quadrupole ion trap mass spectrometer. Samples were diluted in 50:50 water/methanol and then injected into the mass spectrometer by using electrospray ionization (ESI). CID experiments were done using helium as the collision target. The collisional energy was given by the normalized collision energy (NCE) which ranges from 0% to 100%.

5.2.3 Quantum Chemical Calculations

Geometry optimizations and frequency calculations for both ground states and transition states were performed using density functional theory (DFT) with the M06-2X functional[17] and the 6-31++G(d,p) basis set. Calculations were done using Gaussian16.[18] All structures were first drawn in MarvinSketch, and the conformers tool was used to create a maximum of 50 conformers of every structure. These all underwent a geometry optimization, and the lowest energy conformer was selected for constructing energy diagrams and calculating transition states.
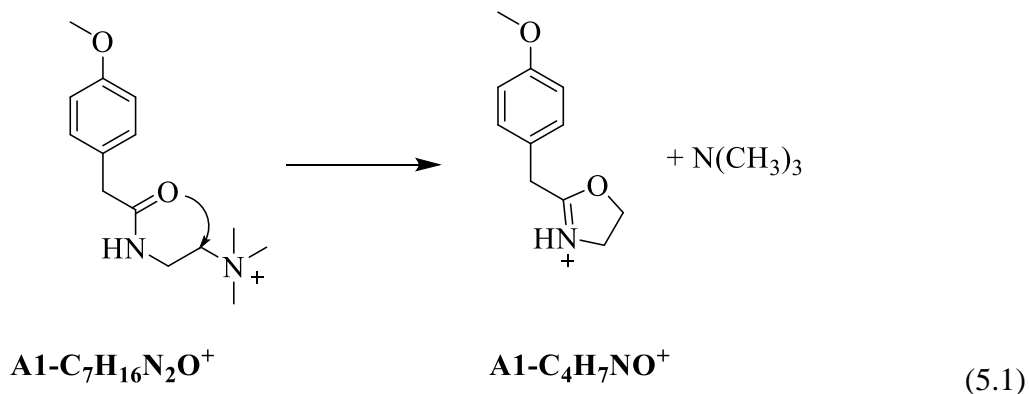
5.3 Results

5.3.1 CID-CRF

Initially, several charge tags were investigated for their ability to facilitate CID-CRF in lignin model compounds. Several methoxy-substituted aromatic compounds containing boron trifluoride groups (BF_3^-) were commercially available, so **A1BF$_3^-$** was purchased and subjected to CID, which is an analog of anisole. A second method was direct sulfonation (**A1SO$_3^-$**), which provided more flexibility in the number of compounds that could be analyzed (Table 5.2). A third approach was addition of cholamine ($C_5H_{16}Cl_2N_2$) to carboxylic acid derivatives (**A1-C$_7$H$_{16}$N$_2$O$^+$**), which are also widely available.

A1BF$_3^-$ **A1SO$_3^-$**   **A1-C$_7$H$_{16}$N$_2$O$^+$**
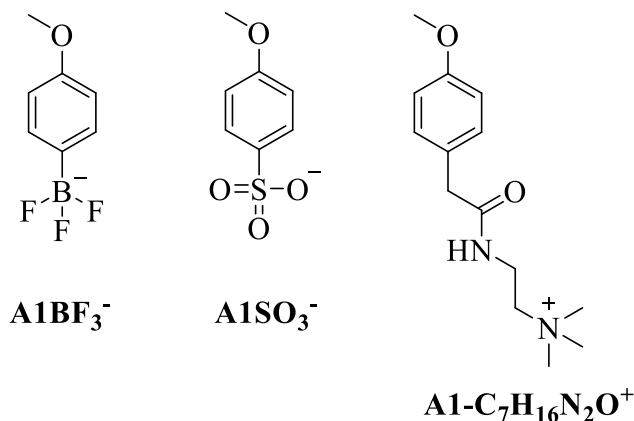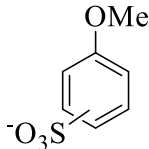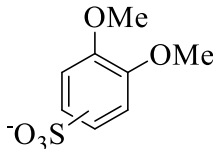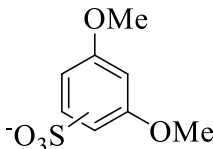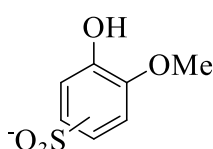
For **A1BF$_3$** and **A1SO$_3^-$**, dissociation occurred by loss of methyl radical to form phenoxy radical. Subsequent CID resulted in cleavage of the charge tag so that no additional dissociation routes could be observed. Upon being collisionally activated, **A1-C$_7$H$_{16}$N$_2$O$^+$** undergoes neutral

loss of trimethylamine ($N(CH_3)_3$),[16] as shown in Equation 5.1. The resulting ion, **A1-C₄H₇NO⁺**
then undergoes CRF and loses methyl radical, similar to **A1BF₃⁻** and **A1SO₃⁻**. However,
subsequent CID also led to charge-driven fragmentations.
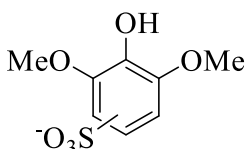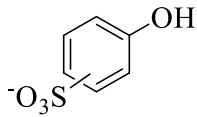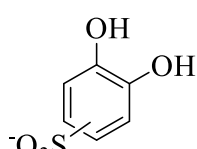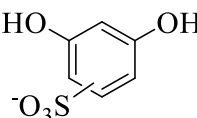

A1-C₇H₁₆N₂O⁺   **A1-C₄H₇NO⁺**

$$\text{(5.1)}$$

The results of CID on additional sulfonated compounds are given in Table 5.2. For these ions,
the first dissociation by CID-CRF was loss of methyl radical to form phenoxy radical unless no
methoxy group was present. In one instance, H_2O was eliminated when two hydroxy groups
were in proximity to one another. The second dissociation step was dominated by elimination of
SO_2 with a few secondary reactions being observed. After loss of SO_2, no further analysis could
be carried out because the charge tag was no longer present on the target analyte.

Table 5.2 MS/MS of directly sulfonated lignin model compounds

Analyte	MS^2	MS^3
	-CH$_3$	
	-CH$_3$	-H, CH$_3$, HCO
	-CH$_3$	-CO
	-CH$_3$	
	-CH$_3$	-CH$_3$
	-H$_2$O	

A final approach for attaching a charge tag to the target molecules was a sulfonated stilbene structure where the charge site was further separated from the dissociation site, as shown in Scheme 5.1. The full MS spectrum and subsequent CID spectra of **A1-C8H6SO3** are given in Chapter 3. In addition to loss of methyl radical, subsequent CID revealed CO loss in competition with SO_2 that was not detected when using the direct sulfonation method. Similar results were seen with other molecules suggesting that the styrene linker made the sulfonate group more robust.

Scheme 5.1
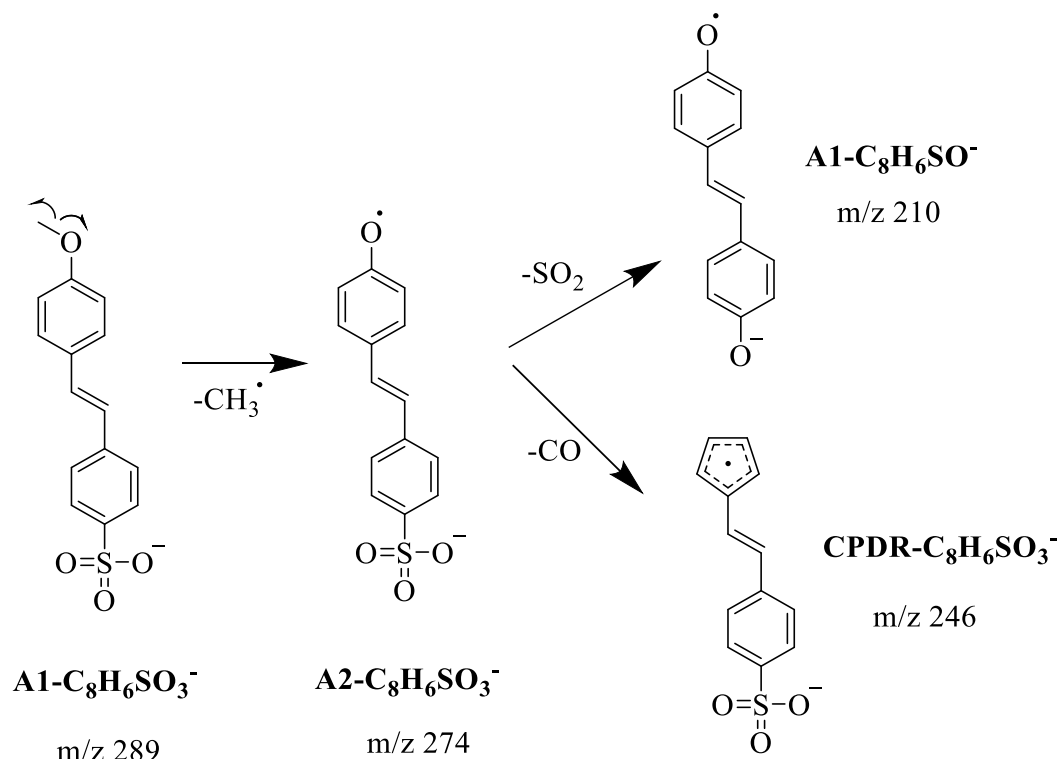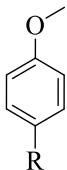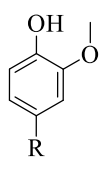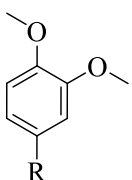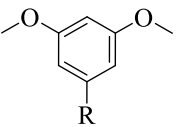
5.3.2 Calculations

The energies for the intermediates and transition states in the dissociation pathways for several model compounds along with their charged analogs were carried out using Gaussian to determine the effects of the charge tags on the dissociation mechanisms. Geometry optimizations and frequency calculations for both ground states and transition states were done using the M06-2X and the 6-31++G(d,p) basis set. Our primary interest was to investigate the effects of the sulfonated stilbene structure because it was the most robust charge tag. The experimental and

calculated bond dissociation energies (BDE) of the first methyl radical loss of the sulfonated structures are shown in Table 5.3.[19, 20] The stilbene tag (R=C$_8$H$_6$SO$_3^-$) lowers the BDE of the first methyl radical loss between 3 to 12 kcal mol^{-1}.

Table 5.3 BDE in kcal mol^{-1} of the first methyl radical loss for several lignin model compounds.

Structure	Experimental[19, 20] R=H	Calculated R=H	Calculated R=SO$_3^-$	Calculated R=C$_8$H$_6$SO$_3^-$
A1	64.7	66	58	56
G1	57.5	58	53	56
O1	60.5	61	54	53
M1	63.7	66	63	62

The sulfonated derivatives of **G1** and **M1** were most similar to the authentic compounds, which both have charge tags *meta* to methoxy groups. This led us to investigate the effects of the position of the charge tag in the ring on the dissociation mechanisms using quantum mechanical calculations. A series of potential energy surface (PES) were constructed of authentic compounds and compared to their charged derivatives, which are given in the discussion section.

5.4 Discussion

5.4.1 ESI operating mode

In order to carry out tandem MS/MS experiments on neutral lignin model compounds, the charge tag must not cleave upon CID. Because charge-driven reactions are far more common than charge-remote fragmentations, strong bonds between the charge tag and the target analyte are desirable. The C-S bond in $R\text{-}SO_3^-$ is strong and easily synthesized via direct sulfonation, which provides a convenient method for ionizing and analyzing aromatic molecules. Additionally, because sulfonates are more stable than sulfates (sulfates are easily hydrolyzed) and are easier to synthesize, we selected SO_3^- for our charge tag. However, sulfur also contains a p orbital in conjugation with the aromatic ring, which provides a stabilization effect that can potentially alter the dissociation lignin. Therefore, additional charge tags were explored that did not add conjugation to the model compounds.

We have observed in general that positive charge tags tend to undergo more rearrangement reactions upon CID, perhaps by lowering the energy barrier of alternate dissociation pathways. Nevertheless, a variety of positive charge-carrying groups are widely available and commonly used to improve the selectivity of analytes by MS, so we investigated the ability of cholamine to facilitate CID-CRF. Lignin model compounds containing carboxylic acid groups are commercially available, so we added cholamine to an anisole derivative containing a carboxylic acid group to make **A1-$C_7H_{16}N_2O^+$**. However, we were unable to carry out multiple MS/MS experiments before cleavage of the charge tag.

Also, because lignin contains many electronegative hydroxy groups, we postulated that the attractive forces between the electron-dense oxygens and a positive charge tag would cause lignin to fold over on itself (Figure 5.3). The labile portions of lignin would then interact with the charge site and undergo charge-driven reactions as opposed to *neutral* dissociations. In contrast, the repulsive forces between the hydroxy groups and a negative charge tag may keep lignin in a more natural state. Because additional product ions beyond the initial methyl radical loss were observed when operating under ESI- (negative mode), we continued with SO_3^- as our charge tag.
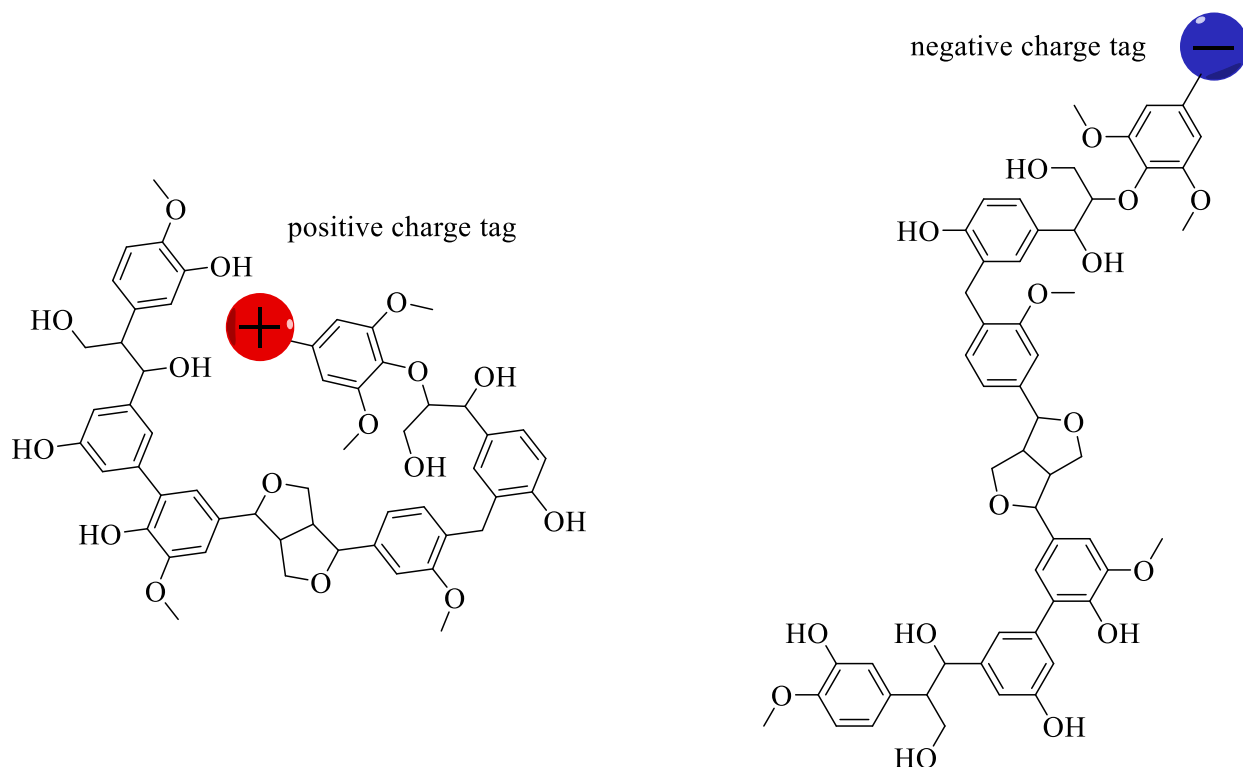
Figure 5.3 Possible effect of the charge on the conformation of lignin

A second approach was used to join the SO_3^- charge tag to the model compounds that involved a styrene linker. The purpose of the linker was to increase the distance between the labile portion of the molecule and the charge site (Figure 5.4). This yielded different intensities of the product ion peaks upon CID. Whereas only the initial methyl radical loss was observed for many directly sulfonated analogs, subsequent CRF was observed when using the styrene linker. Based on the experimental results given in Section 5.3.1, the styrene charge tag was more robust than the directly sulfonated compounds.

Figure 5.4 Scheme of how a linker may be used to increase the distance between a charge tag and a target analyte for CRF

5.4.2 Calculations

A potential obstacle facing the use of charge tags in the analysis of the unimolecular decomposition of lignin model compounds is that the tag may alter the primary route of dissociation by raising or lowering the 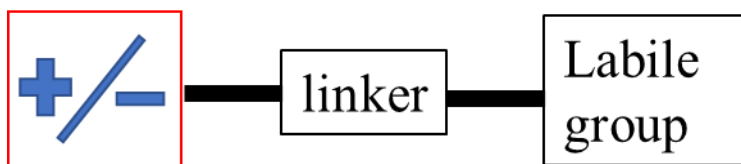energies of the product ions and transition states in the mechanism. The observed ratios of the product ions would then differ from the expected results obtained by pyrolysis. To determine the extent that transition state energies and product ions are changed by addition of a charge tag, we carried out calculations on several lignin model compounds, along with their sulfonated derivatives.

Choosing a basis set, or level of theory, will determine the time and resources required to produce a solution to the energy of a molecule. Generally, the faster the calculation is completed, the more inaccurate it will be. However, increasing the accuracy of a solution requires increasing the time to needed to complete the calculation, and the time requirements may increase exponentially. Two examples of this that are extreme opposites are the B3LYP basis set, which is a fast method but not very accurate, and CCSD(T), which is very accurate but can take months to finish if the molecule being investigated has many atoms.

A good compromise in time and accuracy is the M06-2X basis set. It is a density functional theory (DFT) method that is good for doing thermochemistry calculations, kinetics, and non-covalent interactions of main group atoms. Because lignin contains many electronegative atoms such as O and N, non-covalent interactions should be considered. Thus, M06-2X is a good choice for predicting the reaction pathways, enthalpies, and free energies of intermediates and transition states involved in the dissociation of lignin.

We carried out calculations on sulfonated and non-sulfonated lignin model compounds to predict how the charge tags would affect the ratios of the product ions upon CID. Based on our results, the attachment of SO_3^- lowers the bond dissociation energy (BDE) of the initial methyl radical loss for each of the molecules between 1.7 and 8.7 kcal mol^{-1}. The difference in energy between the authentic compounds and the sulfonated compounds is greatest for **A1** and **O1**, which both have methoxy groups *para* to the charge tag. This energy difference may be explained by the increased resonance contributed by the SO_3^- group to the phenoxy radical products, as shown in Scheme 5.2. No such resonance is present in **G2** and **M2**, which both lose a methoxy group *meta* to the sulfonate tag.

Scheme 5.2
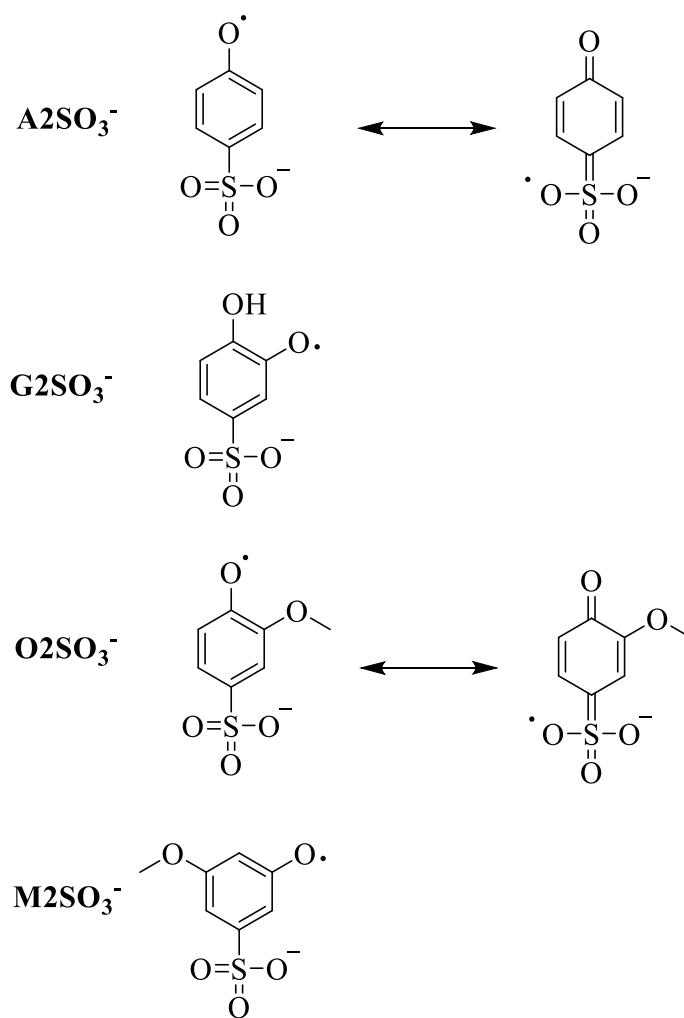
The resonance stabilizing effect seen with **A2SO$_3^-$** and **O2SO$_3^-$** inspired the idea to investigate *meta*-substituted isomers that may have less of an impact on the calculated BDEs. The PES diagrams of authentic anisole along with several charged analogs are shown in Figure 5.5. As can be seen from the figure, the *meta*-substituted tag has the opposite effect of the *para*-substituted versions by lowering the energy of the PES curve relative to the authentic compound. Surprisingly, the *para*-substituted tags destabilize the curve following the initial methyl radical loss. The BF$_3^-$ and SO$_3^-$ groups are indistinguishable from each other. The greatest destabilization is seen with the styrene tag (R=C$_8$H$_6$SO$_3^-$), but it is not differ greatly from the directly sulfonated analog. Thus, the increase in the number of pyrolysis products observed when using the styrene linker is most

likely due to the increased distance between the tag and the labile portion of the molecule as opposed to a change in the energies of the transition states and product ions.
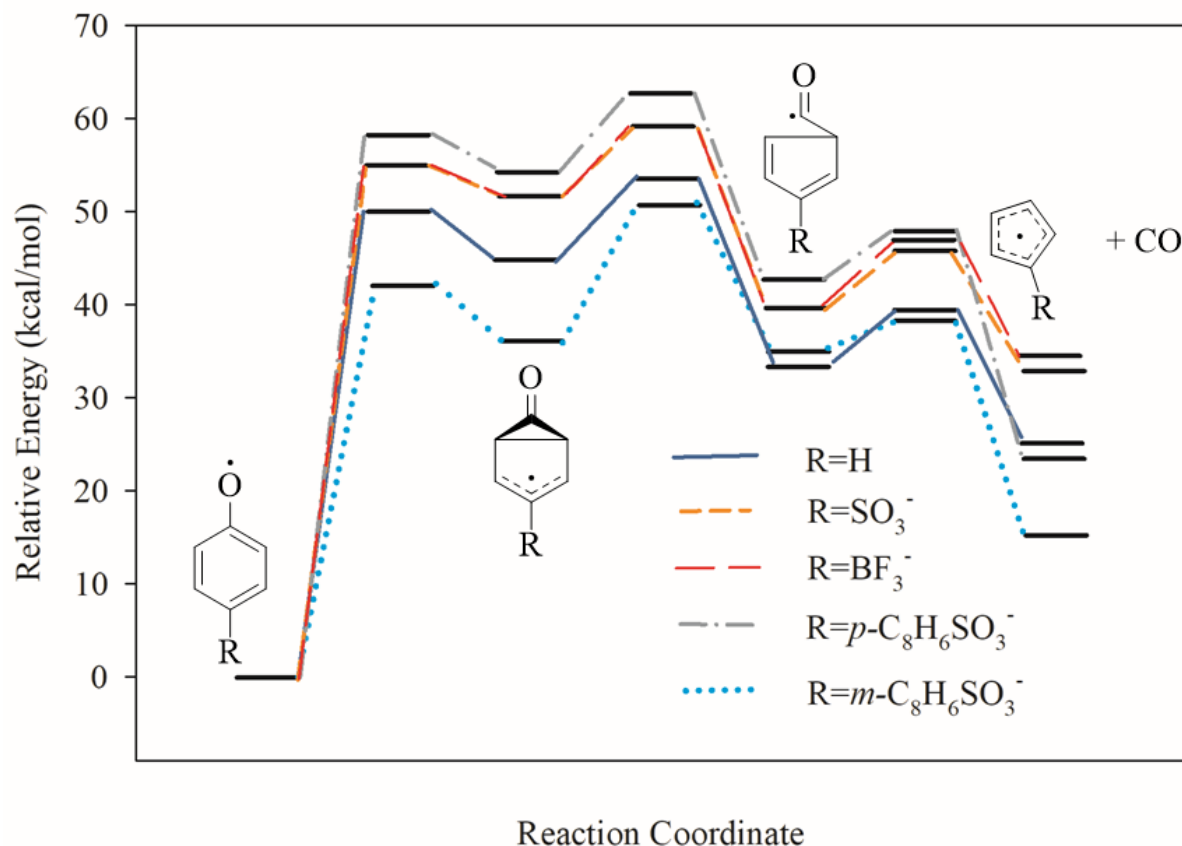
Figure 5.5 PES of anisole dissociation with various charge tags

We also carried out calculations for guaiacol and its charged analogs, and the PES of guaiacol dissociation is shown in Figure 5.6. We were unable to calculate the energy barrier for H loss to form *ortho*-benzoquinone, but it can be assumed that it is close to the BDE of the O-H bond (~70 kcal mol^{-1}) of the phenoxy radical intermediate. Similarly, the energy barrier for formation of the final product is assumed to be the BDE of the O-H bond (~50 kcal mol^{-1}) of the preceding intermediate. The energy effects of the charge tags do not appear to follow the same trend that was observed with anisole dissociation. The SO_3^- and BF_3^- tags are no longer indistinguishable with the SO_3^- falling lower than the authentic molecule and the BF_3^- tag being higher in energy. The *meta-* and *para*-substituted tags appear to be closest in energy to the authentic molecule.
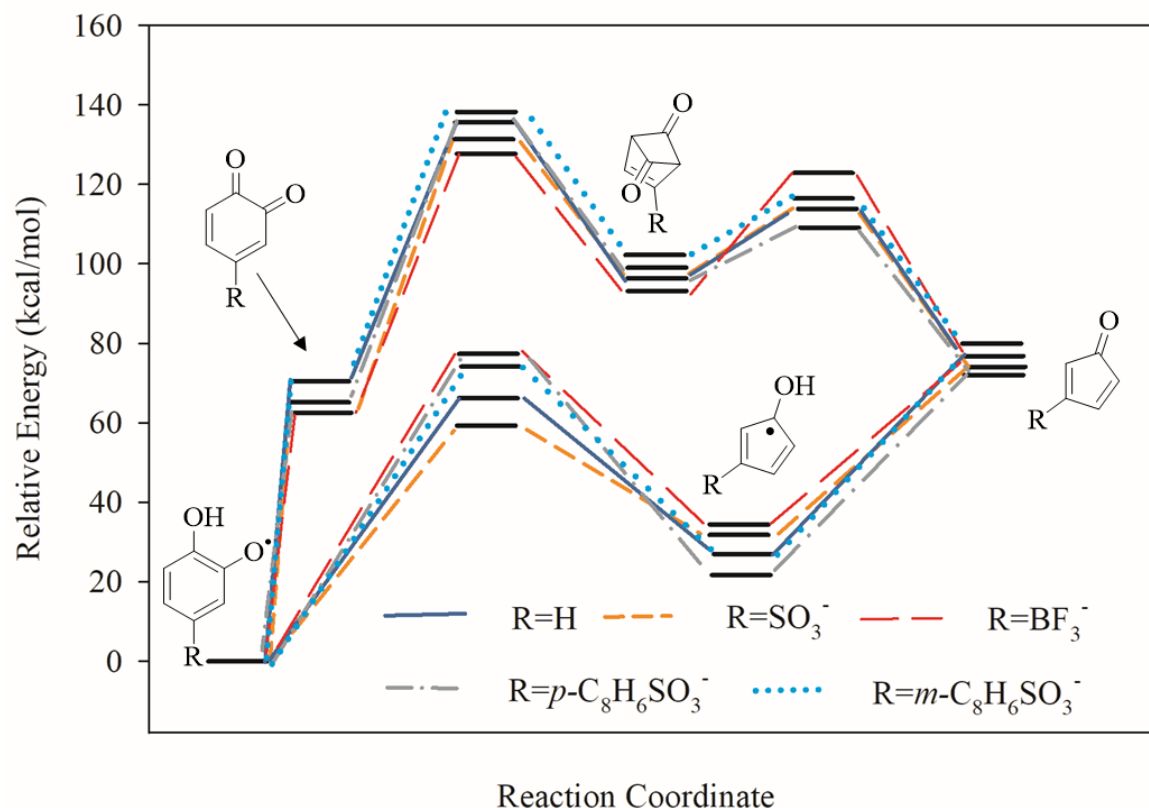
Figure 5.6 PES of guaiacol dissociation with various charge tags

We also carried out calculations for *ortho*-dimethoxybenzene and its sulfonated analogs, which are given in Chapter 3. For this molecule, the *meta-* and *para-* isomers are structurally identical, so no advantage can be gained by changing the orientation of the charge tag. Based on the PES diagrams shown above, it is difficult to choose an optimal charge tag. Because both radical and non-radical intermediates are present in the dissociation mechanisms of lignin model compounds, the argument that added resonance creates a stabilization effect is applicable at every step. Despite many of energies being raised or lowered relative to the authentic molecules, the observed products by CID-CRF were similar to the products observed via pyrolysis, as discussed in Chapters 2 and 3. Thus, the best charge-tag may be the one that gives the best signal intensity of the product ions, which was the *para*-styrene tag.

153

5.5   Conclusion and Future Directions

The advantages of sulfonate charge tags have been discussed here and in Chapter 1, including increasing the volatility and sensitivity of lignin in mass spectrometric analysis, eliminating bimolecular reactions that convolute pyrolysis studies, and facilitating neutral dissociations of lignin model compounds. The sulfonate group has thereby provided insights into the primary pyrolysis of lignin and the formation of reactive intermediates that contribute to PAH formation. In addition, this chapter has focused on experimental and computational results on the effects of varying the charge and location of the charge site on the potential energy surfaces of lignin model compounds. Based on these results, the sulfonate group appears to have a moderate effect on the transition state energies and product ion energies of intermediates involved in the decomposition of lignin. While this may impact the branching ratios of the product ions, the overall dissociation routes remain similar to the authentic molecules.

Nevertheless, the process of CID-CRF can benefit from further optimization of the charge tag. One possibility of accomplishing this is by designing a charge tag that does not contribute resonance stabilization energy to the target compounds. For example, adamantane is the simplest diamondoid and is an sp^3 aliphatic structure.[21] Diamondoids are known for their crystal lattice strength, and their lack of p orbitals would completely isolate the charge site from the labile portion of the molecule.

adamantane
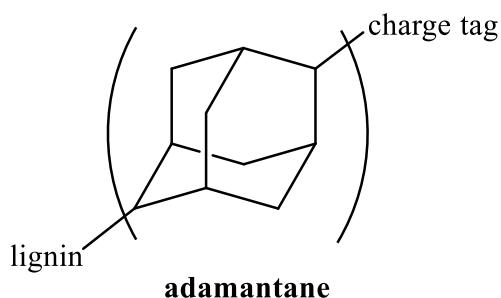
In this work, CID-CRF has been applied to study the pyrolysis of lignin. However, pyrolysis is widespread and is associated with the decomposition of any material under high temperatures. This includes smoking, burning waste, incomplete fuel combustion, forest fires, and cooking.[22-25] In an excellent book on the pyrolysis of organic molecules, Moldoveanu[22] discusses many of these processes including using pyrolysis at a laboratory scale for synthesis as well as at

154

an industrial scale for refining petroleum. CID-CRF could thus be applied to study any number of these molecules to identify their thermal routes of degradation.

In addition to studying pyrolysis, charge tags can also be used to characterize gaseous neutral molecules that would otherwise be difficult to volatilize. For example, amino acids typically exist as zwitterions in solution and are difficult to ionize. However, in the interstellar medium, they would likely have a canonical structure rather than a charge separation. In our earlier work, the neutral dissociation of amino acids and peptides was investigated using a sulfonate charge tag to support this hypothesis.[26, 27] However, this previous work was completed using direct sulfonation to synthesize **PheSO$_3$$^-$**, and a peptide, **GlyPheSO$_3$$^-$**. A repeat of this experiment could be benefited by adding a linker to the charge tag rather than using direct sulfonation.

PheSO$_3$$^-$ **GlyPheSO$_3$$^-$**
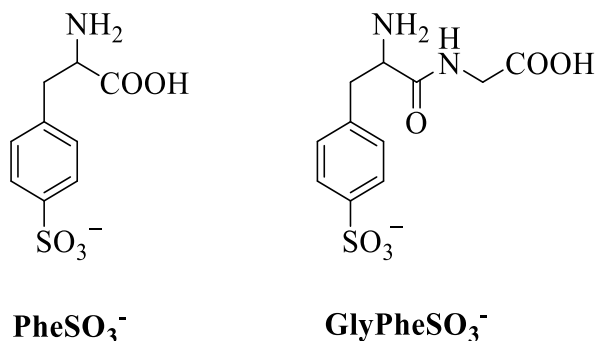
5.6   References

1. Jarrell, T. M.; Marcum, C. L.; Sheng, H.; Owen, B. C.; O'Lenick, C. J.; Maraun, H.; Bozell, J. J.; Kenttämaa, H. I., Characterization of organosolv switchgrass lignin by using high performance liquid chromatography/high resolution tandem mass spectrometry using hydroxide-doped negative-ion mode electrospray ionization. *Green Chemistry* **2014,** *16* (5), 2713-2727.

2. Asare, S. O.; Huang, F.; Lynn, B. C., Characterization and sequencing of lithium cationized β-O-4 lignin oligomers using higher-energy collisional dissociation mass spectrometry. *Analytica Chimica Acta* **2019,** *1047*, 104-114.

3. Banerjee, S.; Mazumdar, S., Electrospray Ionization Mass Spectrometry: A Technique to Access the Information beyond the Molecular Weight of the Analyte. *International Journal of Analytical Chemistry* **2012,** *2012*, 282574.

4. Yan, Y.; Ubukata, M.; Cody, R. B.; Holy, T. E.; Gross, M. L., High-Energy Collision-Induced Dissociation by MALDI TOF/TOF Causes Charge-Remote Fragmentation of Steroid Sulfates. *Journal of The American Society for Mass Spectrometry* **2014,** *25* (8), 1404-1411.

5. Tomer, K. B.; Jensen, N. J.; Gross, M. L.; Whitney, J., Fast atom bombardment combined with tandem mass spectrometry for determination of bile salts and their conjugates. *Biomedical & Environmental Mass Spectrometry* **1986,** *13* (6), 265-272.

6. Adams, J.; Gross, M. L., Charge-remote fragmentations of closed-shell ions. A thermolytic analogy. *Journal of the American Chemical Society* **1989,** *111* (2), 435-440.

7. Fragkaki, A. G.; Petropoulou, G.; Athanasiadou, I.; Kiousi, P.; Kioukia-Fougia, N.; Archontaki, H.; Bakeas, E.; Angelis, Y. S., Determination of anabolic androgenic steroids as imidazole carbamate derivatives in human urine using liquid chromatography–tandem mass spectrometry. *Journal of Separation Science* **2020,** *43* (11), 2154-2161.

8. Zhuang, M.; Hou, Z.; Chen, P.; Liang, G.; Huang, G., Introducing charge tag via click reaction in living cells for single cell mass spectrometry. *Chemical Science* **2020,** *11* (28), 7308-7312.

9. Waliczek, M.; Kijewska, M.; Rudowska, M.; Setner, B.; Stefanowicz, P.; Szewczuk, Z., Peptides Labeled with Pyridinium Salts for Sensitive Detection and Sequencing by Electrospray Tandem Mass Spectrometry. *Scientific Reports* **2016,** *6* (1), 37720.

10. Mayhew, A. W.; Topping, D. O.; Hamilton, J. F., New Approach Combining Molecular Fingerprints and Machine Learning to Estimate Relative Ionization Efficiency in Electrospray Ionization. *ACS Omega* **2020,** *5* (16), 9510-9516.

11. Henriksen, T.; Juhler, R. K.; Svensmark, B.; Cech, N. B., The relative influences of acidity and polarity on responsiveness of small organic molecules to analysis with negative ion electrospray ionization mass spectrometry (ESI-MS). *Journal of the American Society for Mass Spectrometry* **2005,** *16* (4), 446-455.

12. Zolfigol, M. A.; Madrakian, E.; Ghaemi, E., Silica Sulfuric Acid/ $NaNO_2$ as a Novel Heterogeneous System for the Nitration of Phenols under Mild Conditions. *Molecules* **2002,** *7* (10), 734-742.

13. Hajipour, A. R.; Mirjalili, B. B. F.; Zarei, A.; Khazdooz, L.; Ruoho, A. E., A novel method for sulfonation of aromatic rings with silica sulfuric acid. *Tetrahedron Letters* **2004,** *45* (35), 6607-6609.

14. Khemaïs, S.; Kammoun; Majed; Moussaoui, Y.; Salem; Ben, R., The effect of ultrasound on the yields of Heck reaction using Pd-catalyst in DMF/water. *Mediterranean Journal of Chemistry* **2014,** *1*, 13-18.

15. Lamos, S. M.; Shortreed, M. R.; Frey, B. L.; Belshaw, P. J.; Smith, L. M., Relative Quantification of Carboxylic Acid Metabolites by Liquid Chromatography−Mass Spectrometry Using Isotopic Variants of Cholamine. *Analytical Chemistry* **2007,** *79* (14), 5143-5149.

16. Sun, D.; Meng, X.; Ren, T.; Fawcett, J. P.; Wang, H.; Gu, J., Establishment of a Charge Reversal Derivatization Strategy to Improve the Ionization Efficiency of Limaprost and Investigation of the Fragmentation Patterns of Limaprost Derivatives Via Exclusive Neutral Loss and Survival Yield Method. *Journal of The American Society for Mass Spectrometry* **2018,** *29* (7), 1365-1375.

17. Zhao, Y.; Truhlar, D. G., The M06 suite of density functionals for main group thermochemistry, thermochemical kinetics, noncovalent interactions, excited states, and transition elements: two new functionals and systematic testing of four M06-class functionals and 12 other functionals. *Theoretical chemistry accounts* **2008,** *120* (1-3), 215-241.

18. Frisch, M. J.; Trucks, G. W.; Schlegel, H. B.; Scuseria, G. E.; Robb, M. A.; Cheeseman, J. R.; Scalmani, G.; Barone, V.; Petersson, G. A.; Nakatsuji, H.; Li, X.; Caricato, M.; Marenich, A. V.; Bloino, J.; Janesko, B. G.; Gomperts, R.; Mennucci, B.; Hratchian, H. P.; Ortiz, J. V.; Izmaylov, A. F.; Sonnenberg, J. L.; Williams; Ding, F.; Lipparini, F.; Egidi, F.; Goings, J.; Peng, B.; Petrone, A.; Henderson, T.; Ranasinghe, D.; Zakrzewski, V. G.; Gao, J.; Rega, N.; Zheng, G.; Liang, W.; Hada, M.; Ehara, M.; Toyota, K.; Fukuda, R.; Hasegawa, J.; Ishida, M.; Nakajima, T.; Honda, Y.; Kitao, O.; Nakai, H.; Vreven, T.; Throssell, K.; Montgomery Jr., J. A.; Peralta, J. E.; Ogliaro, F.; Bearpark, M. J.; Heyd, J. J.; Brothers, E. N.; Kudin, K. N.; Staroverov, V. N.; Keith, T. A.; Kobayashi, R.; Normand, J.; Raghavachari, K.; Rendell, A. P.; Burant, J. C.; Iyengar, S. S.; Tomasi, J.; Cossi, M.; Millam, J. M.; Klene, M.; Adamo, C.; Cammi, R.; Ochterski, J. W.; Martin, R. L.; Morokuma, K.; Farkas, O.; Foresman, J. B.; Fox, D. J. *Gaussian 16 Rev. C.01*, Wallingford, CT, 2016.

19. Suryan , M. M.; Kafafi , S. A.; Stein, S. E., The thermal decomposition of hydroxy- and methoxy-substituted anisoles. *Journal of the American Chemical Society* **1989,** *4* (111), 1423–1429.

20. Scheer, A. M.; Mukarakate, C.; , D. J. R.; Nimlos, M. R.; Ellison, a. G. B., Thermal Decomposition Mechanisms of the Methoxyphenols: Formation of Phenol, Cyclopentadienone, Vinylacetylene, and Acetylene. *The Journal of Physical Chemistry A* **2011,** *115* (46), 13381-13389.

21. Bouwman, J.; Horst, S.; Oomens, J., Spectroscopic Characterization of the Product Ions Formed by Electron Ionization of Adamantane. *Chemphyschem : a European journal of chemical physics and physical chemistry* **2018,** *19* (23), 3211-3218.

22. Moldoveanu, S. C., Pyrolysis of Organic Molecules with Applications to Health and Environmental Issues. In *Techniques and Instrumentation in Analytical Chemistry*, Elsevier: 2010; Vol. 28, p iii.

23. Eskin, N. A. M.; Ho, C.-T.; Shahidi, F., Chapter 6 - Browning Reactions in Foods. In *Biochemistry of Foods (Third Edition)*, Eskin, N. A. M.; Shahidi, F., Eds. Academic Press: San Diego, 2013; pp 245-289.

24. Johnson, R. R.; Alford, E. D.; Kinzer, G. W., Formation of sucrose pyrolysis products. *Journal of Agricultural and Food Chemistry* **1969,** *17* (1), 22-24.

25. Busch, C.; Streibel, T.; Liu, C.; McAdam, K. G.; Zimmermann, R., Pyrolysis and combustion of tobacco in a cigarette smoking simulator under air and nitrogen atmosphere. *Analytical and Bioanalytical Chemistry* **2012,** *403* (2), 419-430.

26. Koirala, D.; Kodithuwakkuge, S. R.; Wenthold, P. G., Mass spectrometric study of the decomposition pathways of canonical amino acids and α-lactones in the gas phase. *Journal of Physical Organic Chemistry* **2015,** *28* (10), 635-644.

27. Koirala, D.; Mistry, S.; Wenthold, P. G., Participation of C-H Protons in the Dissociation of a Proton Deficient Dipeptide. *Journal of The American Society for Mass Spectrometry* **2017,** *28* (7), 1313-1323.